1984

High temperature thermodynamics of the zirconium-aluminum system

Robert Joseph Kematick
Iowa State University

Kematick, Robert Joseph

HIGH TEMPERATURE THERMODYNAMICS OF THE ZIRCONIUM-ALUMINUM SYSTEM

Iowa State University PH.D. 1984

PLEASE NOTE:

In all cases this material has been filmed in the best possible way from the available copy. Problems encountered with this document have been identified here with a check mark __✓__.

1. Glossy photographs or pages _____
2. Colored illustrations, paper or print _____
3. Photographs with dark background _____
4. Illustrations are poor copy _____
5. Pages with black marks, not original copy _____
6. Print shows through as there is text on both sides of page _____
7. Indistinct, broken or small print on several pages ✓
8. Print exceeds margin requirements _____
9. Tightly bound copy with print lost in spine _____
10. Computer printout pages with indistinct print _____
11. Page(s) _____ lacking when material received, and not available from school or author.
12. Page(s) _____ seem to be missing in numbering only as text follows.
13. Two pages numbered _____. Text follows.
14. Curling and wrinkled pages _____
15. Other _____

High temperature thermodynamics of the zirconium-aluminum system

by

Robert Joseph Kematick

A Dissertation Submitted to the
Graduate Faculty in Partial Fulfillment of the
Requirements for the Degree of
DOCTOR OF PHILOSOPHY

Department: Chemistry
Major: Physical Chemistry

Approved:

Signature was redacted for privacy.

In Charge of Major Work

Signature was redacted for privacy.

For the Major Department

Signature was redacted for privacy.

For the Graduate College

Iowa State University
Ames, Iowa

1984

TABLE OF CONTENTS

I. INTRODUCTION

A. Purpose of Current Project

This project was undertaken to help provide basic chemical and thermochemical information for the various intermetallic compounds formed between zirconium and aluminum. Previous investigations of the phase diagram and crystallography of this system have left some uncertainty regarding the number of compounds formed between zirconium and aluminum and the temperature ranges at which they are stable. To date, reliable thermodynamic data for the system are lacking. Such data are of interest in various metallurgical problems since they relate to segregation and precipitation of intermediate phases in alloy applications and they also provide some basis for the understanding of chemical bonding effects and cohesion in the various compounds.

B. Review of Previous Work on the Zr-Al System

1. Phase diagram and crystallography

Previous investigations of the zirconium aluminum system have centered largely around the establishment of phase diagram features and crystallography of the intermetallic compounds formed. The compounds which have been characterized crystallographically are listed in Table 1.1 along with references to the appropriate literature. These data have been tabulated by Pearson.[12]

Historically, the first zirconium-aluminum compound to be identified was $ZrAl_3$ by Brauer[1] in 1939. The crystal structure of this compound and the related compounds $TiAl_3$, $TaAl_3$, and $NbAl_3$ were reported in this work.

Table 1.1. Crystallographic data for zirconium-aluminides

Compound	Structure Type	Lattice Parameters (Å)	Space Group	Ref.
$ZrAl_3$	DO_{23} tetragonal	a = 4.306, c = 1690	I_4/mmm	1
$ZrAl_2$	C14 ($MgZn_2$) hexagonal	a = 5.282, c = 8.748	$P6_3/mmc$	2
Zr_2Al_3	orthorhombic	a = 9.601, b = 13.906, c = 5.57	Fdd2	3
ZrAl	B_f orthorhombic (CrB)	a = 3.353, b = 10.866, c = 9.266	Cmcm	4
Zr_5Al_4 (h)	hexagonal Ti_5Ga_4	a = 8.447, c = 5.810	$P6_3/mcm$	5
Zr_4Al_3	hexagonal	a = 5.433, c = 5.390	$P\bar{6}$	6
Zr_3Al_2	tetragonal	a = 7.630, c = 6.998	$P4_2/mnm$	7
Zr_5Al_3 (h)	$D8_m$ (W_5Si_3)-tetragonal	a = 11.049, c = 5.396	I4/mcm	8
Zr_2Al	$D8_2$ (Ni_2In)-hexagonal	a = 4.894, c = 5.928	$P6_3/mmc$	9
Zr_3Al	$L1_2$ (Cu_3Au)-cubic	a = 4.372	Pm3m	10
"$Zr_5Al_3O_x$"	$D8_8$ (Mn_5Si_3)-hexagonal	a = 8.184, c = 5.702	$P6_3/mcm$	8,11

Other early work was directed towards the establishment of solidus and liquidus curves in the extreme aluminum-rich end of the phase diagram.[13] Then, in 1954, McPhersen and Hansen[14] reported an investigation of the complete phase diagram of the zirconium-aluminum system, based on results of DTA and metallographical examination of a large number of samples. The compounds $ZrAl_3$, $ZrAl_2$, Zr_2Al_3, ZrAl, Zr_4Al_3, Zr_3Al_2, Zr_5Al_3, Zr_2Al, and Zr_3Al were reported. Three of these, namely Zr_3Al, Zr_2Al, and ZrAl were reported to form in the solid state, while the remaining compounds formed congruently or peritectically from the melt. Zr_5Al_3 was reported to have a minimum temperature of stability, probably decomposing eutectoidally into $Zr_2Al + Zr_3Al_2$, but because of sluggish reaction rates the temperature of decomposition could not be established exactly. To the present time, the phase diagram of the zirconium-aluminum system as it appears in several compilations[15-17] appears to remain basically as established by McPhersen and Hansen without major revisions. This diagram is shown in Figure 1.1.

Following the phase diagram work of McPhersen and Hansen numerous crystallographic studies of the intermetallic compounds were carried out by several investigators.[1-11,18] Edshammar,[18] in 1962 reviewed the crystallography of the zirconium-aluminum system, pointing out potential uncertainties in the structures and existence of some of the compounds. Edshammar was unable to confirm the existence of ZrAl and suggested that this compound may be stabilized by hafnium impurities. He also discussed two observed structures of the compound Zr_5Al_3, one of which is isotypic with Mn_5Si_3 and the other with W_5Si_3. Wilson et al.[11] reported observing

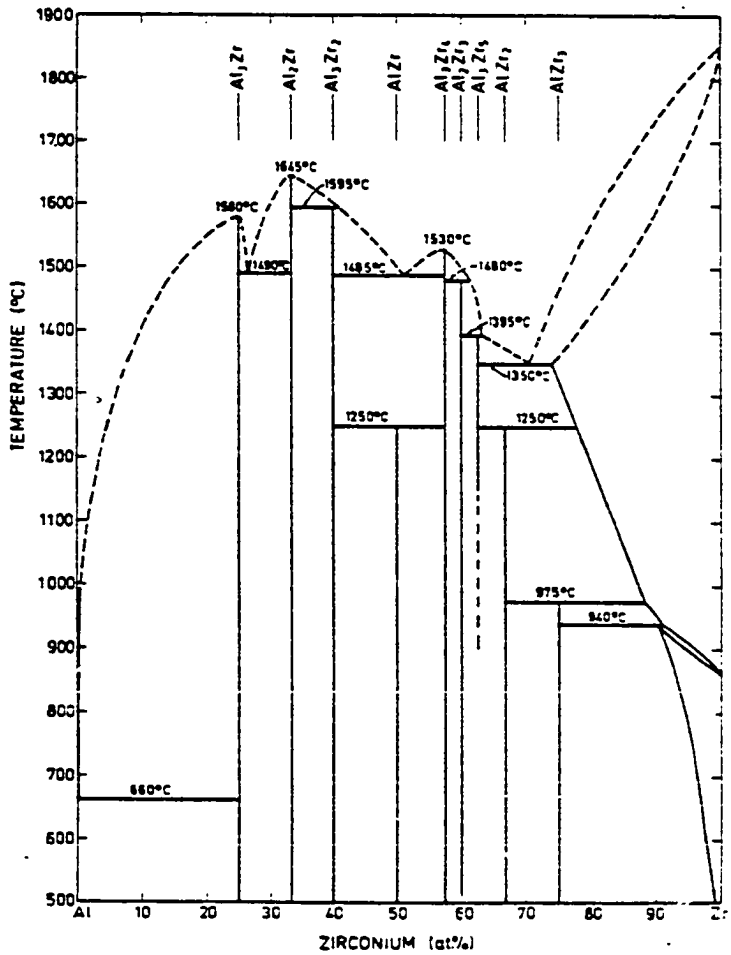

Figure 1.1. The Zr-Al phase diagram of McPhersen and Hansen[14]

a Mn_5Si_3-type phase while Edshammar found a W_5Si_3. Nowotny[19] pointed out that the Mn_5Si_3-type structure is often stabilized by nonmetallic impurities (O,C,B) in octahedral interstices of this structure type. Edshammar believes the same to be true of the Mn_5Si_3 phase occurring in the zirconium-aluminum system. In fact, Edshammar and Andersson[8] arc melted a mixture of Zr, Al, and Al_2O_3 in the ratio Zr_5Al_3O (corresponding to all octahedral interstices filled) and obtained a pure Mn_5Si_3-type phase with lattice parameters near those reported by Wilson for Zr_5Al_3 of the Mn_5Si_3-type. The Mn_5Si_3-type phase is therefore referred to as "$Zr_5Al_3O_x$".

A modification to the phase diagram of McPhersen and Hansen[14] was proposed by Potschke and Schubert in 1962.[20] A new high temperature compound, Zr_5Al_4, was reported to form congruently from the melt at 1530°C and 80.8 wt % Zr instead of the compound Zr_4Al_3 (81.6 wt % Zr). The compound Zr_5Al_4 was reported to be isotypic with the compound Ti_5Ga_4. Potschke and Schubert used the structural data of Ti_5Ga_4 (i.e., the atomic coordinates) to calculate an expected powder pattern of Zr_5Al_4 and reportedly obtained a good match to the observed pattern. The compound Zr_4Al_3, according to Potschke, forms in the solid state at about 1000°C. The phase diagram modification proposed by Potschke and Schubert is illustrated in Figure 1.2. They also report observing "$Zr_5Al_3O_x$" over a wide composition range (50-63 at % Zr). The findings of Potschke and Schubert have not been adopted in phase diagrams appearing in various compilations and remain largely unconfirmed.

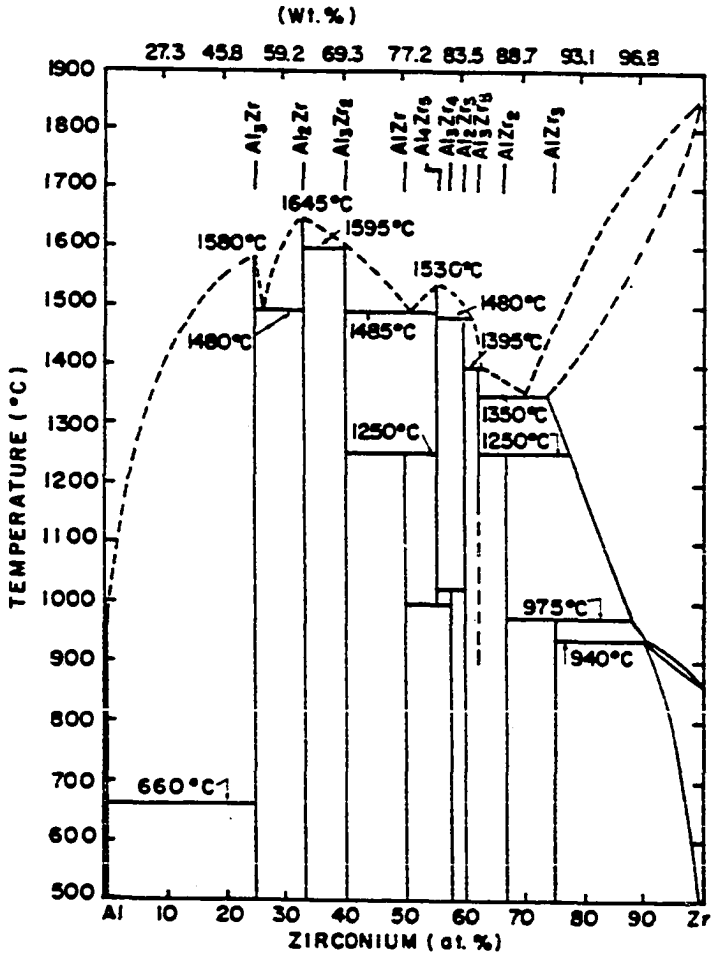

Figure 1.2. The Zr-Al phase diagram as modified by Potschke and Schubert[20]

In summary, the principal phase diagram features of the zirconium-aluminum system are established, but some uncertainty exists regarding the existence of ZrAl and Zr_5Al_4. There has also been some uncertainty as to whether the Mn_5Si_3-type phase appearing in this system is a modification of the binary compound Zr_5Al_3 or a ternary $Zr_5Al_3O_x$ ($x \leq 1$).

2. Previous thermodynamic investigations

Previous thermodynamic investigations of the zirconium-aluminum system are limited to only one. Schneider et al.[21] determined integral free energies of three compounds by measuring the solubility of each component in liquid magnesium at 740°C. They obtained

$$1/3\ ZrAl_2 : \Delta G^\circ_{f,1023\ K} = -13600\ \text{cal/g-atom}$$

$$1/5\ Zr_2Al_3 : \Delta G^\circ_{f,1023\ K} = -12800\ \text{cal/g-atom}$$

$$1/7\ Zr_4Al_3 : \Delta G^\circ_{f,1023\ K} = -10300\ \text{cal/g-atom}.$$

The reliability of these data have been questioned[16] partially because measurements were made at one temperature only, but they constitute all that is known thermochemically about the zirconium-aluminum system.

II. PHASE DIAGRAM SURVEY

A. General Procedures

In view of the fact that there is some uncertainty in the literature regarding the number and composition of the intermetallic phases in the zirconium-aluminum system and the temperature ranges over which these are stable, some effort was placed in the course of this study in preparing and examining, by Guinier X-ray powder diffraction, a number of samples of different compositions subjected to various heat treatment experiments. Many of these experiments were performed in conjunction with Knudsen effusion experiments to be described later. Some of the samples used in heat treatment experiments were also used in effusion experiments, other samples were prepared exclusively for examination of phase changes occurring at specific compositions and temperatures. Aluminum-rich samples were observed to lose weight rather quickly (>0.25 mg/hour) when placed in a tungsten Knudsen cell and heated between 1100-1400°C in vacuum. Some of these samples were deliberately subjected to repeated heat treatment experiments designed to volatilize sufficient aluminum that phase changes occurring with composition could be detected. The major concern throughout these experiments was to verify which compounds were stable at temperatures high enough to volatilize aluminum at a detectable rate. This information is critical to the proper interpretation of any thermodynamic data obtained from high temperature vaporization experiments, and is of interest in clearing up some uncertainties in the reported phase diagrams. Efforts were directed especially towards the examination of the compounds ZrAl, Zr_4Al_3, Zr_5Al_4 and Zr_5Al_3 and

towards the examination of lattice parameter variations with composition and coexisting phases for as many of the compounds as possible.

B. Sample Preparation and Characterization

Zirconium-aluminum alloy samples were prepared by arc melting weighed mixtures of high purity zirconium and aluminum metals. The starting materials were m3N^{+} zirconium foil and m4N8 aluminum shot purchased from the Alfa-Ventron Corporation. The materials were melted on a water cooled copper plate in a helium atmosphere arc welder. A zirconium button was melted to getter oxygen impurities in the helium atmosphere before melting any samples. The sample buttons were turned over and melted several times to help insure homogeneity. Weight loss of the sample could be held to less than about 1% of the total weight with careful technique. The total quantity of material melted at one time was generally 1.5 to 3.0 grams.

After arc melting, the sample buttons were crushed in a tool steel mortar to obtain several coarse chunks of material. These were subjected to various annealing experiments and examined by X-ray powder diffraction afterwards. Portions of the as-cast samples were also subjected to powder diffraction analysis. Samples were ground into as fine a powder as possible using an agate mortar and pestle before the diffraction analyses.

X-ray powder patterns were obtained using a Guinier focusing camera. Small portions of NbS Si were mixed with the samples to provide an internal reference. The positions of all reflections were measured to the nearest 0.01 millimeter using an illuminated fiber viewing device.

Powder patterns and observed intensities were compared to expected powder patterns calculated (using reported structural data) by a powder pattern program developed at Penn State.[22] Lattice parameters were refined by least squares fitting of the observed $1/d^2$ values using a computer program developed at the Ames Laboratory.[23]

In the various heat treatment experiments, different heat sources were used depending on the temperature to which the sample was to be heated and the length of time it would remain at temperature. Higher temperature anneals ($\gtrsim$1000°C) were performed by placing the sample in a tungsten crucible and inductively heating it in a high vacuum using the apparatus shown in Figure 2.1. Lower temperature anneals were performed by wrapping the sample in tantalum foil, sealing it in an evacuated fused silica tube, and heating it in a resistance tube furnace. The inductive heating method provides a cleaner atmosphere for heating the samples, but the sample temperature can not be quenched so rapidly. The fused silica tubes on the other hand were generally dropped into a pan of water at the end of the heat treatment to rapidly quench the sample temperature. No major differences were observed, however, in powder patterns of samples heated by both methods.

C. Results and Discussion

The results of various heat treatment experiments and a summary of the phases observed at different compositions and temperatures is given in Table 2.1. Observed versus calculated patterns of selected phases observed during the course of this phase diagram survey have been accumulated in Appendix A.

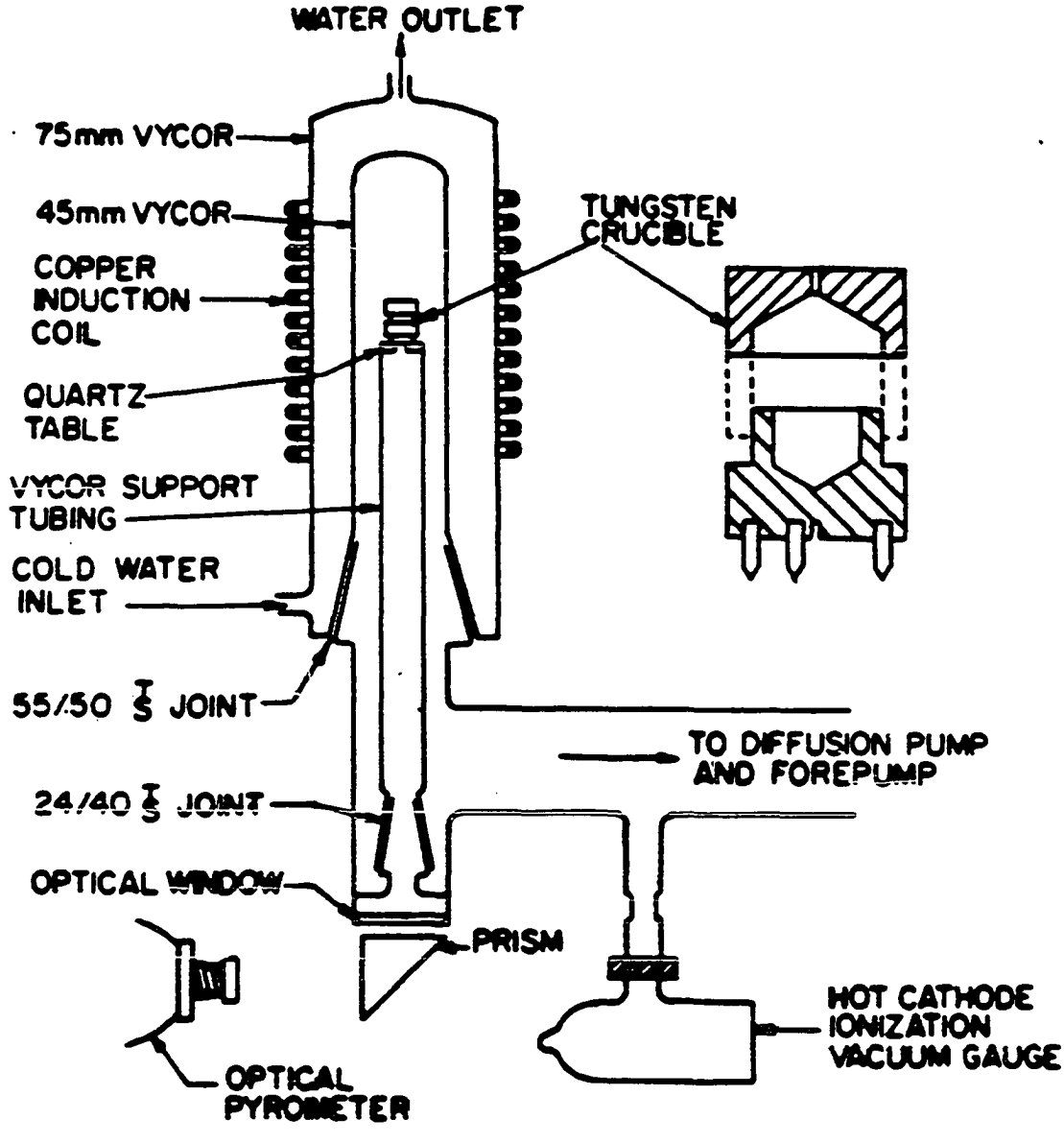

Figure 2.1. The apparatus used to anneal Zr-Al alloys at high temperature

Table 2.1. Phases observed

Phase	Lattice parameters (Å)		
$ZrAl_3$	a = 4.0074 (6)	c = 17.286 (4)	
lit	a = 4.010 (2)	c = 17.310 (8)	
$ZrAl_2$	a = 5.2792 (7)	c = 8.747 (2)	
	a = 5.2807 (5)	c = 8.749 (1)	
	a = 5.2880 (5)	c = 8.760 (1)	
lit	a = 5.2824	c = 8.7482	
Zr_2Al_3	a = 9.603 (4)	b = 13.927 (5)	c = 5.578 (2)
	a = 9.617 (3)	b = 13.934 (3)	c = 5.584 (2)
	a = 9.609 (3)	b = 13.917 (6)	c = 5.575 (3)
lit	a = 9.601	b = 13.906	c = 5.574
ZrAl	a = 3.362 (1)	b = 10.892 (3)	c = 4.274 (2)
	a = 3.362 (2)	b = 10.903 (3)	c = 4.281 (2)
lit	a = 3.353	b = 10.866	c = 4.266
Zr_4Al_3	a = 5.424 (1)	c = 5.405 (2)	
	a = 5.432 (1)	c = 5.396 (1)	
	a = 5.428 (1)	c = 5.387 (1)	
lit	a = 5.433	c = 5.390	
Zr_5Al_4	a = 8.459 (4)	c = 5.784 (4)	
	a = 8.432 (2)	c = 5.791 (2)	
lit	a = 8.447	c = 5.810	
Zr_3Al_2	a = 7.6333 (8)	c = 6.996 (2)	
	a = 7.6342 (8)	c = 6.989 (2)	
lit	a = 7.630	c = 6.998	
Zr_5Al_3	a = 11.043 (2)	c = 5.392 (1)	
lit	a = 11.049	c = 5.396	

Comments
Single phase, annealed ~1100°C. Coex with $ZrAl_2$, annealed ~1100°C
Trace $ZrAl_3$, annealed 1 wk at 1000°C. Single phase ~1200°C. Coex Zr_2Al_3, annealed at ~1200°C.
Coex $ZrAl_2$, annealed ~1200°C. Single phase ~1200°C. Coex Zr_5Al_4, 76 wt% Zr as-cast sample.
77 wt% Zr, annealed 1200°C, trace Zr_2Al_3. 81 wt% Zr, annealed 935°C, coex Zr_4Al_3.
81 wt% Zr, annealed 800°C, 2 wks, trace $Zr_5Al_3O_x$; 81 wt% Zr, annealed at 935°C, 4 days, coex ZrAl, $Zr_5Al_3O_x$; 82.2 wt% Zr, annealed 750°C, coex with Zr_3Al_2, $Zr_5Al_3O_x$.
81 wt % as-cast. 81 wt% Zr, annealed 800°C, 2 wks, 1200°C, 24 hrs coexisting with ZrAl, $Zr_5Al_3O_x$.
82.2 wt% Zr, coex with Zr_5Al_4, annealed 1150°C; 84.2 wt% Zr, coex with Zr_5Al_3, annealed 1150°C.
Coex with Zr_3Al_2, annealed 1100°C.

The more aluminum-rich compounds $ZrAl_3$, $ZrAl_2$ and Zr_2Al_3 consistently gave sharp powder patterns and samples containing these phases were fairly crystalline. In fact, single crystals of $ZrAl_3$, and $ZrAl_2$ were isolated in some of the as-cast samples after crushing. Powder patterns showing the presence of one phase only could be obtained for each of the above compounds from samples prepared either by comelting stoichiometric amounts of zirconium and aluminum or by volatilizing aluminum out of $ZrAl_3$ at high temperature. No indication of any deviations from the reported crystal structures of the above compounds was obtained from either powder diffraction or single crystal diffraction patterns. The variation of the lattice parameters with composition and coexisting phases appear to be small, indicating rather small ranges of nonstoichiometry. The cell volume of $ZrAl_2$ does appear to increase slightly with zirconium content, however, indicating a possible range of nonstoichiometry.

It was more difficult to obtain sharp powder diffraction patterns from compositions containing more zirconium than the composition Zr_2Al_3, and single phase samples were only rarely obtained. Of particular interest in clarifying the phase diagram features are the phase changes which were observed in samples of nominal composition 76, 81, and 82.5 weight percent zirconium. Samples of these compositions were examined immediately after arc-melting (as-cast) and after annealing at various temperatures. The as-cast samples were useful in establishing the compounds stable at high temperature since these samples were very rapidly

quenched from the melt to room temperature during the arc-melting process.

The observed powder pattern of an as-cast 76 wt % Zr sample, Table 2.2, showed lines from the phases Zr_2Al_3 and Zr_5Al_4. The diffraction lines were rather weak and diffuse, especially for the Zr_5Al_4 phase. Annealing this sample at 1200°C for 12 hours eliminated the Zr_5Al_4 phase completely, and resulted in the formation of nearly single phase ZrAl, with only two weak lines of Zr_2Al_3 appearing, Table 2.3.

An 81 wt % Zr sample showed several phase changes when annealed at different temperatures. The composition of this sample is close to both Zr_5Al_4 (80.8 wt % Zr) and Zr_4Al_3 (81.6 wt % Zr). The powder pattern of the as-cast sample, Table 2.4, showed nearly single phase Zr_5Al_4 (of the Ti_5Ga_4 type). The observed diffraction lines were quite weak and diffuse as is nearly always the case both for as-cast and annealed samples near this composition. Portions of this sample were subjected to repeated heat treatment experiments at temperatures of 800°C, 935°C, 1000°C, 1075°C, 1160°C and 1200°C for time periods ranging from 2 weeks at 800°C to 12 hours at 1200°C. The powder pattern of the sample annealed for 2 weeks at 800°C showed the presence of nearly single phase Zr_4Al_3, Table 2.5, with a few weak reflections that corresponded to the strongest calculated reflections of the phase $Zr_5Al_3O_x$ (Mn_5Si_3-type). The Zr_4Al_3 phase remained present in portions of the sample annealed at temperatures up to 1075°C. Portions of the sample annealed at 935°C or higher (up to 1200°C) also showed the presence of ZrAl. The Zr_5Al_4 phase began to reappear somewhere between 1000°C and 1075°C, it was not present in the

Table 2.2. Observed powder pattern - 76 wt % zirconium sample as-cast

$2\Theta_{obs}$	I_{obs}	Zr_2Al_3 hkℓ	Zr_5Al_4 hkℓ	Zr_2Al_3 I_{calc}	Zr_5Al_4 I_{calc}
19.32	VW	1,1,1		27.2	
22.35	W	2,2,0		26.6	
24.20	W		2,0,0		12.1
25.99	MW		1,1,1		47.5
26.53	W	1,3,1		46.8	
30.68	W		0,0,2		4.3
31.61	MW	2,4,0		62.0	
32.31	W		2,1,0		12.2
32.84	MW	3,1,1		62.2	
34.66	W	0,2,2		45.1	
35.94	MW		2,1,1		32.0
36.84	MS		3,0,0		90.5
37.28	S	2,0,2 1,5,1		49/9. 100.0	
37.51	S		1,1,2		100.0
37.68	S	3,3,1		43.6	
39.54	M	2,2,2		51.8	
49.58	W	1,7,1		19.8	
50.67	VW	5,1,1		7.7	
53.51	W		2,2,2		32.7
54.01	W	1,3,3		16.8	
54.91	W	2,6,2		10.4	
57.03	M	4,4,2	3,2,1	34.3	10.4
59.17	VW	6,2,0		11.5	
59.56	VW		4,0,2		10.9
59.96	VW	4,1,1			7.3
60.59	VW	1,5,3		19.7	
60.94	VVW	5,5,1		5.5	
64.32	M	6,4,0	0,0,4	10.0	9.3
66.20	VW		3,3,0		10.5
67.40	VW	6,0,2		16.6	
69.54	VW	3,9,1		11.8	
70.10	W	5,7,1		15.9	
73.92	W	7,3,1	5,1,1	8.4	14.2

Cu Kα λ = 1.5406 Å

Table 2.3. Observed powder pattern - 76 wt % zirconium sample annealed at 1200°C

$2\theta_{obs}$	ZrAl hkℓ	I_{obs}	I_{calc}	
16.18	020	M	13.5	
26.46	021	MS	43.3	
27.72	110	W	6.0	
32.86	040	M	13.7	
34.65	-	-	-	022, Zr_2Al_3
34.91	111	S	100.0	
36.37	130	S	49.3	
37.26	-	W	-	202, 151 Zr_2Al_3
39.17	041	M	44.8	
42.22	002	M	25.7	
49.87	150	W	7.4	
50.22	060	W	4.9	
54.56	151	MS	16.2	
56.96	132	MS	30.4	
61.69	221	MW	9.9	
65.11	240	W	4.7	
66.17	170	MW	8.4	
67.41	152	W	7.2	
70.15	171	MW	9.3	
71.35	202	MW	14.6	
72.52	113	MW	16.7	
72.79	081	MW	10.7	
77.26	260	VW	4.0	
80.72	242	W	6.9	
81.66	172	W	12.6	

Cu Kα λ = 1.5406 A

Table 2.4. Observed powder pattern of an 81 wt % Zr as-cast sample

$2\Theta_{obs}$	Zr_5Al_4 hkℓ	I_{obs}	I_{calc}
24.34	200	VW	12.1
26.18	111	MW	47.5
30.78	002	VW	4.3
32.38	210	W	12.2
33.22	102	W	9.8
36.01	211	M	32.0
36.89	300	MS	90.5
37.65	112	MS	100.0
53.62	222	VW	32.7
59.64	402	W	10.9
64.35	004	W	9.3

All lines observed were quite broad ($\gtrsim 0.1°$ in 2Θ and a high background was present.

Cu Kα $\lambda = 1.5406$ Å

Table 2.5. Observed powder pattern - 81 wt % Zr sample annealed at 800°C

$2\theta_{obs}$	Zr_4Al_3 hkℓ	I_{obs}	I_{calc}	
16.35	001	W	16.0	
18.80	100	MW	14.3	
25.06	101	W	14.3	
26.82	-	VW	-	111 "$Zr_5Al_3O_x$"
32.96	110	S	96.6	
33.44	-	VW		210 "$Zr_5Al_3O_x$"
34.00	-	VW		102 "$Zr_5Al_3O_x$"
37.10	111	S	53.7	
38.27	200	S	16.4	
38.45	102	S	100.0	
41.88	201	M	25.7	
51.55	202	M	18.9	
58.95	300	M	20.4	
61.70	301	MW	13.9	
62.58	212	M	27.7	
65.37	203	W	8.1	
69.17	220	MS	24.3	
71.63	221	VVW	2.4	
75.09	213	VVW	2.1	
79.14	114	W	22.4	
82.00	132	W	17.0	

powder pattern of a sample annealed at 1000°C, but a few of the stronger reflections of the Zr_5Al_4 phase were present in the sample annealed at 1075°C. The Zr_4Al_3 phase was not present at 1160° or 1200°C.

The "$Zr_5Al_3O_x$" phase was observed quite often in an 81 wt % Zr sample annealed at different temperatures. The intensities of the $Zr_5Al_3O_x$ reflections relative to the coexisting phases varied strongly with the heat treatment of the samples. Samples heated at 800°, 935°, 1000° and 1075°C showed $Zr_5Al_3O_x$ reflections which were weak relative to the other phases present (Zr_4Al_3 and ZrAl). Samples annealed at 1160° and 1200°C showed $Zr_5Al_3O_x$ reflections of intensity comparable to the coexisting phases (Zr_5Al_4, ZrAl). The $Zr_5Al_3O_x$ reflections were not observed in an 81 wt % Zr as-cast sample. Faint reflections from this phase also appeared in a 76 wt % Zr sample and an 82.5 wt % Zr sample.

The phase changes observed in the 81 wt % Zr sample and the relative intensities of the $Zr_5Al_3O_x$ lines were reversible with temperature. For example, a sample annealed at 935°C for 4 days, 1160°C for 13 hours, and 935°C for 24 hours showed a powder pattern identical to that of the same sample annealed at 935°C for 4 days. It therefore, seems unlikely that the increase in relative intensity of the "$Zr_5Al_3O_x$" diffraction lines at 1160° and 1200°C is due to sample oxidation on prolonged annealing since the lines become weaker again when the sample is reannealed at a lower temperature. The compound Zr_4Al_3 also disappeared and reappeared reversibly in the sample annealed at 935°C, then 1160°C, and then 935°C.

The formation and decomposition of the high temperature compound Zr_5Al_4 was also observed in a sample containing 82.5 wt % Zr. The as-cast sample of this composition yielded a powder pattern exhibiting lines primarily of the phases Zr_5Al_4 and Zr_3Al_2; annealing this sample at ca. 1000°C for 24 hours resulted in a mixture of Zr_4Al_3 and Zr_3Al_2. A few weak lines of the phase '$Zr_5Al_3O_x$' generally appeared in these powder patterns also. The disappearance of Zr_4Al_3 and appearance of Zr_5Al_4 at ~1000°C was thus observed with samples containing both more and less zirconium than the stoichiometric formula Zr_5Al_4, and Zr_5Al_4 was observed coexisting with neighboring phases on both sides.

The remaining phases which were observed in this survey were Zr_3Al_2, coexisting with Zr_5Al_4 in an 82 wt % Zr sample and with Zr_5Al_3 in an 84 wt % Zr sample, and Zr_5Al_3 (W_5Si_3-type) coexisting with Zr_3Al_2 in an 84 wt % Zr sample. A sample of composition 87 wt % Zr was also prepared, and attempts were made to anneal this sample at temperatures between 1250°C and 1350°C to form a mixture of Zr_5Al_3 and Zr(ss). These attempts were unsuccessful, powder patterns showing Zr_5Al_3 coexisting with the Zr(ss) were not obtained, but extremely diffuse powder patterns of Zr_2Al (Ni_2In-type) resulted apparently due to difficulty in properly quenching the samples.

D. Conclusions

The results of the previously described phase diagram experiments have in most ways duplicated the results reported by Potschke and Schubert,[20] especially as regards the existence/nonexistence of

Zr_5Al_4/Zr_4Al_3 at high temperatures. The alleged ternary phase "$Zr_5Al_3O_x$" was also observed, at least in trace amounts, over a wide composition range coexisting with several intermetallic phases (between Zr_2Al_3 and Zr_5Al_3).

To help determine the effects that impurities may have had on the phases observed in various X-ray powder patterns several chemical analyses were performed on the starting material and an 82 wt % Zr sample.

The 10 major impurities identified by a spark source mass spectrometric analysis of the zirconium and aluminum metals used in the sample preparations are as follows (concentrations in atomic ppm):

Major element Zr:	Mn	N	Ni	Cr	Si	Hf	Al	O	Fe	C
	15	20	35	70	80	100	160	700	730	1000

Major element Al:	P	C	Ni	Ti	Cu	O	Ga	Zn	Si	Fe
	5	5	10	10	12	20	32	69	100	400

The results obtained for C and O in this analysis may be high since the spark source mass spectrometric method is somewhat surface sensitive. The metallic impurities appear quite low, and hafnium in particular is present at only 100 ppm in the zirconium used. A vacuum fusion analysis of an 82 wt % Zr sample (one in which the alleged ternary phase "$Zr_5Al_3O_x$" of the Mn_5Si_5-type was observed) was also performed. The total O, C, N, H impurities added up to less than 700 ppm by weight in this sample, which should be typical of the contamination in all other samples since all were similarly prepared. An acknowledgement is made to

the Ames Laboratory analytical service groups for performing these analyses.

Using the results of the impurity analyses and the observations made in various heat treatment-X-ray diffraction experiments several conclusions can be made relative to previous reports on the Zr-Al phase diagram. The 1:1 compound ZrAl was observed in this study in samples of composition from 76 wt % Zr to 81 wt % Zr annealed at temperatures less than 1250°C. The proposal by Edshammar that this phase is a hafnium stabilized ternary appears to be unlikely since the hafnium impurity in the zirconium metal used was only 100 ppm. This phase is undoubtedly a binary, and perhaps Edshammar's annealing temperature, stated to be 850°C, was too low to equilibrate an arc-melted mixture near this composition (which consisted of Zr_2Al_3 + Zr_5Al_4 in the present study) in a reasonable time period.

The phase diagram modification proposed by Potschke and Schubert appears to be basically correct. Zr_4Al_3 is clearly absent in powder photographs of samples annealed above about 1075°C, and a Ti_5Ga_4-type phase is present in samples cooled from above this temperature. The powder patterns of samples of 76-83 wt % Zr (~50-60 atomic % Zr) always show an apparent Ti_5Ga_4-type phase, Zr_5Al_4, when cooled from high ($\gtrsim$1200°C) temperature. The powder patterns are invariably diffuse, probably because of difficulty in quenching these samples quickly enough.

The major remaining uncertainty in the zirconium-aluminum diagram is the identity of the Mn_5Si_3-type phase. In the course of this series of

experiments, an apparent Mn_5Si_3-type phase appeared quite strongly with an 81 wt % Zr (55 atomic %) heated to 1200°C and quenched in H_2O. The appearance of this phase accompanied the appearance of the Ti_5Ga_4-type phase, Zr_5Al_4, and the disappearance of the Zr_4Al_3 phase on heating. In view of the low content of nonmetallic impurities found in the vacuum fusion analysis (≲700 ppm), it is unlikely that this phase is a ternary, such as "$Zr_5Al_3O_x$". In this context, it is interesting to note that there is a close relationship between the Mn_5Si_3-type structure and the Ti_5Ga_4 structure. In fact, if the octahedral voids that Edshammar and Nowotny have postulated are partially filled with oxygen were to be completely filled by aluminum, a Ti_5Ga_4 phase results. This suggests the possibility of Zr_5Al_4 ordering on cooling in a manner which would result in what appears to be a Mn_5Si_3-type diffraction pattern. The powder patterns obtained from the heat treatment-quenching experiments performed in this survey are not very sharp and the fact that several phases appear simultaneously makes it difficult to unambiguously index the films. Still, the simultaneous appearance of two hexagonal phases, one a Ti_5Ga_4-type and the other a Mn_5Si_3-type, occurred reproducibly in different experiments. This would be an interesting problem for future experimental work, which may include high temperature X-ray diffraction experiments of samples of nominal composition Zr_5Al_4 over the temperature range 900-1400°C. In view of the fact that the Mn_5Si_3-type phase is possibly stabilized by interstitial impurities, extreme care would have to be taken in such experiments to avoid sample contamination.

III. VAPORIZATION STUDY

A. Knudsen Effusion Method

The technique used to investigate the thermodynamic properties of the zirconium-aluminum system is a variation of the Knudsen effusion method, named after M. Knudsen[24] who originally discussed the basic principles behind the method. The Knudsen effusion method has its roots in simple kinetic gas theory. It is assumed that the distribution of molecular speeds in a low pressure gas follows a Maxwell-Boltzmann type of distribution

$$\frac{dN(c)}{No} = 4\pi \left(\frac{M}{2\pi RT} \right)^{3/2} c^2 \exp\left(Mc^2/RT\right) \qquad (1)$$

where $\frac{dN(c)}{No}$ is the fraction of molecules having speed c, N is the molecular weight, T the absolute temperature, and R the gas constant. The average molecular speed for a gas obeying the above distribution law is

$$\bar{c} = (8RT/\pi n)^{1/2} = (8kT/\pi m)^{1/2} \qquad (2)$$

and the rate of the molecules colliding on a unit area of the container wall per unit time is

$$Zo = \frac{z}{At} = \frac{n}{V}\frac{\bar{c}}{4} \qquad (3)$$

where N/V is the number of molecules per unit volume. For an ideal gas

$$P = \frac{N}{V} kT = \frac{n}{V} RT \qquad (4)$$

where n is the number of moles, k the Boltzmann constant. Combining

equations (2), (3), and (4) yields

$$P = 4Zo\ kT\ (\pi m/8kT)^{1/2} = \frac{Z}{A}\ (2\pi kTm)^{1/2} \qquad (5)$$

which is the Knudsen equation. In terms of the weight of molecules colliding per unit time it can be written as

$$P = \frac{W}{At}\ \sqrt{\left(\frac{2\pi RT}{M}\right)}\ . \qquad (6)$$

Equation (5) relates the partial pressure of a gas species to the rate at which collisions take place with a unit area of the container wall. Experimental Knudsen effusion techniques are based on the assumption that a small cross-sectional area of the wall can be removed and equation (6) will then give the rate at which mass is lost due to effusion through this orifice. This assumption is strictly valid only for infinitely thin walls, in real orifices a correction known as a clausing factor is often applied to compensate for finite wall thickness. With careful machining, however, of the cell orifice the clausing factor becomes very nearly unity. In order to obtain meaningful thermodynamic data, it is also important that the saturation pressure of the gas species be maintained inside the container.

There are several variations of Knudsen effusion method depending mainly on the technique used to identify and quantify the species effusing through the orifice of the Knudsen cell.[25,26] The most straightforward way is simply to place a weighed sample into the cell, heat it at constant temperature for a measured time period, and weigh it again. Other common techniques are to condense a known fraction of the effusate

on a cold target placed coaxially with the cell orifice and to determine the amount of condensate by chemical or radiochemical analysis. Another common technique is to use a mass spectrometer to study the vapor effusing from the cell. This last method provides a means of identifying all vapor species effusing from the cell, and relative ratios of one to another, but poses experimental problems in the calibration of the mass-spectrometer to determine absolute partial pressures.

It is worth discussing the principles of a Knudsen cell mass-spectrometer in slightly more detail. The measured quantity in a mass spectrometric experiment is an ion current at a given mass setting I_i^+. This current is related to the molecular flux z and the time spent in the ionization chamber via

$$I_i^+ \propto Zt \propto \frac{z}{v} \qquad v = \text{molecular velocity.}$$

From the Maxwell-Boltzmann distribution the molecular velocity v is exactly $\bar{c}$ of equation (2) which is proportional to the square root of the temperature

$$v \propto T^{1/2}.$$

The Knudsen equation also implies that

$$P_i \propto T^{1/2} z$$

combining gives

$$I_i^+ \propto \frac{P_i}{T} \quad \text{or} \quad P_i = kI_i^+T .$$

The instrumental constant k incorporates several other factors including the ionization cross-section σ, a transmission factor τ, a mass-spectrometer electron multiplier response function s, and various instrumental and geometric factors that are constant for different masses.

$$k = \frac{G\ (\text{Inst factors-Geom})}{\sigma\ s\ \tau} \quad .$$

The problem of calibration of the mass-spectrometer is essentially that of determination of the proportionality constant k.

This brings us to the exact experimental method used in the study of the zirconium-aluminum system. A simple but effective way of calibrating the mass-spectrometer would be provided if a means of monitoring the total weight of the sample at a given time could be coupled to simultaneous mass-spectrometer measurements. Then since

$$P_i = \frac{W_i}{At} \sqrt{\left(\frac{2\pi RT}{M_i}\right)} = kI_i^+T$$

the pressure obtained from the weight loss data could be used to calibrate the mass-spectrometer constant k. An apparatus possessing these capabilities will now be described.

B. Description of Experimental Apparatus

The apparatus used in this study of the vaporization properties in the zirconium-aluminum system is illustrated schematically in Figures 3.1, 3.2. A stainless steel high vacuum system houses the various components shown. Access to the system is obtained by breaking vacuum and

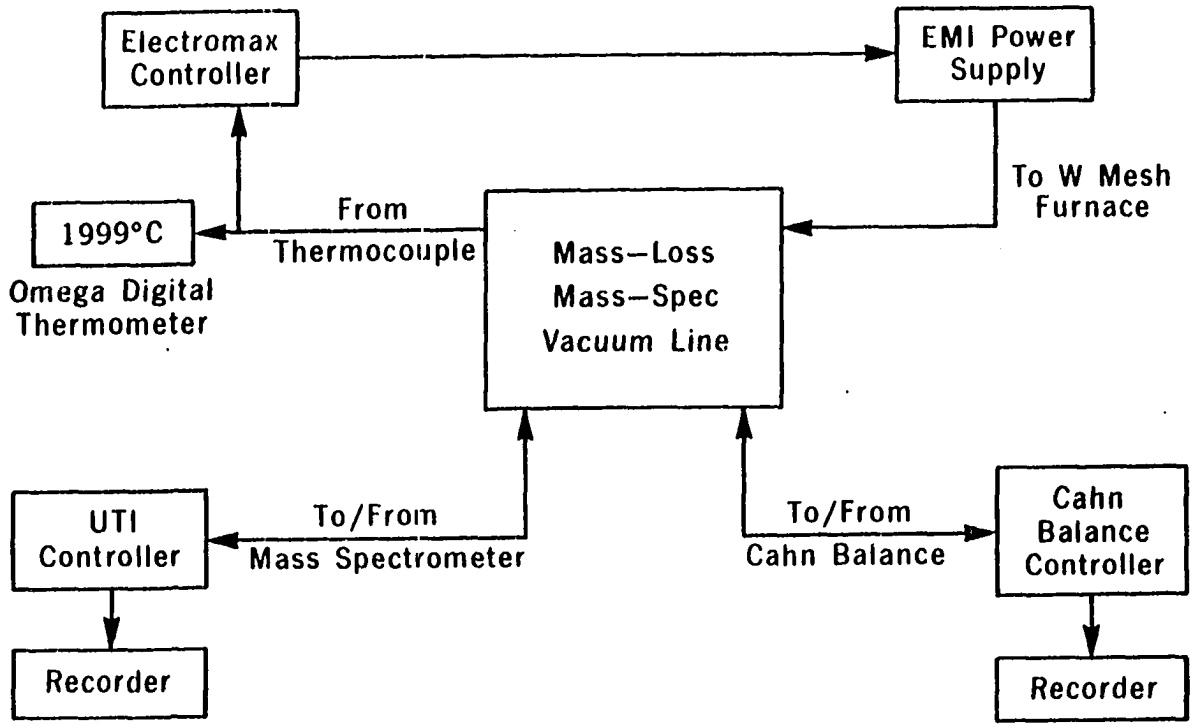

Figure 3.1. The mass-loss-mass-spectrometer apparatus block diagram

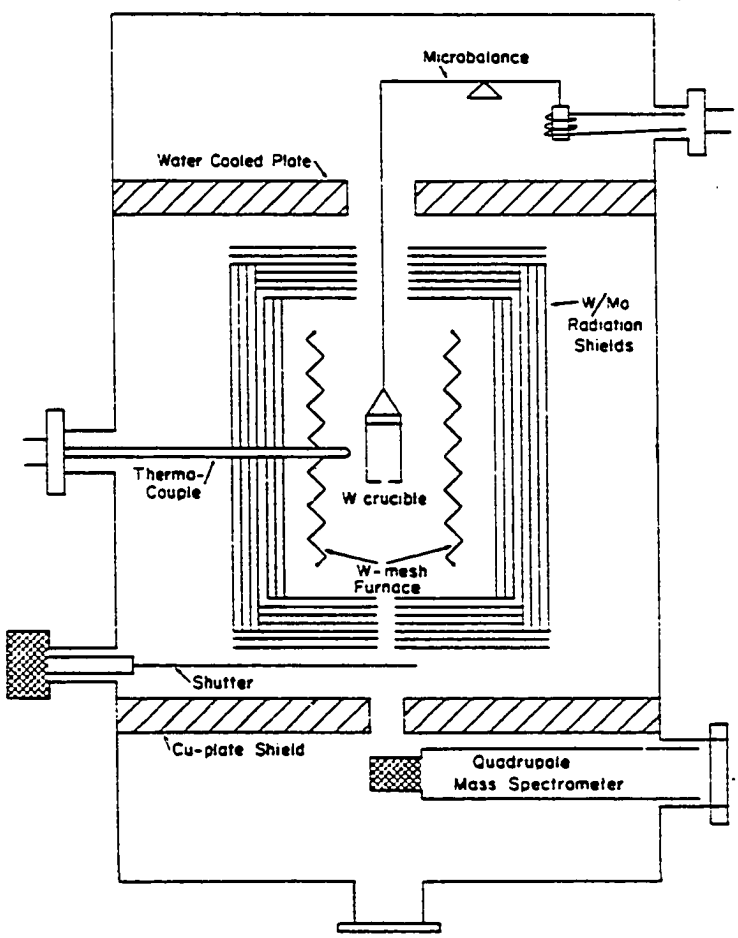

Figure 3.2. The major components inside the mass-loss-mass-spectrometer vacuum system

raising or lowering a glass bell jar which rests on top of the main stainless steel assembly. The system is pumped by a liquid nitrogen trapped Varian 4" diffusion pump and mechanical forepump, and after thorough outgassing the residual pressure in the vacuum system reaches about $5x10^{-8}$ torr. The major components inside the vacuum system are a Cahn RH recording microbalance, a UTI 1-400 amu quadrupole mass-spectrometer, a Sylvania tungsten mesh heating element, a shutter, and a tantalum sheathed W5% Re vs W26% Re thermocouple which is inserted through an O-ring sealed feed-through from outside the vacuum system. A sample is placed into a tungsten Knudsen cell with a knife edge orifice on the bottom and is suspended between the tungsten mesh heating elements from the arm of the Cahn balance. The effusing vapor is directed towards the quadrupole mass-spectrometer. The tip of the W5% Re vs W26% Re thermocouple is a few millimeters from the effusion cell, and the output of this thermocouple provides a signal which is used to control the cell temperature and also provides a close measure of the cell temperature since the tungsten mesh furnace creates a large uniform temperature zone. The output of the recording balance is routed to a strip chart recorder having a sensitivity of 1 mV full scale. The balance is usually operated on a range which gives a 1 mV change in the output signal for a 1 mg change in the sample weight, so that weight loss can be continually monitored with a sensitivity of at least ±0.1 mg. The signal from the mass-spectrometer is similarly routed to a chart recorder and/or an oscilloscope after having been amplified by a high speed picoammeter. It is thus possible to make simultaneous measurements of mass-loss and mass-

spectra, and to calibrate the mass-spectrometer ion intensities against partial pressures calculated from the balance data. The material effusing from the Knudsen cell towards the mass-spectrometer can be blocked by a mechanical shutter to permit readings of the background gas level, thus improving sensitivity.

The major components of the mass-loss-mass-spectrometer system exterior to the vacuum system are a Leeds & Northrup Electromax temperature controller, an EMI 10 Kw DC power supply (for the tungsten mesh furnace), an Omega digital thermometer which displays the furnace temperature, and the associated electronic units for the Cahn balance and mass-spectrometer. The Electromax controller monitors the output of the W5% Re-W26%Re thermocouple and sends a signal to the EMI power supply which regulates the power applied to the tungsten mesh elements. The controller provides excellent long term temperature stability and reproducible temperature setpoints, the temperature of the furnace and Knudsen cell can be held to ±2°C for several days without readjustment.

The mass-loss-mass-spectrometric technique is particularly well-suited to the study of incongruent vaporization processes, and has been successfully applied to several such investigations.[27-29] The ability of the mass-spectrometer to make measurements relatively quickly, and the rapid response and excellent stability of the temperature control system (≲3 minutes to stabilize temperature after a setpoint change) are tremendous assets in the study of incongruent vaporization where problems due to slow diffusion and surface depletion in the solid sample often arise. With the mass-spectrometer measurements at comparatively high

temperatures can be made quickly and the temperature can then be lowered to anneal the sample and restore the volatile component to the sample surface before proceeding with vapor pressure measurements. Weight loss vs mass-spectrometer calibration data can also often be collected during these annealing periods at lower temperature where kinetic problems are less pronounced. The long term temperature stability provided by this apparatus is also vital in the study of samples which require extensive in situ annealing, and in the measurement of extremely low vapor pressures where the sample loses weight slowly. Such experiments would be difficult, if not impossible, to perform with other experimental variations of the Knudsen effusion technique.

C. Treatment of Vaporization Data

The raw data collected in a mass-loss-mass-spectrometric experiment are the sample rate of weight loss (mg/min), the temperature, and the mass-spectrometer ion intensities. In the case of the present study, the only vapor species of importance is atomic aluminum at 27 amu, so the treatment of the data is simplified. However, it is useful to know the criteria for making useful measurements.

In order to make meaningful vapor pressure measurements, the variables upon which these pressures depend should be known and/or controlled. For a two component system, the important variables are the composition of the sample being studied and the temperature. If a single solid phase coexists with a vapor phase, $p = 2$, and the phase rule implies $f = c - p + 2 = 2 - 2 + 2 = 2$, i.e., there are two degrees of

freedom and the vapor pressures of the components are not uniquely defined by fixing the temperature of the sample. On the other hand, partial pressures over a three phase (two solids and the vapor) sample are dependent solely on temperature since f = 1 in this case. The experimental observables related to the partial pressures of the various gas species in equilibrium with the solid sample, i.e., the rate of weight loss and mass-spectrometer ion intensities, are then also fixed by fixing the temperature and will remain constant so long as the two solid phases coexist. Experimentally, it is usually easiest to work with an univariant system.

The vaporization processes in the zirconium-aluminum system are incongruent, i.e., aluminum is preferentially lost from the solid until no aluminum remains. By measuring rates of weight loss and aluminum mass spectrometric ion intensities over compositions at which two solid phases coexist, thermodynamic data for the various intermetallic phases can be established. The first step is conversion of the raw data to equilibrium partial pressures. The rate at which the sample loses weight is established by examining chart recordings of weight loss vs time, for an univariant process these are linear. Partial pressures of aluminum can be calculated directly from the weight loss data using the Knudsen equations in the form

$$P = \frac{3.76 \times 10^{-7}}{A} \quad R \quad \sqrt{(T/M)}$$

where P = pressure (atmospheres), A = area of the effusion cell orifice (cm^2), T = absolute temperature, R = observed rate of weight loss

(mg/min), M = molecular weight of effusing species = 26.9815, and the numerical factor 3.76×10^{-7} is a product of several constants necessary to provide dimensional consistency. The pressures thus calculated from the balance data are used in the relation

$$P_{balance} = kI_{27}^{+}T$$

with aluminum ion intensities I_{27}^{+} measured simultaneously with the weight loss data and the proportionality constant k evaluated. This constant k can then be used to convert mass-spectrometer measurements for which no simultaneous weight loss data were obtained into partial pressures. Because mass-spectrometer measurements can be obtained much more quickly than weight loss data there are generally very many mass-spectrometer measurements for which simultaneous weight loss data are not available. The conversion of the mass-spectrometer measurements to partial pressures by calibration against the balance data reduces the statistical error in subsequently derived quantities by providing many more partial pressure data points.

Derivation of thermodynamic values from the temperature vs partial pressure data invariably centers around first using the partial pressure data to calculate an equilibrium constant (K) for some vaporization reaction. Two methods of treating the data are then commonly used.[30] The first, referred to as the second law method, starts with the relation

$$\Delta G^{\circ} = -RT \ln K = \Delta H_T^{\circ} - T\Delta S_T^{\circ} .$$

The standard enthalpy change ΔH_T° and entropy change ΔS_T° can be

evaluated by plotting or least squares fitting of observed ln K values vs 1/T. ΔH_T° and ΔS_T° follow from the slope and intercept, respectively, of the straight line obtained. The temperature assigned to these ΔH_T°, ΔS_T° values is generally the median temperature over which data were collected. The enthalpy change at some reference temperature, i.e., ΔH_{298}°, can then be calculated from the relation

$$\Delta H_T^\circ = \Delta H_{298}^\circ + \int_{298}^{T} \Delta C_p \, dT \, .$$

Second law heats at 298 K can also be evaluated from the slope of a plot of ($R \ln K + \Delta fef_T$) vs 1/T, referred to as a $\underline{\Sigma'}$ plot.[31]

Another method, referred to as the third law method, uses the relation

$$\Delta fef_T = \frac{\Delta G_T^\circ - \Delta H_{298}^\circ}{T} = \frac{-RT \ln K - \Delta H_{298}^\circ}{T} \, .$$

Calculated or estimated free energy function changes for the vaporization reaction being considered are evaluated at each experimental temperature point, and from these and the observed ln K values a value for ΔH_{298}° is computed. One ΔH_{298}° value is obtained for each experimental temperature vs ln K data point and these are then averaged.

In the current study, seven different vaporization processes were examined by measuring aluminum partial pressures over samples in which two zirconium-aluminum intermediate compounds coexist. The processes are as follows:

1. $ZrAl_3(s) \rightarrow ZrAl_2(s) + Al(g)$
2. $2ZrAl_2(s) \rightarrow Zr_2Al_3(s) + Al(g)$
3. $Zr_2Al_3(s) \rightarrow 2ZrAl(s) + Al(g)$
4. $^5/_7Zr_2Al_3(s) \rightarrow {}^2/_7Zr_5Al_4(s) + Al(g)$
5. $^3/_2Zr_5Al_4(s) \rightarrow {}^5/_2Zr_3Al_2(s) + Al(g)$
6. $5Zr_3Al_2(s) \rightarrow 3Zr_5Al_3(s) + Al(g)$
7. $^1/_3Zr_5Al_3(s)$ $^5/3Zr(ss) + Al(g)$.

The equilibrium constant for all the above reactions is $K = P_{Al}$. Second law enthalpy and entropy changes at the median temperatures can be evaluated from the slopes and intercepts of plots of ln K vs 1/T (second law plots). The calculation of second and third law standard enthalpy changes (ΔH°_{298}) involves an estimation of heat capacity and free energy function changes for the above processes.

Heat capacities of intermetallic phases are generally lacking and therefore estimates of C_p values are required. These values are usually estimated using the so called Neumann-Kopp rule.[32] According to this procedure the change in heat capacity ΔC_p for an all solid reaction such as

$$x\ Zr(s) + y\ Al(s) = Zr_xAl_y(s)$$

is $\Delta C_p = 0$. This implies that the heat capacity of a solid compound is the sum of the heat capacities of the constituent elements. Since free energy function changes for an all solid reaction are related to the heat capacity changes via

$$\Delta fef_T = \frac{1}{T} \int_o^T \Delta C_p(T')dT' - \int_o^T \frac{\Delta C_p(T')}{T'} dT'$$

these are also identically zero. Subject to this assumption the free energy function changes for reactions 1 through 7 above are the same as for the vaporization of pure aluminum at the same temperature. Data for elemental Al necessary to perform second and third law calculations for reactions 1-7 were taken from the compilation of Hultgren et al.[33]

D. Experiments Performed with Aluminum-Rich Compositions

The experimental approach used in the various vaporization experiments performed on zirconium-aluminum samples varied somewhat with the composition of the sample being studied, but can roughly be separated into experiments performed with zirconium-rich or aluminum-rich compositions. Aluminum-rich compositions were studied with the apparatus as previously described and will be discussed in this section, while zirconium-rich compositions were examined after making some modifications to the experimental apparatus and will be discussed later. The term 'aluminum-rich' will be rather loosely used to describe compositions between 53 and 82 wt % zirconium, or the approximate stoichiometries $ZrAl_3$ to Zr_5Al_4. Eight different experiments (MLMS-1 through MLMS-8) were performed using samples in this composition range. The various experiments are compared in Table 3.1, where "processes examined" refers to the vaporization reactions 1-7 described in the previous section. Experiments MLMS-1 through MLMS-4 were preliminary experiments of 1 to 2 days duration designed to check the feasibility of measuring aluminum partial pressures over this composition range and to establish temperature ranges over which measurements could be made. Experiments MLMS-5

Table 3.1. Experiments performed with aluminum-rich compositions

Experiment	Phase present at start	Phase present at end	Cell orifice areas (cm^2)	Reaction[a]
MLMS 1	$ZrAl_3$+$ZrAl_2$	Zr_5Al_4	$2.03x10^{-2}$	-[b]
MLMS 2	$ZrAl_3$+$ZrAl_2$	melted	$2.03x10^{-2}$	-[b]
MLMS 3	$ZrAl_3$	Zr_2Al_3+Zr_5Al_4	$2.03x10^{-2}$	-[b]
MLMS 4	$ZrAl_3$	Zr_2Al_3+Zr_5Al_4	$6.76x10^{-3}$	2,3
MLMS 5	$ZrAl_3$+$ZrAl_2$	Zr_5Al_4	$6.76x10^{-3}$	1,2,3,4
MLMS 6	Zr_2Al_3+ZrAl	Zr_5Al_4+Zr_3Al_2	$2.43x10^{-2}$	3,4
MLMS 7		aborted	$6.76x10^{-3}$	
MLMS 8	$ZrAl_3$	Zr_2Al_3	$6.76x10^{-3}$	1,2

[a]Processes examined refers to decomposition reactions listed in Section III.C.

[b]Experiments performed isothermally, no temperature dependent data.

through MLMS-8 were longer duration, 1 to 3 week experiments performed using larger quantities of sample than the first four and most of the useful data obtained were from these later experiments.

The experimental procedure used was essentially as follows. Samples were prepared by arc-melting elemental zirconium and aluminum, and the phases present in the prepared samples were established by examining X-ray powder diffraction photographs. The sample to be studied in the vaporization experiment was placed in semi-toroidal tantalum liners inside a tungsten Knudsen cell. The tantalum liners, sample, and various parts of the Knudsen cell were carefully weighed on a separate Mettler analytical balance before being placed in the Knudsen effusion apparatus. The vacuum system was then evacuated and the temperature of the sample

slowly raised to approximately 100°C below the point where the sample began to lose weight at an appreciable rate. The temperature was then held at this point for 12 to 24 hours to anneal the sample before beginning any measurements. By the end of the annealing period, the residual pressure in the vacuum system also reached a stable level, facilitating mass-spectrometer measurements. The temperature of the Knudsen cell was then raised by raising the power setting to the furnace assembly and measurements of mass-spectrometer ion intensities and rate of weight loss could commence. The only vapor species effusing from the Knudsen cell that could be detected by the mass-spectrometer were elemental aluminum at 27 amu and Al_2O at 70 amu, both of which gave signals above the background level as established with a shutter blocking the vapor stream. The Al_2O signal was generally 100 to 1000 times lower than the Al signal. All mass-spectrometer ion intensities recorded were obtained by subtracting readings taken with the shutter blocking the effusing vapor from the Knudsen cell from those obtained with the shutter open. At the end of the experiment, the sample and parts of the Knudsen cell were again weighed on a separate balance to check the weight loss as recorded by the Cahn balance during the experiment and to verify that no reaction had taken place with the crucible. Residues were also examined by X-ray powder diffraction to verify that no side reactions had taken place during the experiment.

The preliminary experiments MLMS-1 through MLMS-4, in addition to establishing working temperature ranges for subsequent experiments, also pointed to the existence of a potential diffusion controlled vaporization

process. All of these experiments were begun by loading a sample of composition close to $ZrAl_3$, heating the effusion cell to a temperature which gave a fairly high rate of weight loss (~1 mg in 30 mins), and then holding the temperature constant at this point. It was hoped that by following a procedure of this sort that single phase compositions and boundaries for the intermediate compounds could be established, and that a series of such experiments performed at different temperatures would yield accurate phase boundary as well as thermodynamic data. It was found, however, that, if the temperature was held constant for a long period of time at a relatively high value that the observed ion intensities at 27 amu and rate of sample weight loss fell continually with time, even when the composition of the sample was such that two solid phases should coexist. This problem was especially pronounced when the composition of the sample approached the composition of one of the intermetallic compounds. The mass-spectrometer ion currents often began to drop as expected near single phase compositions ($ZrAl_2$ or Zr_2Al_3) but did not seem to become constant (independent of time) again at compositions expected to give constant values. It was observed, however, that if the sample in the Knudsen cell was held at a temperature low enough to give a relatively small rate of weight loss and measurements at higher temperatures were made as quickly as possible using the mass spectrometer that reproducible results were obtained in measurement over a two-phase sample. Similar experimental problems were being encountered by another worker[28,29] at the Ames Laboratory studying the Nb-Al system at about the same time, the effect was even more pronounced in the Nb-Al

experiments where the working temperature range and aluminum partial pressures were considerably higher. It was concluded that the diffusion processes in these systems are relatively slow, and that at a sufficiently high temperature the rate at which aluminum vaporizes from the surface of the material is faster than the rate at which diffusion restores it, so that the observed partial pressures are limited by the slower diffusion process. However, if the sample temperatures were lowered so that the rate of aluminum loss was relatively slow (~1 mg in 4 to 12 hrs) then the diffusion rate apparently overtakes the vaporization rate and the surface composition of the sample can be equilibrated with the bulk. These conclusions led to the adoption of the experimental approach used in the remaining experiments. All high temperature measurements of aluminum ion currents and weight loss rates were obtained as quickly as possible and the sample temperature was then lowered for in situ annealing. Fortunately, the tungsten mesh furnace and Electromax controller permit fairly quick temperature changes and after changing the setpoint the cell temperature stabilizes in 1-3 minutes.

With regard to absence of technical problems and the total amount of data collected experiment MLMS-5 was the most successful experiment performed over the composition range ~$ZrAl_3$ to ~Zr_5Al_4. In order to accommodate the total sample mass used (199 mg), 3 semi-toroidal tantalum liners were stacked one on top of another inside the effusion cell. The sample was then heated to temperatures sufficiently high to volatalize aluminum and mass-loss and mass-spectrometer data were recorded. The temperature was periodically cycled through the entire temperature range

over which mass-spectrometer measurements could be taken and then held constant again to volatilize aluminum, record weight loss data, and/or anneal the sample. During the temperature cycling process, the temperature was generally changed in increments of 25°C and held at each temperature until the observed aluminum ion currents became constant, which usually took 3 minutes or less. This experiment lasted two weeks. The sample temperature was lowered and the sample annealed overnight and measurements were taken during the day. Sufficient data were collected to enable the construction of the mass-spectrometer calibration curve of Figure 3.3. The value of $k = P/I^{+}_{27}T$ obtained was $k = 0.85 \pm 0.07$. Aluminum ion current vs total weight loss data were also accumulated at various temperatures as a by-product of the temperature cycling procedure described above, and the data at T = 1674, 1646, 1591, 1564, 1538, and 1511 K were used to construct the isotherms shown in Figure 3.4. From these isotherms it is obvious that three univariant regions were examined during the course of this experiment. These were the ranges of coexistence of $ZrAl_3 + ZrAl_2$, $ZrAl_2 + Zr_2Al_3$, and $Zr_2Al_3 + Zr_5Al_4$, respectively. From the partial pressure vs temperature data collected over these regions, second law plots were constructed for the processes 1) to 3)

1) $ZrAl_3 \rightarrow ZrAl_2 + Al(g)$

2) $2ZrAl_2 \rightarrow Zr_2Al_3 + Al(g)$

3) $^{5}/_{7}Zr_2Al_3 \rightarrow {}^{2}/_{7}Zr_5Al_4 + Al(g)$.

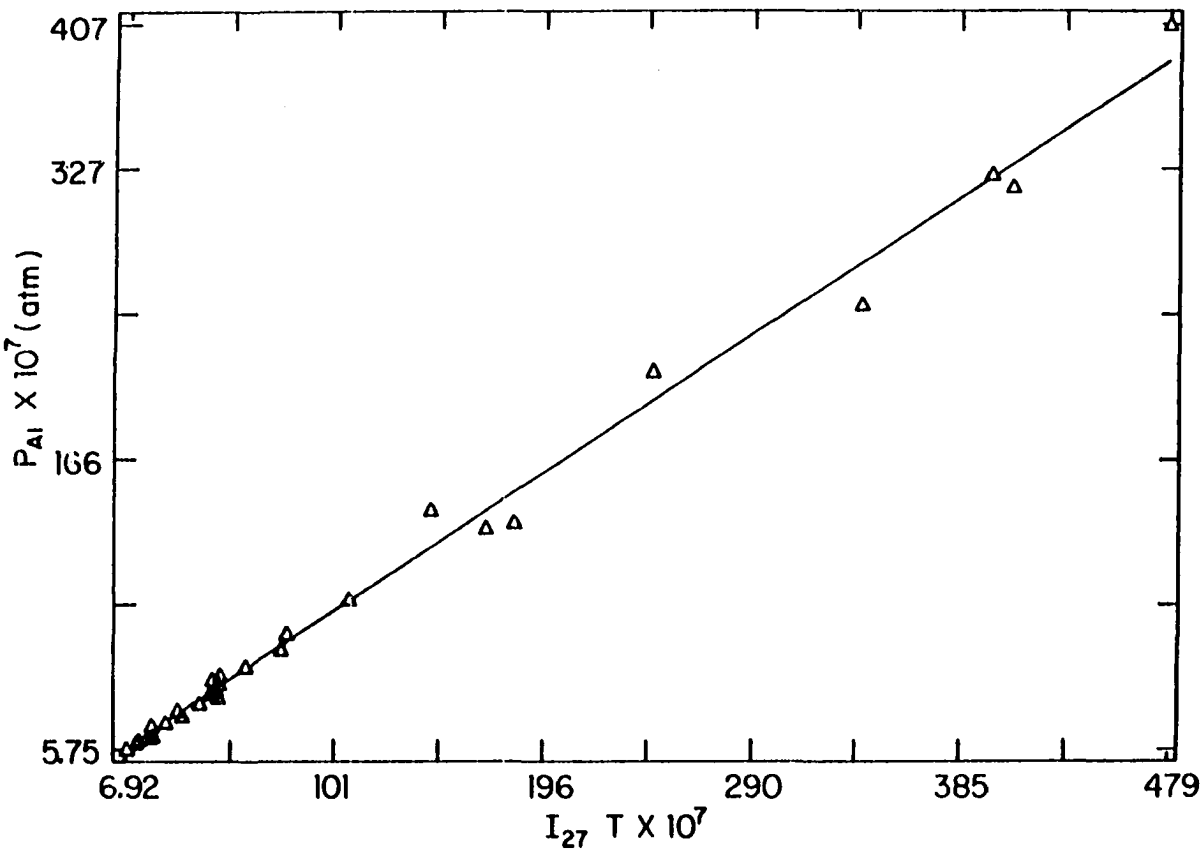

Figure 3.3. Mass-spectrometer calibration curve, experiment MLMS-5

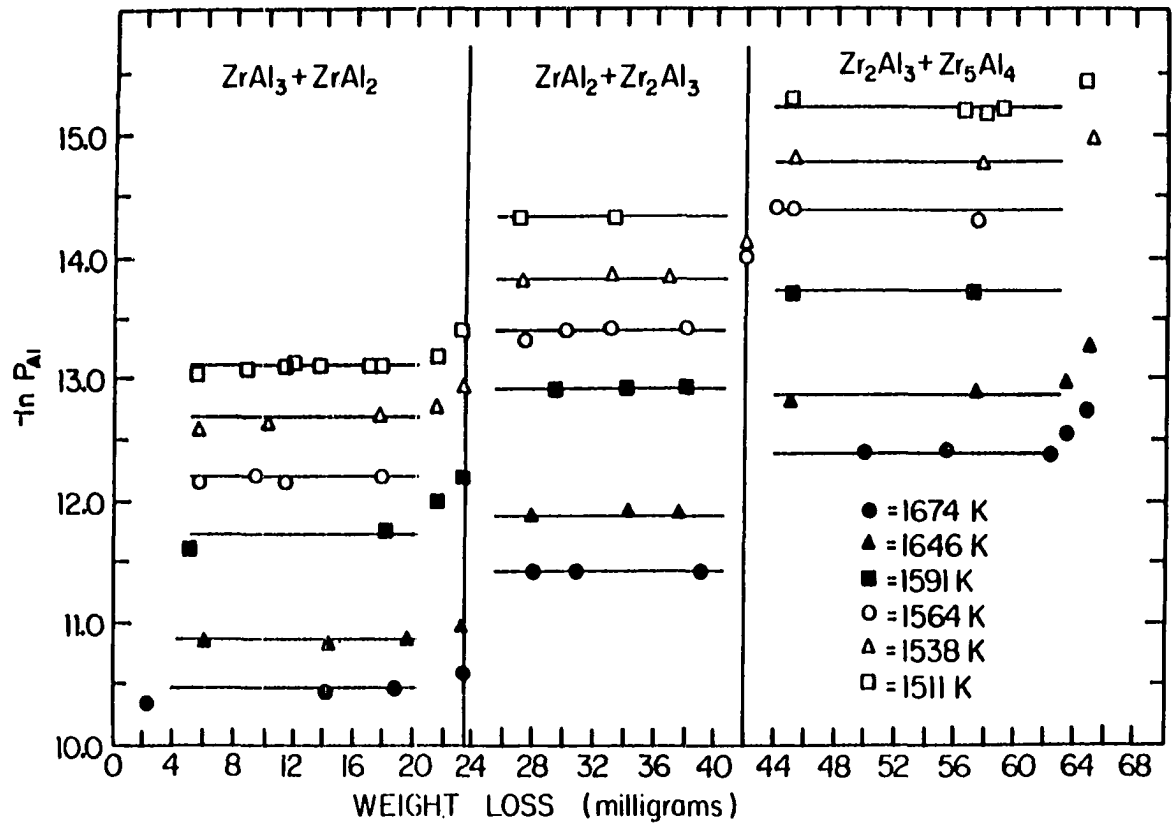

Figure 3.4. Isotherms, experiment MLMS-5

Some data at lower temperature ($\lesssim$1250°C) were also collected over the two phase Zr_2Al_3 + ZrAl region, relating to the reaction

4) $Zr_2Al_3 \rightarrow 2ZrAl + Al(g)$.

The second law plots obtained are shown in Figure 3.5. A second law plot for reaction 4) was not constructed because measurements could be made over a temperature of only 60 K, however, these data points appeared to fall on the same line as those for reaction 3). If it were not for independent X-ray evidence pointing to the formation/decomposition of ZrAl at ~1250°C it would not be possible to distinguish between reactions 3) and 4).

The remaining experiments MLMS-6 through MLMS-8 primarily checked for reproducibility of results obtained with samples of different starting composition and effusion cells of different orifice areas. In MLMS-6, an attempt was made to make measurements at compositions more zirconium-rich than Zr_5Al_4. Technical problems complicated these experiments. MLMS-6 was interrupted because of a malfunctioning thermocouple and MLMS-7 was aborted before any useful data were obtained because of a vacuum leak in the effusion apparatus. MLMS-8 was deliberately interrupted twice to remove part of the sample for X-ray diffraction analysis and thereby confirm which intermediate phases were participating in the vaporization processes. Because of these interruptions, data for construction of isotherms analagous to Figure 3.4 were not obtained. Sufficient temperature dependent data were obtained over two phase samples to permit second and third law treatments for the relevant decomposition reactions to be performed. The results were quite similar to those of

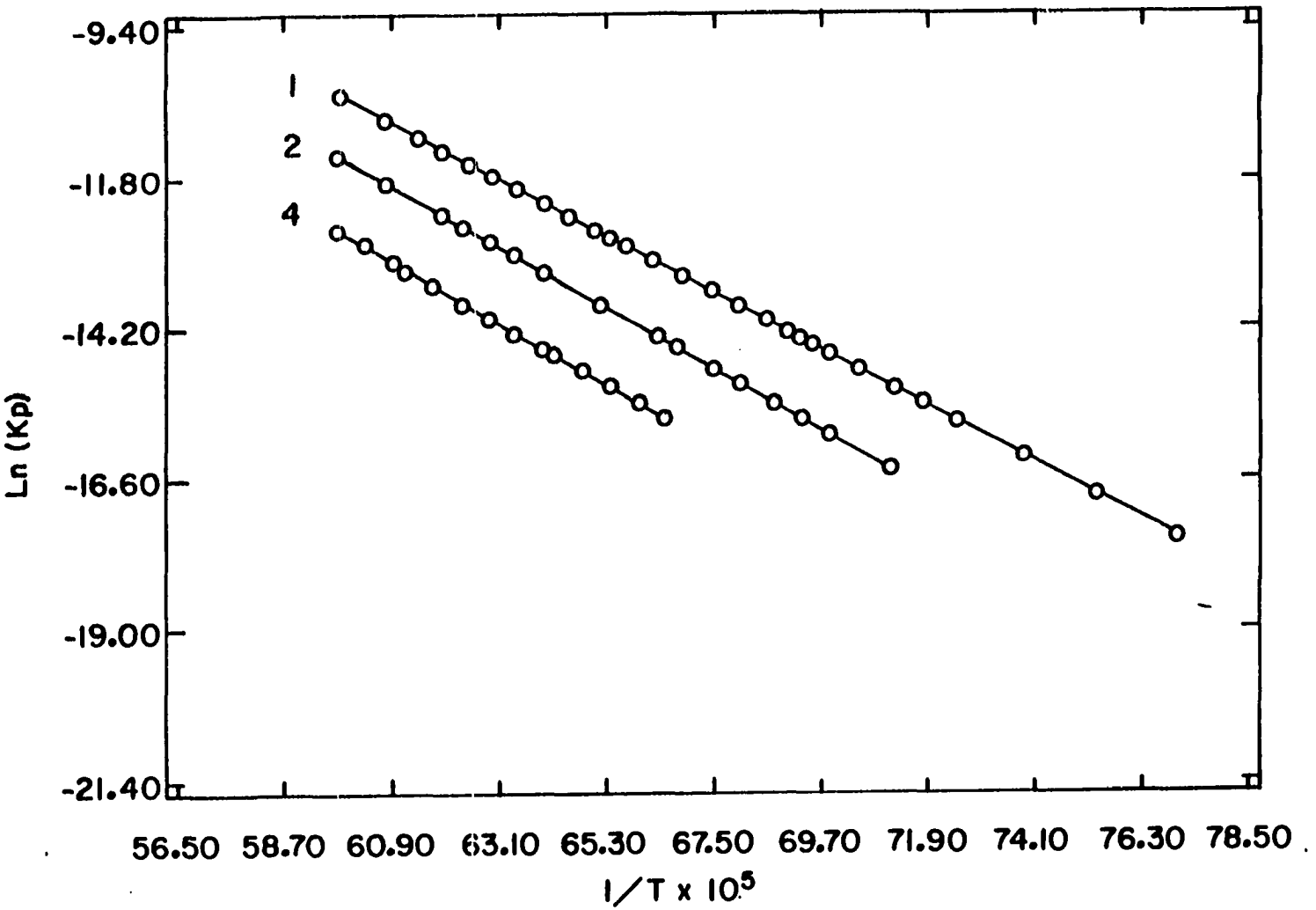

Figure 3.5. Second law plots, experiment MLMS-5. Numbers refer to reactions listed in text

MLMS-5. Probably the most useful information obtained from experiments MLMS-6 and MLMS-8 was in the X-ray powder diffraction patterns of the residues. The residue of experiment MLMS-6 gave a powder pattern which exhibited lines of Zr_5Al_4 and Zr_3Al_2 (Table 3.2) and essentially confirmed that the high temperature compound Zr_5Al_4 was participating in the vaporization processes. The residue of MLMS-5 also showed nearly single phase Zr_5Al_4, although the observed pattern was quite diffuse. It is interesting to note that Zr_5Al_4 can be prepared by arc-melting zirconium and aluminum in a 5/4 ratio (Chapter 2) or by volatilizing aluminum from a more aluminum-rich composition as was done in vaporization experiments MLMS-4,5,6. It again appears that Potschke and Schubert's conclusions on the decomposition of Zr_4Al_3 and the formation of Zr_5Al_4 at or around 1000°C are correct.

The results of second and third law treatments of the experimental data obtained in experiments MLMS-1 through MLMS-8 are given in Table 3.3. Actual tables of experimental aluminum vapor pressure vs temperature data collected over the various two-phase ranges are accumulated in Appendix B.

Table 3.2. Observed powder pattern - residue of experiment MLMS-6

$2\theta_{obs}$	I_{obs}	Zr_5Al_4 hkℓ	Zr_3Al_2 hkℓ	Zr_5Al_4 I_{calc}	Zr_3Al_2 I_{calc}
12.01	W	100		5.5	
16.38	VW		110		6.1
20.99	W	110		3.6	
24.29	M	200		12.1	
26.05	S	111	210	47.5	33.9
30.39	M		112		35.8
30.78	W	002		4.3	
32.36	M	210		12.2	
33.18	S	102	220	9.8	38.1
34.75	S		202		100.0
35.92	M	211		32.0	
36.75	VS	300	212	90.5	98.3
37.60	VS	112		100.0	
39.43	M		131		15.6
40.38	VW		103		3.5
42.22	VW		222		0.5
42.72	VW	220		1.4	
45.63	W	221	312		4.4
49.15	M		410	5.7	19.3
52.26	M		004		18.7
53.74	M	222		32.7	
54.72	MW		402,313		6.6
57.13	VW	321		10.4	
57.58	M		332		30.3
59.28	MW		214		12.1

Table 3.3. Results of experiments MLMS-1 through MLMS-8

Experiment	Rxn	ΔH°_{T}(kcal)	ΔS°_{T}(cal)	II ΔH°_{298}(kcal)	III ΔH°_{298}(kcal)	Temperature Range
MLMS-3	1	80(2)	27(2)	-	-	1406-1668
	2	89.1(9)	30.6(6)	-	-	1413-1668
	4	90.2(6)	29.4(4)	-	-	1500-1668
MLMS-5	1	81.6(2)	28.0(1)	86.5(2)	84.8(1)	1328-1673
	2	87.5(4)	29.6(3)	92.7(4)	88.3(2)	1406-1673
	4	86.2(3)	26.9(2)	91.6(3)	91.1(1)	1526-1670
MLMS-6	4	86.2(4)	27.4(3)	91.3(4)	90.6(1)	1527-1668
MLMS-8	1	81.7(5)	27.6(3)	86.8(5)	85.6(2)	1379-1663
	2	88.5(7)	30.1(4)	93.7(7)	88.5(3)	1432-1663

Reactions:

1 $ZrAl_3(s) \rightarrow ZrAl_2(s) + Al(g)$

2 $2ZrAl_2(s) \rightarrow Zr_2Al_3(s) + Al(g)$

4 $^{5}/_{7}Zr_2Al_3 \rightarrow {}^{2}/_{7}Zr_5Al_4 + Al(g)$

E. Experimental Problems with Zirconium-Rich Phases

Measuring aluminum vapor pressures in equilibrium with zirconium-rich samples (samples containing more zirconium than Zr_5Al_4 = 81 wt % Zr) proved to be a difficult experimental problem. Part of the problems arose from uncertainties as to whether Zr_4Al_3 or Zr_3Al_2 was, at high temperatures, the stable compound neighboring Zr_5Al_4 on the zirconium-rich side. The powder pattern of the residue of MLMS-6 (Table 3.2) showed lines of Zr_5Al_4 and Zr_3Al_2 indicating that Zr_4Al_3 was not important in the vaporization reactions. The results of the heat treatment experiments described in Chapter 2 (performed partly in conjunction with vaporization experiments) also indicated that Zr_4Al_3 was unstable above ~1050°C, and it was therefore concluded that Zr_4Al_3 was not taking part in the high temperature vaporization processes.

The major experimental problems in measuring aluminum pressures beyond Zr_5Al_4 arose from the fact that, below the melting points of the solid compounds, the aluminum vapor pressures are very low. The observed rates of weight loss near the end of experiments MLMS-5,6 were less than about 1 milligram per 12 hrs except at temperatures very near the melting point of the sample. The mass-spectrometer ion signal at 27 amu (aluminum) with the shutter open was less than twice the shutter closed signal near the melting point, and at lower temperatures the ion signal eventually disappeared. Mass-spectrometer measurements could be made only over narrow (ca. 50-100 K) temperature ranges. Both mass-loss and mass-spectrometer data collection were thus hampered.

Other complicating factors that need to be considered are that the melting points of the compounds drop with increasing zirconium content (see, for example, Figure 1.1) and that the compounds Zr_5Al_4, Zr_3Al_2, and Zr_5Al_3 are fairly close in composition.

The combination of experimental problems described above forced certain changes in both the experimental procedure and the instrumentation before attempting to measure aluminum pressures over zirconium-rich samples. Since the compounds Zr_5Al_4, Zr_3Al_2, and Zr_5Al_3 are fairly close in composition (80.8, 82.5, 84.9 wt % Zr) and the melting points drop quickly with increasing zirconium content, composition drift due to aluminum loss had to be minimized in order to avoid accidentally melting the sample, and in order to know for certain which phases were coexisting in the sample. Separate samples of nominal compositions 82.2, 84.2, and 87.1 wt % Zr were prepared to examine the aluminum partial pressures over the Zr_5Al_4 + Zr_3Al_2, Zr_3Al_2 + Zr_5Al_3, and Zr_5Al_3 + Zr(ss) two-phase regions. The approach decided upon was to place as large a quantity of these materials as could be contained into the Knudsen cell and to use the mass-spectrometer to collect data (I^+_{27} vs T) while trying to minimize the total weight loss from the sample. Due to the low aluminum volatility in these samples the mass 27 ion signal with the shutter open was only slightly higher (~50%) than with the shutter closed, and instrumental noise complicated mass-spectrometer measurements at this low level. To overcome and help combat the electronic noise accompanying the mass-spectrometer signal a minicomputer system was added to the Knudsen

effusion apparatus. The computer was used to automate the experiments and signal average the mass-spectrometer output.

F. Addition of Minicomputer System to Effusion Apparatus

A DEC MINC-11/3 minicomputer system was interfaced to the mass-loss-mass-spectrometer apparatus as illustrated in Figure 3.6. The MINC interface features four 12 bit digital to analog converters (DACs) with switch selectable output voltage ranges, 16 lines of digital output, 16 lines of digital input, a multichannel 12 bit analog to digital (A/D) converter and a preamplifier which amplifies or attenuates signals before analog to digital conversion. One of the DAC outputs is used to generate a ramp voltage which is routed to the UTI mass-spectrometer control unit to select the ionic charge to mass ratio. One of the remaining DACs is used to send a temperature setpoint control signal to the Electromax temperature controller, the other two drive or offset strip chart recorders. Two of the digital output lines activate an electric motor which opens and closes the shutter and five more control mass-spectrometer functions and picoammeter range selection. The output of the Cahn recording balance and temperature measurement thermocouple are routed to the A/D converter after passing through signal amplification and isolation devices. The output signal from the mass-spectrometer is also routed to the A/D converter through one of the preamplifier channels. The electronic accessories (signal conditioners and switching devices) used with the MINC interface were constructed by James Anderegg of the Ames Laboratory.

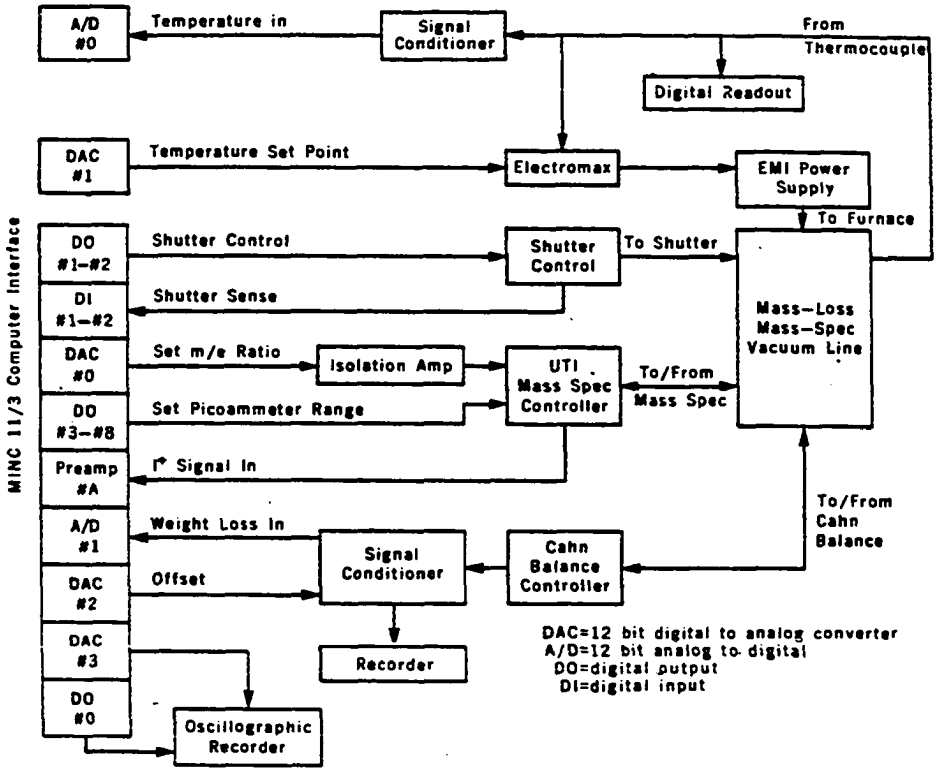

Figure 3.6. The MINC computer to MLMS apparatus interface

Software to control the mass-loss-mass-spectrometer experiments using the MINC system was developed in collaboration with Jim Anderegg. All of the various functions such as digital to analog and analog to digital conversions, picoammeter range selection, and shutter opening or closing are performed under direct program control. One of the more useful implementations, at least as regards the zirconium-aluminum study, is the ability to program the computer system to generate a mass-spectrometer scan and then digitize and average the resulting mass spectra. The signal averaging procedure used is illustrated in Figure 3.7. The user enters starting and final a.m.u. values for the charge to mass ratio scan, the number of data channels into which the mass spectrum is accumulated, the number of scans, and the scan time. The program then computes a ramp voltage increment used in stepping through the mass range and the number of mass-spectrometer readings to be taken and averaged in each channel. Two types of averaging are performed. At each step on the mass scan, multiple mass-spectrometer measurements are taken and averaged to provide an average for that particular channel. The ramp voltage is then incremented and the process repeated in the next channel until the final mass has been reached. Multiple sweeps of the mass range are also taken and the average values obtained in each channel and the various sweeps are again averaged. The multiple sampling of each channel on each sweep prefilters the signal by performing a real time running average and the higher frequency noise is reduced. The multi-sweep averaging is more effective with low frequency noise. The averaging is performed by maintaining running sums so the individual measurements are not available.

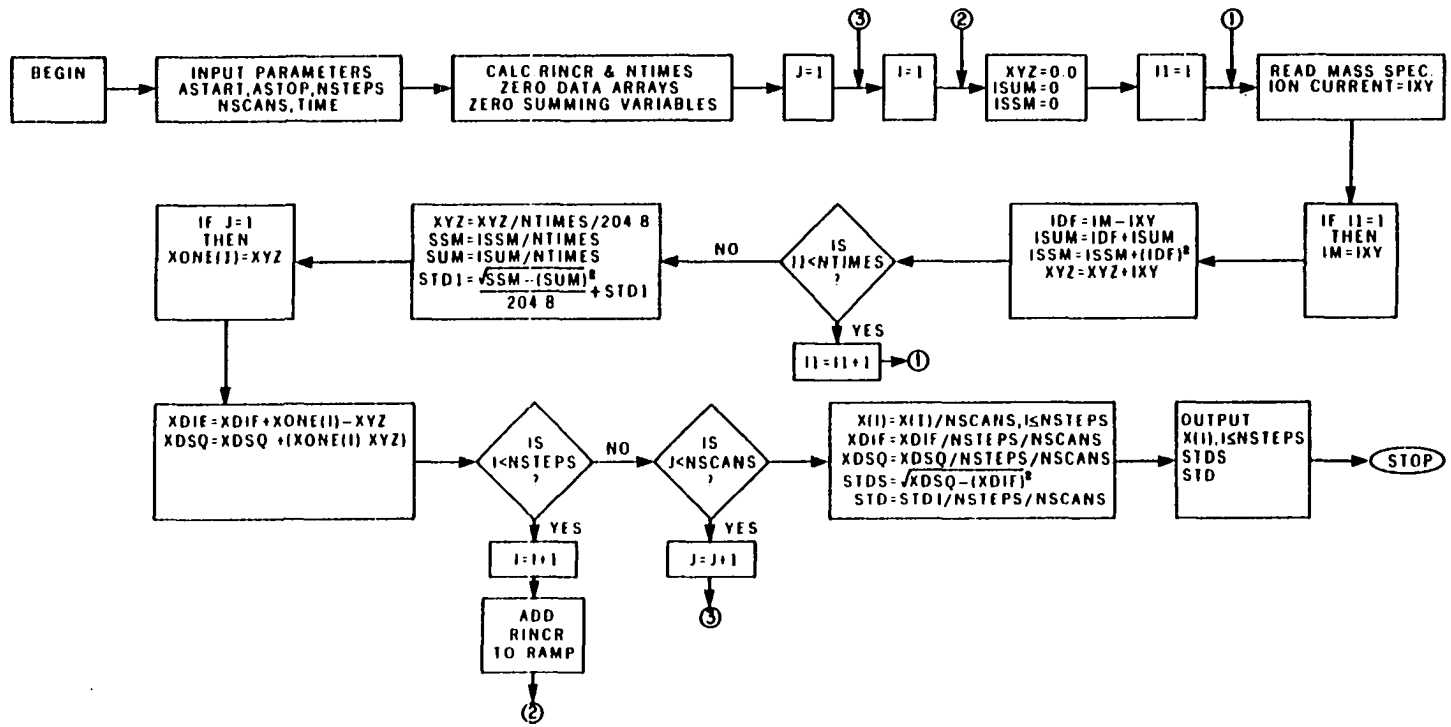

Figure 3.7. A flowchart of mass-spectrometer signal averaging procedure used

By maintaining running sums of differences from a chosen working mean, and the differences squared, variance or standard deviations from the calculated averages are also obtained. These calculated standard deviations provide a quantitative estimate of the system noise and established some criteria for judging how large the difference between the shutter open and shutter closed mass-spectrometer signals need to be before concluding that the material effusing from the Knudsen cell has indeed been measured. The mass-spectrometer data averaging was crucial in measuring aluminum vapor pressures over zirconium-rich zirconium-aluminum phases. The data averaging and digital filtering routines developed were partially based on the discussion of references 34 and 35.

G. Experiments Performed Using Computer Automation

A series of vaporization experiments on zirconium-aluminum samples was performed using the computer to signal average the extremely low aluminum ion signals. The resulting increased sensitivity due to the signal averaging was crucial in performing these experiments and collecting data over a wide enough temperature range to derive meaningful results. The aluminum vapor pressures over zirconium-aluminum samples containing more zirconium than Zr_5Al_4 are on the order of 10^{-8} atm or less. Before the addition of the minicomputer control system, aluminum partial pressures less than about $5x10^{-8}$ atm could not be reliably measured (experiments MLMS-1 through MLMS-8). Using the signal averaging process, described previously, and the computer calculated noise figures to evaluate the significance of small shutter open minus shutter closed

mass spectra data it was possible to measure aluminum partial pressures down to $1x10^{-9}$ atm.

Table 3.4 compares the various experiments performed after adding the computer system to the mass-spectrometer system. Experiments MLMS-9,10,11, and 14 were performed to collect vapor pressure data over the Zr_5Al_4 + Zr_3Al_2, Zr_3Al_2 + Zr_5Al_3, and Zr_5Al_3 + Zr(ss) two phase regions. These experiments were all performed quite similarly. Samples of nominal composition 82.2, 84.2, and 87.1 wt % Zr corresponding to mixtures of Zr_5Al_4 + Zr_3Al_2, Zr_3Al_2 + Zr_5Al_3 and Zr_5Al_3 + Zr(ss) ('Zr_2Al' at <1250°C) were prepared and examined by X-ray powder diffraction to verify the phases present. As much of these materials as could be transferred to the Knudsen cell were transferred. Samples in this composition range are difficult to grind and coarse samples and chunks needed to be contained, so instead of using semi-toroidal shaped liners as done in previous experiments, tungsten or tantalum cup-shaped liners were used. Since the orifice of the Knudsen cell is on the bottom, split tungsten rings were placed underneath the cup-shaped liners to avoid blocking the orifice. The temperature of the Knudsen cell was then raised and measurements commenced.

A computer program that cycled the temperature between an upper and lower limit, in increments of 5°C, was used in these experiments. At each temperature the ion intensity at 27 amu (Al) was signal averaged identically with the shutter closed, and then open, and differences computed and recorded. The amount of averaging used varied somewhat, but typically 5 to 10 scans, were taken over the range 26.75 - 27.25 amu with

Table 3.4. Comparison of experiments MLMS-9 through MLMS-15

	Cell orifice Area cm^2	Phases at start	Phases at end	Reactions studied
MLMS-9	0.0580	Zr_5Al_4+Zr_3Al_2	Zr_5Al_4+Zr_5Al_2	5
MLMS-10	0.0580	Zr_3Al_2+Zr_5Al_3	Zr_3Al_2+Zr_5Al_3	6
MLMS-11	0.0580	Zr_2Al	W_2Zr[a]	7
MLMS-12	0.0580	Zr_3Al	W_2Zr	-[b]
MLMS-14	0.0580	Zr_2Al	Zr_5Al_3+Zr_2Al	7
MLMS-15	0.0580	$ZrAl_3$	Zr_2Al_3+Zr_5Al_4	3,4

Reactions:

3: $Zr_2Al_3 \rightarrow 2ZrAl + Al(g)$

4: $^5/_7Zr_2Al_3 \rightarrow {}^2/_7Zr_5Al_4 + Al(g)$

5: $^3/_2Zr_5Al_4 \rightarrow {}^5/_2Zr_3Al_2$+$Al(g)$

6: $5Zr_3Al_2 \rightarrow 3Zr_5Al_3$+$Al(g)$

7: $^1/_3Zr_5Al_3 \rightarrow {}^5/_3Zr(ss)$+$Al(g)$

[a]Sample reacted with container and some of the higher temperature data had to be discarded.

[b]Measurement of Al partial pressures over bcc Zr solid solution.

10 data channels and approximately 600 voltage measurements per channel were averaged on each single sweep. Lower signals required more averaging in order to obtain reproducible measurements.

The results of measurements taken over the Zr_5Al_4 + Zr_3Al_2 (MLMS-9) two-phase region, the Zr_3Al_2 + Zr_5Al_3 (MLMS-10) region, and the Zr_5Al_3 +

Zr(ss) (MLMS-11 and MLMS-14) region are presented in the second law plots of Figures 3.8 through 3.10 and in Table 3.5. Two experiments were performed with samples in the Zr_5Al_3 + Zr(ss) region. In the first of these (MLMS-11) the compound W_2Zr was identified in the residue indicating that the sample had partially reacted with the tungsten container. The second experiment (MLMS-14) was performed using a tantalum container inserted into the tungsten effusion cell, and more care was taken to not heat the sample to temperatures near the Zr_5Al_3 + Zr eutectic melting point (1350°C) for extended time periods.

Measurements of aluminum partial pressure vs composition across the solid solution of aluminum in body centered cubic (bcc) zirconium were made in experiment MLMS-12. A sample of nominal composition 75 at% Zr ("Zr_3Al") was loaded into a tungsten effusion cell with orifice area 0.0580 cm^2. The sample and cell were then heated to 1583 K and held at this temperature for 12 days while the computer continually logged Al ion current, total milligrams of weight loss, and time of day data. The aluminum partial pressure fell during this time period from about $2x10^{-6}$ atm to $1x10^{-9}$ atm as aluminum was lost and the sample composition approached pure zirconium. Near the end of this experiment, the temperature was raised from 1583 K to 1673 K, 1723 K, and 1773 K. It was found that above 1723 K the sample began to react rapidly with the tungsten container, as evidenced by an unexpected drop in the rate of change of the aluminum ion signal and by the presence of W_2Zr in the residue of the experiment. Data collected above 1723 K were therefore discarded. Plots of the 1583 K and 1673 K isotherms are shown in Figure 3.11. Henry's law

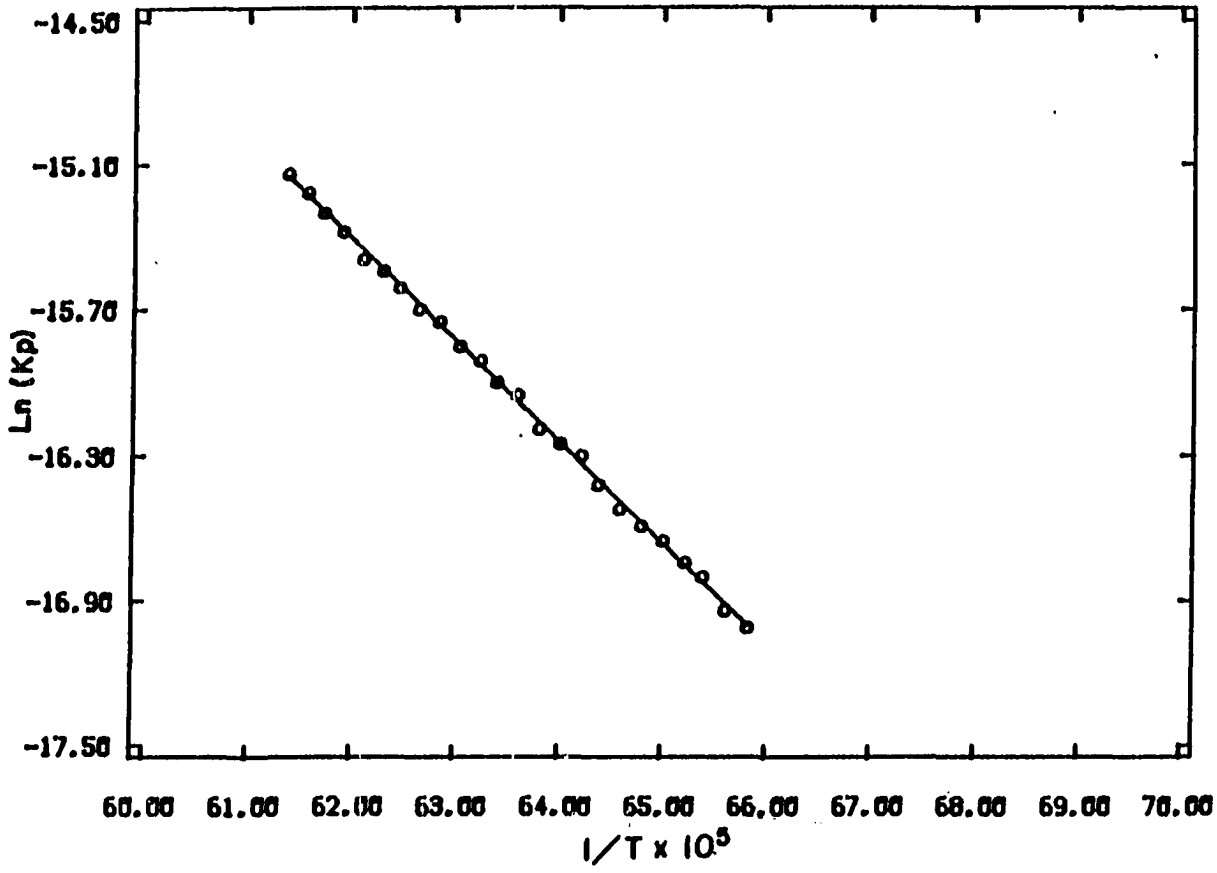

Figure 3.8. Second law plot, Zr_5Al_4 + Zr_3Al_2 region, experiment MLMS-9

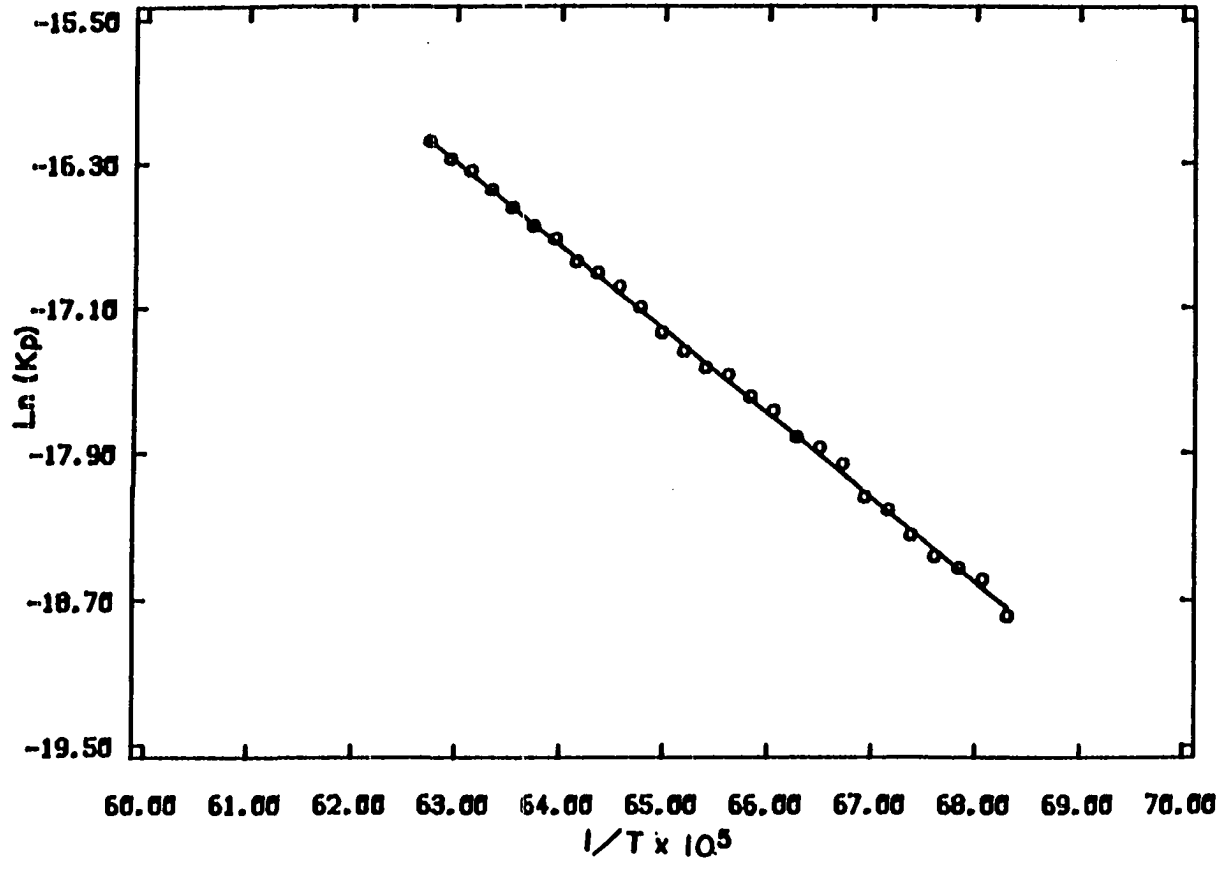

Figure 3.9. Second law plot, Zr_3Al_2 + Zr_5Al_3 region, experiment MLMS-10

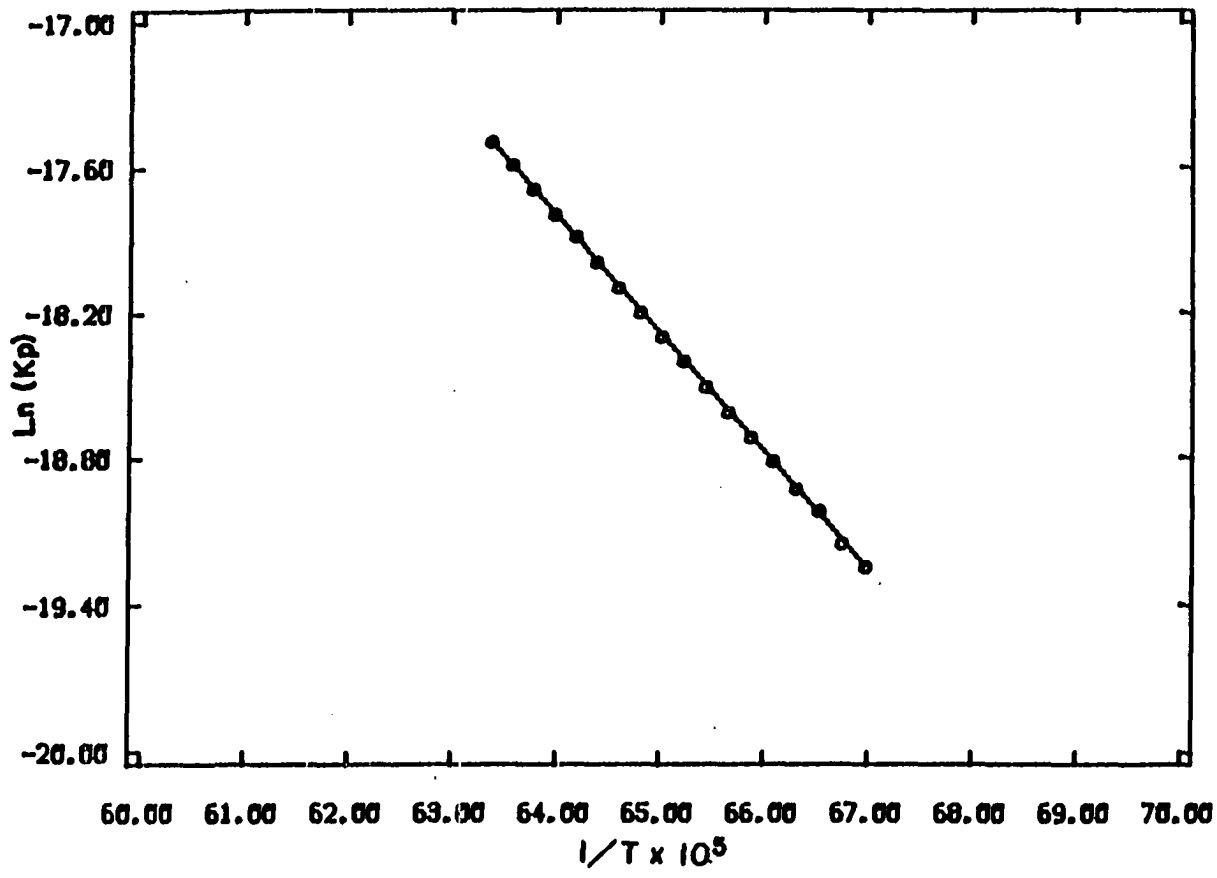

Figure 3.10. Second law plot, Zr_5Al_3 + Zr(ss) region, experiment MLMS-14

Table 3.5. Results of Experiments MLMS-9 through MLMS-15

Experiment	Rxn	ΔH°_T(kcal)	ΔS°_T(cal)	II ΔH°_{298}(kcal)	III ΔH°_{298}(kcal)	Temperature Range
MLMS-9	5	82.6(5)	20.6(3)	88.0(5)	97.5(2)	1519-1629
MLMS-10	6	91.7(6)	25.4(4)	96.8(6)	98.9(1)	1464-1594
MLMS-11	7	91.1(1)	23.3(6)	96.2(9)	101.6(1)	1479-1569
MLMS-14	7	96.6(2)	26.5(1)	101.8(3)	102.2(1)	1493-1578
MLMS-15	3	89.1(8)	28.3(5)	93.5(8)	92.1(1)	1338-1473
MLMS-15	4	88.3(3)	27.6(2)	93.8(3)	92.0(1)	1503-1673

Reactions:

3 $Zr_2Al_3 \rightarrow 2ZrAl + Al(g)$

4 $^5/_7 Zr_2Al_3 \rightarrow {}^2/_7 Zr_5Al_4 + Al(g)$

5 $^3/_2 Zr_5Al_4 \rightarrow {}^5/_2 Zr_3Al_2 + Al(g)$

6 $5Zr_3Al_2 \rightarrow 3Zr_5Al_3 + Al(g)$

7 $^1/_3 Zr_5Al_3 \rightarrow {}^5/_3 Zr(ss) + Al(g)$

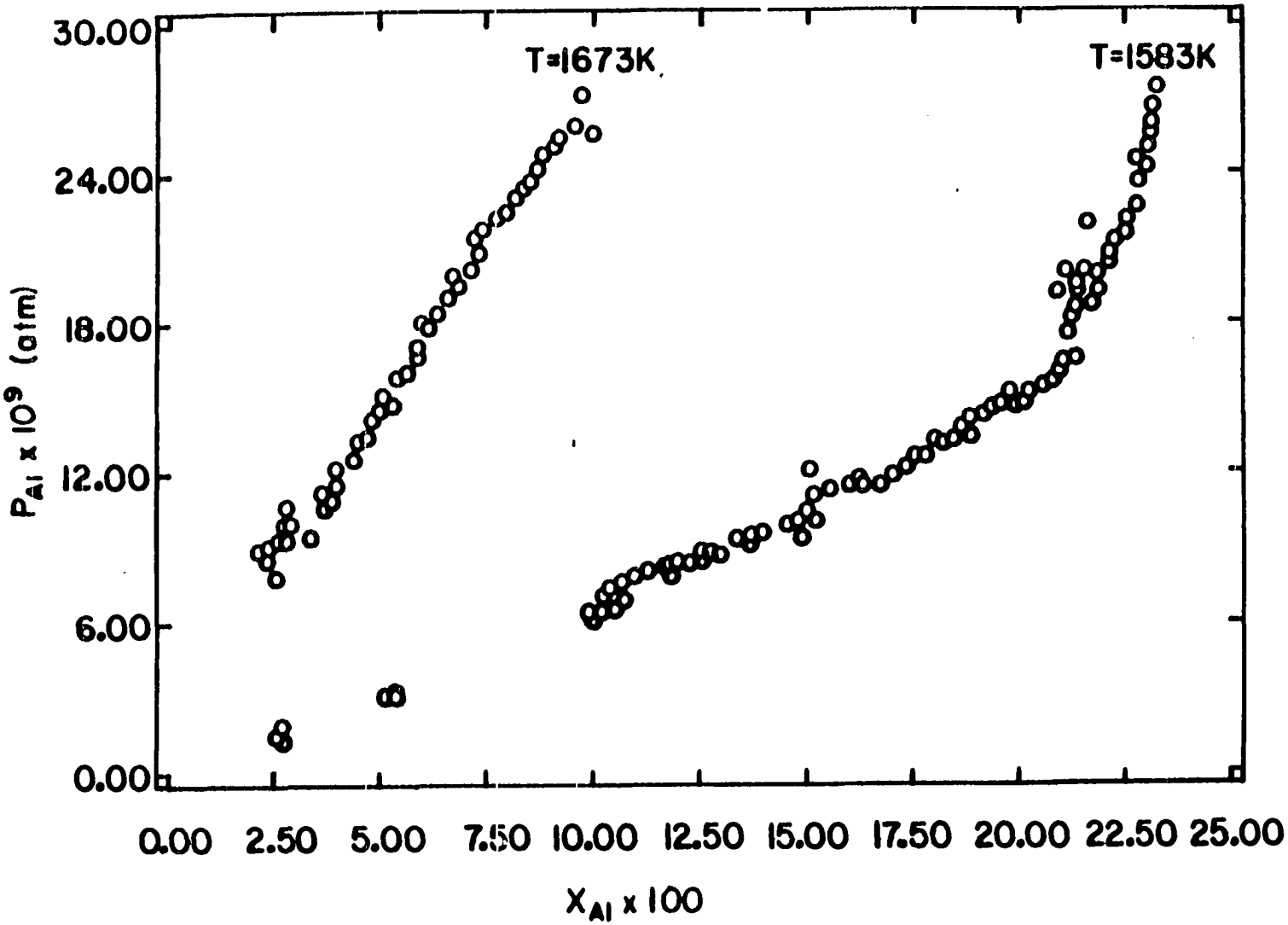

Figure 3.11. Aluminum pressure data collected over the bcc Zr(ss) region

behavior of aluminum was observed for compositions containing more than ~80 atomic % zirconium.

A final experiment, MLMS-15, was performed using the computer automation and signal averaging procedures. In this experiment a sample of X-ray pure $ZrAl_3$ was loaded into the effusion apparatus and ion intensity measurements were recorded vs temperature and total weight loss. There were several purposes for performing this experiment. All other experiments performed after adding the minicomputer system had been performed with zirconium-rich samples (MLMS-9 through MLMS-14) while more aluminum-rich samples were studied earlier. One purpose of performing this experiment was, therefore, to insure that there were no systematic differences between the two types of experiments. An attempt was also made to use the computer to log a large number of data points (ion current vs weight loss) along one isotherm (1473 K) and thereby more accurately estimate the phase width of $ZrAl_2$, which experiment MLMS-5 (Figure 3.4) and various X-ray powder patterns (Table 2.1) indicated may have a measureable (though small) range of nonstoichiometry. The signal averaging procedure was also used to extend the temperature range over which measurements could be made to lower temperatures, providing a better opportunity to make measurements at temperatures at which ZrAl is stable. The reactions $^5/_7Zr_2Al_3 \rightarrow {}^2/_7Zr_5Al_4 + Al(g)$ and especially $Zr_2Al_3 \rightarrow 2ZrAl + Al(g)$ could thus be more readily investigated, and sufficient data were collected for the latter reaction to enable construction of second law plots (Figure 3.12) which were difficult to obtain previously because measurements were made over a limited temperature range. Data points

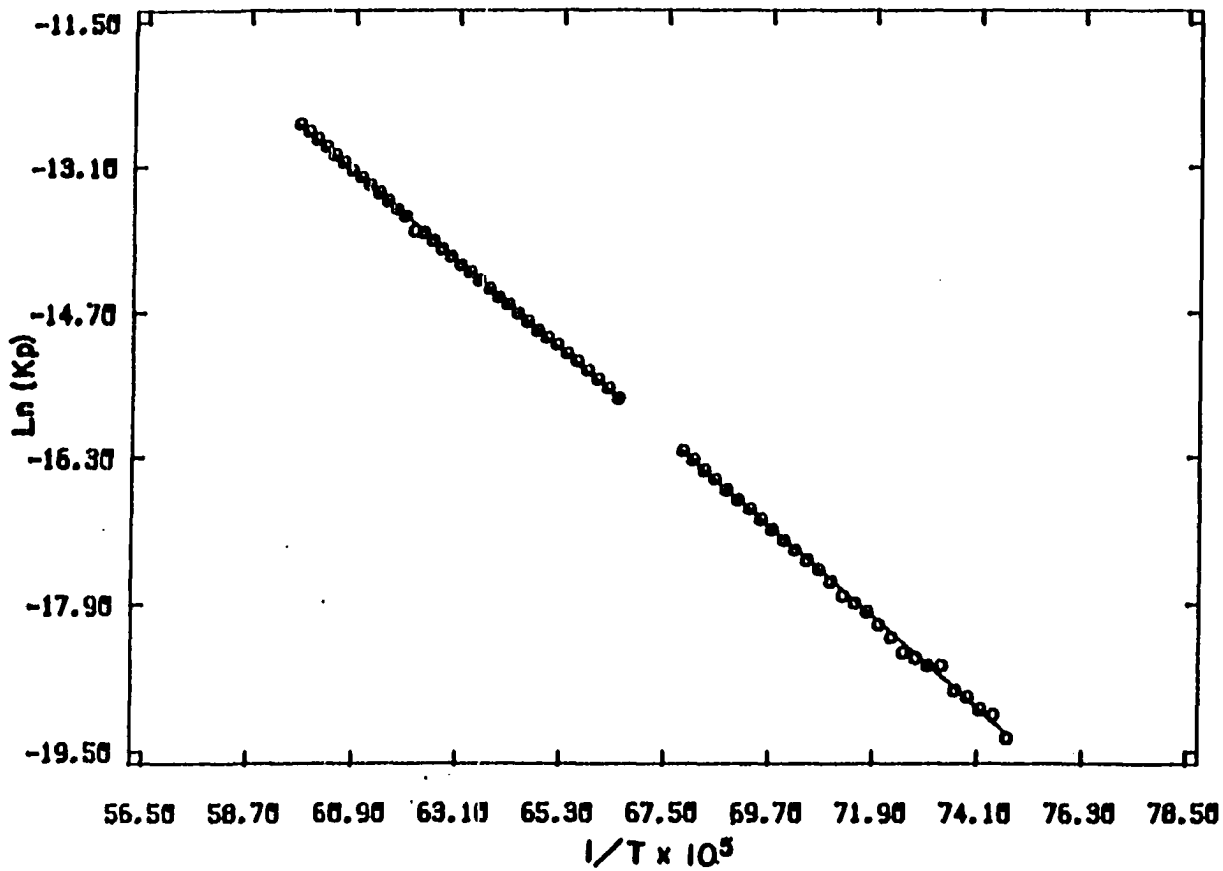

Figure 3.12. Second law plots, Zr_2Al_3 + ZrAl and Zr_2Al_3 + Zr_5Al_4 regions, experiment MLMS-15

for the two processes again appear to fall on nearly the same line. The data collected along the 1473 K isotherm are also shown in Figure 3.13. The temperature was held constant for about 2 days to collect these data, and previously mentioned diffusion effects interferred with the data collection as evidenced by the slight drop in the observed aluminum ion intensities across the $ZrAl_3$ + $ZrAl_2$ coexistence region. The ion intensities never stabilized after the composition drifted across the $ZrAl_2$ single phase region. The $ZrAl_2$ region appears to extend, however, from X_{Al} = 0.662 to X_{Al} = 0.618. The sample temperature was lowered after 16 mg weight loss for in situ annealing, and attempts to follow the 1473 K isotherm across the Zr_2Al_3 region were unsuccessful. Temperature dependent data were collected over the $ZrAl_2$ + Zr_2Al_3, Zr_2Al_3 + Zr_5Al_4, and Zr_2Al_3 + ZrAl coexistence regions.

A summary of the various experiments MLMS-9 through MLMS-15 appear in Table 3.5.

H. Results and Discussion

Sufficient data were obtained in the previously described experiments to permit calculation of enthalpies of atomization and formation of the various zirconium-aluminum intermetallic compounds. The partial pressure of zirconium at the boundary between the bcc zirconium solid solution and the Zr_5Al_3 + Zr(ss) coexistence region at 1583 K was calculated using the Gibbs-Duhem[30] equation in the form

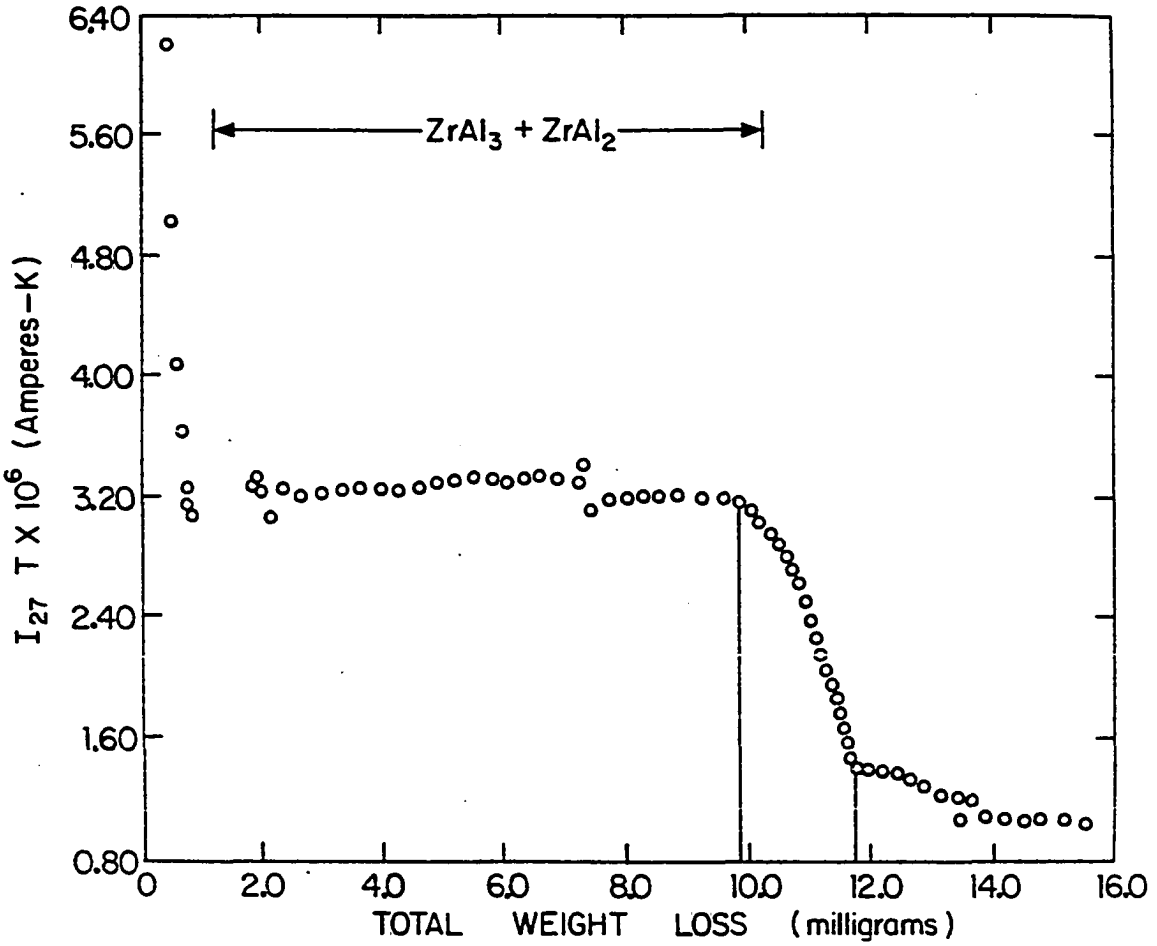

Figure 3.13. T = 1473 isotherm, experiment MLMS-15

$$\ln P_{Zr} = \int \frac{X_{Al}}{X_{Zr}} d \ln P_{Al} .$$

The integral was evaluated graphically from the area under the curve of a plot of $\frac{X_{Al}}{X_{Zr}}$ vs. ln P_{Al}. The aluminum pressures were taken from the 1583 K isotherm of Figure 3.11. The position of the phase boundary was estimated to be at a composition of 23.5 atomic percent aluminum by extrapolating the 1583 K isotherm (Figure 3.11) back to the aluminum partial pressure measured over the Zr_5Al_3 + Zr(ss) region. The phase boundary position agrees well with the phase diagram work of McPhersen and Hansen.[14] The value of the zirconium partial pressure at this composition and temperature was calculated to be 1.14×10^{-13} atmospheres. The measured aluminum pressure at the same point is 2.80×10^{-8} atm. These values can be combined to yield an equilibrium constant for the atomization of Zr_5Al_3

8) $Zr_5Al_3(s) \rightarrow 5Zr(g) + 3Al(g)$

of $K = 4.198 \times 10^{-88}$. The change in the free energy function Δfef for the above reaction (at 1583 K) can be estimated from the free energy function changes for the vaporization of the pure elements

$$\Delta fef^{vap}(Zr_5Al_3) = 5\Delta fef^{vap}(Zr) + 3\Delta fef^{vap}(Al) = 256.27 \text{ eu.}$$

The equilibrium constant at 1583 K combined with the Δfef value can be used to calculate the enthalpy of atomization of Zr_5Al_3 at 298 K

$$-(R \ln K + \Delta fef) = \Delta H^\circ_{298}/T$$

$$-(1583)((1.987)(-201.2) + -256.3) = 1038.2 \text{ kcal.}$$

The enthalpy change for reaction (8) is thus 1038.2 kcal at 298 K. The enthalpy of formation of Zr_5Al_3 can be determined by subtracting the enthalpies of vaporization of the elements from the above enthalpy of atomization, yielding a value of -74.6 kcal/mole. It is interesting to compare these results to those that could be derived, assuming Raoult's law behavior for zirconium across the bcc solid solution region. The zirconium partial pressure at the Zr_5Al_3 + Zr(ss) boundary (23.5 atomic % Al) at 1583 K calculated via Raoult's law would be $0.765 \times 1.77 \times 10^{-13}$ atm, combining this with the measured aluminum pressure at the same temperature over the Zr_5Al_3 + Zr(ss) region would yield an atomization enthalpy (at 298 K) of 1036 kcal for Zr_5Al_3 and a heat of formation of -72.4 kcal/mole.

The enthalpies of atomization and formation of the remaining zirconium-aluminum compounds can be determined by coupling the heat of formation of Zr_5Al_3, as derived above, with data on the various vaporization reactions 1-6, listed in Section IIIC. For example, using the results of experiment MLMS-10 for the decomposition reaction 6 and the above heat of formation at 298 K of Zr_5Al_3 gives

III

6) $5Zr_3Al_2 \rightarrow 3Zr_5Al_3 + Al(g)$ $\quad \Delta H^\circ_{298} = 98.9$ kcal

$3Zr_5Al_3 \rightarrow 15Zr(s) + 9Al(s)$ $\quad \Delta H^\circ_{298} = 3(74.6)$

$Al(g) \rightarrow Al(s)$ $\quad \Delta H^\circ_{298} = -78.7$

$5Zr_3Al_2 \rightarrow 15Zr(s) + 10Al(s)$ $\quad \Delta H^\circ_{298} = 244$.

so that the enthalpy of formation of Zr_3Al_2 would be -244/5 = -48.8 kcal. This value can then be used along with data collected for the vaporization reaction

5) $^3/_2Zr_5Al_4 \rightarrow {}^5/_2Ar_3Al_2 + Al(g)$

to calculate the enthalpy of formation of Zr_5Al_4. This process can be continued in this manner towards the more aluminum-rich compounds, finally stopping at $ZrAl_3$. The enthalpies of formation of the compounds thus determined are listed in Table 3.6. The enthalpies of formation of the compounds divided by the number of atoms in the stoichiometric formula ($^1/_4ZrAl_3$, $^1/_3ZrAl_2$, etc.) are plotted vs composition in Figure 3.14. Enthalpies of formation at selected compositions in the bcc zirconium solid solution region are also indicated on Figure 3.14. These were calculated using aluminum pressures taken from the linear portion of the 1583 K isotherm (Figure 3.11) and zirconium pressures calculated by Raoult's law. It should be noted that a value of 145.5 kcal was used for the heat of vaporization of pure zirconium and 78.7 kcal for Al throughout the thermodynamic calculations, and data for the elements when needed were taken from Hultgren et al.[33]

Table 3.6. Enthalpies of formation and atomization of zirconium-aluminides

Enthalpies of formation of zirconium-aluminides

	$\Delta H^\circ_{f,298}$ (kcal/mole)
$Zr(s) + 3Al(s) \rightarrow ZrAl_3(s)$	-38.96
$Zr(s) + 2Al(s) \rightarrow ZrAl_2(s)$	-32.86
$2Zr(s) + 3Al(s) \rightarrow Zr_2Al_3(s)$	-56.12
$Zr(s) + 3Al(s) \rightarrow ZrAl(s)$	-21.36
$5Zr(s) + 4Al(s) \rightarrow Zr_5Al_4(s)$	-93.76
$3Zr(s) + 2Al(s) \rightarrow Zr_3Al_2(s)$	-48.78
$5Zr(s) + 3Al(s) \rightarrow Zr_5Al_3(s)$	-74.57

Enthalpies of atomization of zirconium-aluminides

	ΔH°_{298} (kcal/mole)
$ZrAl_3(s) \rightarrow Zr(g) + 3Al(g)$	420.56
$ZrAl_2(s) \rightarrow Zr(g) + 2Al(g)$	335.76
$Zr_2Al_3 \rightarrow Zr(g) + Al(g)$	583.22
$ZrAl \rightarrow 2Zr(g) + 3Al(g)$	245.56
$Zr_5Al_4(s) \rightarrow 5Zr(g) + 4Al(g)$	1136.06
$Zr_3Al_2(s) \rightarrow 3Zr(g) + 2Al(g)$	642.68
$Zr_5Al_3(s) \rightarrow 5Zr(g) + 3Al(g)$	1038.17

Comparison of heats of formation of zirconium and hafnium-alumides

$\frac{1}{1+y} M(s) + \frac{y}{1+y} Al(s) \rightarrow \frac{1}{1+y} MAl_y(s)$ $-\Delta H^\circ_{f,298}$ kcal/g-atom

	I	II	III	
$^1/_4ZrAl_3$	9.74	14.28	9.99	$^1/_4HfAl_3$
$^1/_3ZrAl_2$	10.95	17.83	11.54	$^1/_3HfAl_2$
$^1/_5Zr_2Al_3$	11.22	19.53	11.35	$^1/_5Hf_2Al_3$
$^1/_2ZrAl$	10.68	19.79	11.06	$^1/_2HfAl$
$^1/_9Zr_5Al_4$	10.42	18.84	10.6	$^1/_7Hf_4Al_3$
$^1/_5Zr_3Al_2$	9.76	17.61	10.4	$^1/_5Hf_3Al_2$
$^1/_8Zr_5Al_3$	9.32	16.76	9.8	$^1/_3Hf_2Al$
			7.95	$^1/_4Hf_3Al$

I. This work
II. Miedema's empirical model - see text.
III. Hf-Al system - Kaufmann and Nesor, ref. 36

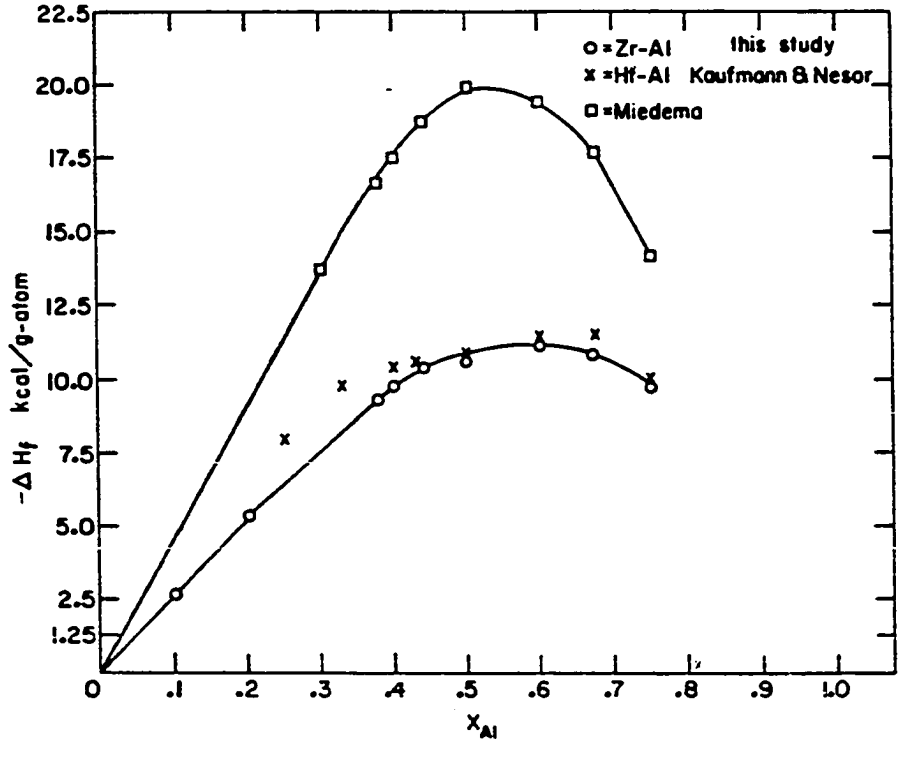

Figure 3.14. The enthalpies of formation of zirconium and hafnium aluminides

Having successfully measured aluminum pressures across the Zr-Al system and derived values for enthalpies of atomization and formation of the various compounds, it is interesting to compare the results to existing experimental data on similar transition metal aluminum systems. Unfortunately, such experimental data are relatively scarce, and for the zirconium-aluminum system existing experimental data are completely lacking. The enthalpies of formation of the various hafnium aluminum compounds have been estimated by Kaufmann and Nesor[36] by a computer fitting of the Hf-Al phase diagram. These values are plotted in Figure 3.14 along with values for the zirconium aluminides determined in this study. The agreement is surprisingly close even though there is no particular reason why it should be. The Zr-Al heats of formation have greater magnitude (~1.5 kcal/g-atom) than experimental values for the Ti-Al system[16] but vary similarly with composition. The heats of formation of corresponding titanium, zirconium, and hafnium aluminides seem to also approximately vary as the atomization heat of the transition metal, zirconium and hafnium aluminides have heats of formation approximately equal with magnitude higher than the titanium aluminides while zirconium and hafnium metals have nearly equal atomization heats (145.5 kcal and 148 kcal) greater than that of titanium (113 kcal).

The possible uncertainties in the enthalpies of formation of the zirconium-aluminum compounds derived from the results of this study should be commented upon. There are several factors which could contribute to errors in these derived results, and the total effect is hard to estimate with complete accuracy. The enthalpies of formation

and atomization of all of the zirconium-aluminum compounds containing more aluminum than Zr_5Al_3 are dependent on the value obtained for Zr_5Al_3, which is in turn dependent on the measured and Gibbs-Duhem derived aluminum and zirconium partial pressures over the bcc zirconium solid solution. The observed deviation of the aluminum partial pressures over the solid solution region from Henry's law behavior (Figure 3.11) at compositions near the Zr_5Al_3 + Zr(ss) two-phase boundary is a potential cause of concern, especially in view of the fact that previous studies at the Ames Laboratory[28,29] of Nb-Al and Mo-Al systems have shown Henry's law to hold accurately over the transition metal-rich solid solution. Since the zirconium and aluminum activities over the solid solution are coupled via the Gibbs-Duhem equation, the deviation of the aluminum activity from Henry's law implies a deviation of the zirconium activity from Raoult's law. The overall effect is that the zirconium activity at the solid solution boundary is somewhat lower than would be predicted by Raoult's law, as previously mentioned, the calculated enthalpy of formation of Zr_5Al_3 would differ by 2 kcal/mole from what might be calculated assuming Raoult's law. Since the 1583 K isotherm of Figure 3.11 extrapolates well to both the aluminum pressure measurement over the Zr_5Al_3 + Zr(ss) region and the phase boundary position established by McPhersen and Hansen, it would seem that the observed deviation from Henry's law behavior is not a spurious or erroneous effect. Further evidence indicating the observed deviation from ideal Henry's law behavior is correct is that a similar effect has been observed over the titanium-rich solid solution in the titanium aluminum system.[37]

Further errors in the derived heats of formation and atomization of the zirconium-aluminum compounds, as well as in the energetics of the vaporization reactions 1-7, could be caused by systematic experimental error in the vapor pressure measurements, or error in the free energy function changes estimated assuming the Neumann-Kopp rule. Possible limits to these errors can be estimated by comparing partial pressure measurements in different experiments, the agreement between second and third law enthalpy changes, and the scatter with temperature of the individual third law enthalpy changes calculated for the various vaporization reactions. The agreement or disagreement of second and third law heats of reaction is generally taken as an indication of the effect of systematic errors in the experimental measurements. The individual third law enthalpy changes calculated from various experimental temperature showed little, if any, temperature dependent trends throughout the course of this study ($\lesssim$500 cal over ~200°C range). The agreement between second and average third law heats of reaction (see for example Tables 3.3 and 3.5) is generally good except for reaction

5) $^{3}/_{2}Zr_5Al_4 \rightarrow {}^{5}/_{2}Zr_3Al_2 + Al(g)$.

The disagreement in this case is somewhat puzzling. It may be that in the process of making the aluminum pressure measurements that the temperature was cycled across a phase transition temperature of some sort and that insufficient annealing time was allowed. The powder patterns of the sample used in this experiment, and the residue obtained, showed the presence of Zr_5Al_4 and Zr_3Al_2, and the temperature range of thermodynamic measurements was above the decomposition temperature of Zr_4Al_3, so that

Zr_5Al_4 and Zr_3Al_2 should coexist at the temperature of the experiment. Heat treatment experiments on samples near this composition often resulted in the formation of a Mn_5Si_3-type phase, which if it is an equilibrium binary phase, may complicate the interpretation of the vapor pressure data collected with this 82.5 wt % Zr sample (Zr_5Al_4 + Zr_3Al_2 ?). In any event, an examination of the second and third law results for the vaporization reactions attempting to explain all disagreements as due to errors in estimated free energy functions indicates that the estimated fef's are accurate to ±0.5 cal/g-atom. Aluminum partial pressure measurements on separate experiments agree to within at least ±15%, so that a conservative estimate of the error in the measured pressures would be ±20%. Errors of these magnitudes give a worst case estimate of the heat of formation of Zr_5Al_3 of about ±6 kcal/mole, or about ±0.75 kcal/g-atom of $^1/_8Zr_5Al_3$. The heats of formation of the remaining compounds were derived from the value obtained for Zr_5Al_3, so that the estimated error of 0.75 kcal/g-atom would hold for these also.

The experimentally determined cohesive energies of the zirconium aluminides can be compared to results predicted from different bonding models in an attempt to glean some indirect bonding information from the results and to check the applicability of the models. Unfortunately, there are no absolutely reliable models, short of a detailed quantum mechanical total energy calculation, which can accurately predict cohesive properties of solid compounds. Existing models therefore are of an empirical nature. Perhaps, two of the more successful models for

rationalizing cohesive properties of metals and alloys are the Brewer-Engel[38,39] model and the Miedema model.[40,41]

The Brewer-Engel model[38] involves several fundamental chemical concepts. A correlation is made between the crystal structures of the metallic elements and the number of bonding s and p type electrons, one s-p electron is correlated with the bcc type structure, two s-p electrons with the hcp structure, and three with the fcc structure. Unpaired s-p electrons in singly occupied orbitals are considered available for bonding, and promotion to low lying electronic levels above the ground state occurs to maximize the number of s-p electrons available for bonding. Thus, sodium with an s^1 configuration forms a bcc structure, magnesium s^2 promotes to s^1p^1 and forms an hcp structure, and aluminum with an s^2p configuration promotes to sp^2 to form an fcc metal. Transition metals promote from a $d^{n-2}s^2$ configuration to $d^{n-1}s$, $d^{n-2}sp$, or $d^{n-3}sp^2$ to form the solid metals of bcc, hcp, or fcc structure. Brewer then asserts that each bonding electron contributes a certain fraction of the bonding energy of a metal. Crystal structure is "determined" by s,p electrons, s-p electrons give similar contributions to the total bonding energy of the solid, and d-electrons contribute to the bonding energy but are not viewed as having a direct effect on crystal structure. By using experimental thermodynamic and atomic spectroscopic data for the metallic elements and correlating the above postulated electronic configurations with the observed crystal structures of the metals, Brewer has self-consistently explained the occurrence of the various crystal structures bcc, hcp and fcc in the metallic elements, and derived

values for the contribution of an electron of a given type to the total bonding energy of a metal in one of the three transition series. The concepts invoked in the Brewer-Engel model are, unfortunately, often difficult to apply to alloy systems and intermetallic compounds where it is not always obvious how a complicated alloy crystal structure is related to one of the simpler bcc, hcp, or fcc types found in pure metals. The idea of attributing a certain fraction of the total bonding energy to each electron is not, however, unique to the Brewer-Engel model and has been applied by others to model the stabilities of the transition metals.[42] This concept is also not necessarily dependent on any correlation between electronic and crystal structures.

An attempt to partition the atomization enthalpies of the zirconium aluminides according to the total number of bonding electrons can be made as follows. Assuming each zirconium electron contributes an amount "A" and each aluminum electron an amount "B" to the atomization enthalpy per mole of each of the seven zirconium aluminides for which data were collected the following set of equations can be formed.

$ZrAl_3$: 4A + 9B = 420.56 kcal/mole

$ZrAl_2$: 4A + 6B = 335.76

Zr_2Al_3: 8A + 9B = 583.22

ZrAl : 4A + 3B = 245.56

Zr_5Al_4: 20A + 12B = 1136.06

Zr_3Al_2: 12A + 6B = 642.68

Zr_5Al_3: 20A + 9B = 1038.17

The bonding energy per zirconium electron "A" and per aluminum electron

"B" are multiplied by the total number of zirconium and aluminum electrons in the above equations. Values for these bonding energies determined by a least squares solution of these equations are A = 38.55 ± 0.36 kcal/Zr e^- and B = 30.13 ± 0.24 kcal/Al e^-. These values can be compared with the bonding energy per Zr electron of pure zirconium which is 145.5 kcal/4 = 36.38 kcal (heat of sublimation divided by the number of valence electrons), and the bonding energy per Al electron of pure aluminum which is 78.7/3 = 26.23 kcal. It appears that aluminum is stabilized slightly more than zirconium in zirconium-aluminum alloys. The derived values of "A" and "B", when substituted back into the above equation set, give a fairly close fit to the experimental data as shown by the following table.

Compound	Observed $\Delta H_{atomization}$	Predicted $\Delta H_{atomization}$
$ZrAl_3$	420.56 kcal/mole	425.37 kcal/mole
$ZrAl_2$	335.76	334.98
Zr_2Al_3	583.22	579.57
ZrAl	245.56	244.59
Zr_5Al_4	1136.06	1132.56
Zr_3Al_2	642.68	643.38
Zr_5Al_3	1038.17	1042.17

This demonstrates that the idea of attributing a certain bonding energy to each bonding electron is reasonably valid.

The above described procedure was carried through for all of the first and second row transition metal aluminum compounds for which data could be readily obtained.[16] The following bonding energies (kcal/electron) per aluminum electron were obtained in the indicated systems.

Sc	Ti	V	Cr	Mn	Fe	Co	Ni
-	29.68	29.05	27.48	26.14	28.68	27.18	30.37
Y	Zr	Nb	Mo	Tc	Ru	Rh	Pd
-	30.13	29.35	30.2	-	-	-	29.46

There is a noticeable trend across the first transition series with the bonding energy per aluminum electron reaching a minimum value very nearly the same as the value for pure aluminum in the Mn-Al system. Data for the second row aluminides are more scarce, but the trend of the first transition series does not seem to be occurring. The values for second row transition metal aluminum compounds appear nearly constant. Data are lacking, however, for Ru and Rh systems and these may prove to differ. The comparison does seem to indicate that the values obtained for the Zr-Al system are consistent with other similar systems.

Miedema and coworkers, have in the last few years[40,41] developed a phenomological model for predicting enthalpies of formation of alloys and intermetallic compounds. The model is based on a "macroscopic atom" approach. An alloy is pictured, to a first approximation, as being a mechanical mixture of Wigner-Seitz atomic cells corresponding to the pure metals. The major energy effects taking place at the cell boundaries are then considered to be related to the discontinuities of the charge

density Δn and electron chemical potential $\Delta\phi^*$ (related to the electronegativity difference). The heat of solution of a metal A in metal B is then given as

$$\Delta H_{sol'n}^{A \text{ in } B} = \frac{V_A}{(n_{WS}^A)^{-1/3} + (n_{WS}^B)^{-1/3}} \left[-P(\Delta\phi^*)^2 + Q(\Delta n_{WS}^{1/3}) - R\right]$$

and the heat of formation of an ordered intermetallic compound as

$$\Delta H_f^{A \text{ in } B} = c_A^S f_B^A \Delta H_{sol'n}^{A \text{ in } B}$$

where f_B^A is the surface area fraction of A atomic cells in contact with B cells, c_A^S and c_B^S are used to designate concentrations (i.e., mole fractions) adjusted according to the total Wigner-Seitz cell surface area, i.e.,

$$c_A^S = \frac{c_A V_A^{2/3}}{(c_A V_A^{2/3} + c_B V_B^{2/3})}$$

with c_A and c_B normal mole fractions. The fraction of A atoms in contact with B atoms, which in effect establishes the concentration dependence of the heats of formation, has been estimated by Miedema as

$$f_B^A = (1-c_A^S)\ \{1+8(c_A^S)^2(1-c_A^S)^2\}.$$

The parameter R in the heat of solution equation was introduced by Miedema to account for hybridization effects in alloy formation. Three different sets of the empirical parameters P,Q,R, are used for liquid alloys of two transition metals, solid alloys of two transition metals, and solid alloys of a transition metal and a p-type nontransition metal.

It is then a straightforward problem to use values of $\Delta\phi^*$ and Δn_{WS} tabulated by Miedema to predict heats of formation for almost any binary alloy system. The values calculated for the Zr-Al system are indicated on the heat of formation plot of Figure 3.14. The values are more negative by nearly a factor of two than the experimentally determined values. Miedema's predictions have also been shown inadequate to model the heats of formation of Nb-Al compounds.[28] It would appear that the nature of bonding in these compounds is significantly different than in the systems considered by Miedema in the evaluation of his parameters, or that the cohesive properties of Zr-Al and Nb-Al simply cannot be parameterized in terms of $\Delta\phi^*$ and Δn_{WS}. It may also be that the model overestimates charge transfer effects.

It is interesting to note that in the process of developing his model, Miedema et al. surveyed the available heat of formation data for binary alloy systems and correlated the number of compounds forming a binary system with the heat of formation of the 1:1 (or interpolated to 1:1 if none actually exists) compound.[43] They found that the average number of compounds increases from 1 for ΔH_f° (AB) between -4 and -10 kJ/g-atom to 3 for ΔH_f°(AB) between -20 and -40 kJ/g-atom and 5 for ΔH_f° (AB) more negative than -75 kJ/g-atom. Interestingly, there are 9 compounds in the Zr-Al system and the heat of formation of the 1:1 compound is only about -45 kJ/g-atom. The Zr-Al system is thus rather unusual in the large number of compounds forming with relatively small heats of formation.

In summary, the thermodynamic data obtained in this study of the Zr-Al system are consistent with available experimental data for similar systems. The enthalpies of atomization of the compounds can be successfully modeled by assigning each valence electron a certain binding energy, and the binding energy per electron values obtained are consistent with values similarly obtained for other transition metal aluminum systems. The empirical model of Miedema et al. which has become popular in the literature does not successfully model the results, however.

IV. ELECTRONIC STRUCTURE OF Zr_2Al

A. Introduction

In order to provide a basis for the discussion of bonding in the zirconium-aluminum compounds, and a possible comparison to empirical bonding models (such as those of Brewer and Miedema) and previous electronic structure calculations of early transition metal sulfides,[44-46] a nonself-consistent, nonrelativistic calculation of the band structure of the intermetallic compound Zr_2Al was performed. Recent collaborative efforts between J. Nakahara and H. Franzen (ISU Chemistry Department) and D. K. Misemer (ISU Physics Department)[46] have made available a set of computer programs which enable solid state band structure calculations for compounds with NiAs-type crystal structures to be performed by the KKR method.[47] The crystal structure of Zr_2Al is closely related to the NiAs-type structure.

Zr_2Al crystallizes in a hexagonal Ni_2In type structure, space group $P6_3/mmc$, with lattice constants a = 4.8939 Å and c = 5.9283 Å. There are 6 atoms in the hexagonal unit cell, 2 at each of 3 crystallographically distinct sites. The positions of the atoms are

Zr_1	0 0 0
Zr_1	0 0 $^1/_2$
Zr_2	$^1/_3$ $^2/_3$ $^3/_4$
Zr_2	$^2/_3$ $^1/_3$ $^1/_4$
Al	$^1/_3$ $^2/_3$ $^1/_4$
Al	$^2/_3$ $^1/_3$ $^3/_4$

Zr_1 and Zr_2 designate zirconium atoms on distinct sites. The structure is shown drawn on the hexagonal 110 plane in Figure 4.1a. The structure can be thought of as consisting of hexagonal Zr_2-Al nets at height $z = {}^1/_4$ or $z = {}^3/_4$ with columns of Zr_1 atoms at height $z = 0$ or $z = {}^1/_2$ running through the center of the Zr_2-Al hexagons. The Zr_1 atoms at $z = 0$ or $z = {}^1/_2$ also form a larger hexagonal net, so that the structure can also be thought of as being built up by an alternate stacking of the large Zr_1 hexagonal nets and the smaller Zr_2-Al nets with the stacking along the z-axis. Two layers of the structure as seen along the z-axis are shown in Figure 4.1b, along with the orientation of the cartesian coordinates x,y relative to the hexagonal crystal axes.

B. Description of Calculation

The crystal eigenvalues and eigenfunctions for Zr_2Al were calculated by the Korringa-Kohn-Rostoker (KKR) or Green's function method. A description of the method, at least as it pertains to a monatomic lattice, can be found in most solid state physics textbooks.[48] The problem is to solve a one-electron Schrödinger equation of the form

$$\left[\frac{-h^2}{2m}\nabla^2 + U(\vec{r})\right]\psi(\vec{r}) = \varepsilon\psi(\vec{r})$$

where the potential $U(\vec{r})$ is periodic in the Bravais lattice vectors $\vec{R}$

$$U(\vec{r}+\vec{R}) = U(\vec{r}).$$

A theorem known as Bloch's theorem asserts that for a potential having the above property the eigenfunctions ψ have the form

$$\psi_{n\vec{k}}(\vec{r}) = e^{i\vec{k}\cdot\vec{r}}u_{n\vec{k}}(\vec{r})$$

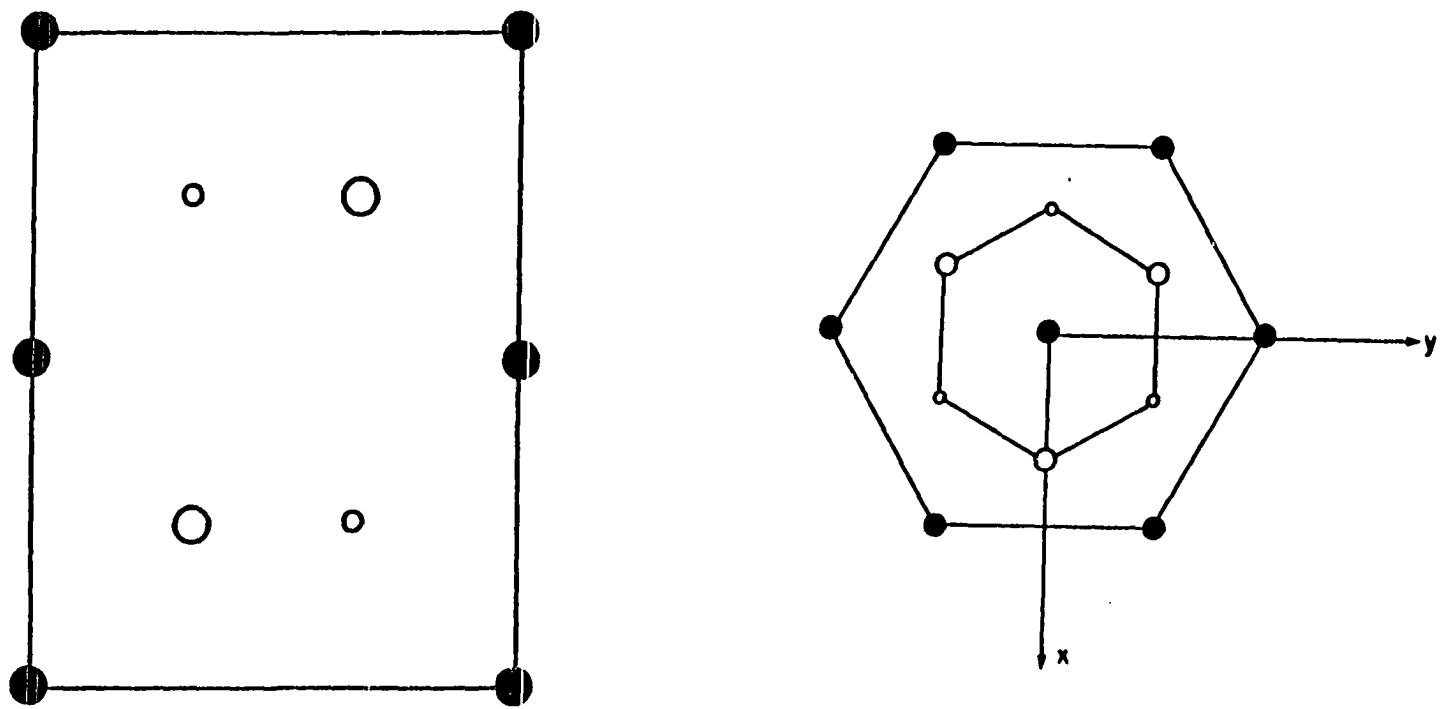

(a) (b)

Figure 4.1. The crystal structure of Zr_2Al
a) drawn on the hexagonal 110 plane
b) the z=0 and z=$^1/_4$ layers projected on the a-b plane.
Large open circles denote Zr_1 atoms, large filled circles Zr_2 atoms, and small open circles Al atoms

where the function $u_{n\vec{k}}(\vec{r})$ has the periodicity of the lattice

$$u_{nk}\to(\vec{r}+\vec{R}) = u_{n\vec{k}}(\vec{r}).$$

The Bloch wave vector $\vec{k}$ can be thought of as a quantum number characteristic of the translational symmetry of the crystal. The quantum number n, called the band index, counts the eigenvalues at a particular k-point. Because of the periodic property of the function $u_{n\vec{k}}(\vec{r})$ the eigenfunctions ψ also have the property

$$\psi_{n\vec{k}}(\vec{r}+\vec{R}) = e^{i\vec{k}\cdot\vec{R}}\,\psi_{n\vec{k}}(\vec{r}) .$$

It is convenient when working with periodic solids to define a so-called reciprocal lattice which is comprised of all wave vectors $\vec{K}$ which yield plane waves with the periodicity of the lattice, i.e.,

$$e^{i\vec{K}\cdot\vec{R}} = 1$$

for all lattice translations $\vec{R}$. Because of Bloch's theorem it then follows that if the wave vector $\vec{k}$ is augmented by a reciprocal lattice vector $\vec{K}$ then

$$\psi_{n,\vec{k}+\vec{K}}(\vec{r}+\vec{R}) = e^{i(\vec{k}+\vec{K})\cdot\vec{R}}\,\psi_{n,\vec{k}+\vec{K}}(\vec{r}) = e^{i\vec{k}\cdot\vec{R}}\psi_{n,\vec{k}+\vec{K}}(\vec{r})$$

and the state with wave vector $\vec{k}+\vec{K}$ behaves the same as that with wave vector $\vec{k}$. Because of this property, the Bloch wave vectors $\vec{k}$ can be limited to a primitive cell in reciprocal space called a Brillouin zone.

The KKR method[47] solves the crystal Schrödinger equation by casting it into an equivalent integral form using a Green's function technique. One of the fundamental assumptions made is that the crystal potential $U(\vec{r}+\vec{R}) = U(\vec{r})$ can be modeled by a so-called "muffin-tin" potential. The muffin-tin approximation replaces the actual crystal potential with one that is spherical (atomic-like) within a certain radius (the muffin-tin sphere radius) of an atomic center and zero in the interstitial region between the spheres. The other major approximation of the KKR method is that the wave function inside a sphere can be expanded in a truncated series of the form.

$$\psi^{\text{inside}}_{\varepsilon,\vec{k}}(\vec{r}) = \sum_{\ell,m} c^{\varepsilon,\vec{k}}_{\ell,m} \; f^{\varepsilon,\vec{k}}_{\ell}(r) \; Y_{\ell,m}(\theta,\phi).$$

The energy eigenvalues and eigenfunctions for Zr_2Al were calculated using the Ames Laboratory KKR programs.[49] The calculation was nonrelativistic and nonself-consistent. The muffin-tin radii of zirconium and aluminum were chosen to be 1.484 Å and 1.270 Å, respectively, these radii were chosen by dividing the shortest Zr-Al distance in the Zr_2Al structure into segments proportional to the Pauling radii of zirconium and aluminum. The muffin-tin spheres thus constructed filled 58.58% of the total cell volume and 96.18% of the charge was inside the spheres. The muffin-tin potential was constructed using atomic charge densities of $5s^24d^2$ zirconium and $3s^23p^1$ aluminum which were calculated by the self-consistent Hartree-Fock-Slater method using a variation of the Hermann and Skillman program.[50] The procedure used was developed by Matheiss.[51]

The potential consists of both a coulombic part and an exchange contribution. The coulombic part results from the combination of individual atomic charge densities and spherical terms of a Löwdin-Alpa expansion of neighboring atom charge densities.[52] The exchange component was calculated using Slater's free electron exchange approximation.[53] The wave function expansion inside the aluminum muffin-tin spheres included spherical harmonics up to $\ell = 1$ and inside the zirconium spheres through $\ell = 2$. Energy eigenvalues and eigenfunctions were calculated for 63 general $\vec{k}$-points and 6 high symmetry points in $^1/_{24}$th of the hexagonal Brillouin zone. The Brillouin zone points chosen were the same as those used previously in calculations performed for TiS and VS of the NiAs-type structure.[46] Eighteen energy bands were calculated in the energy range 0 to 1.2 R_y. The electronic density of states was evaluated by a simple histogram type procedure, i.e., the density of states $\rho(\varepsilon)$ at energy ε was obtained by counting the number of $\vec{k}$-points for which eigenvalues between ε and $\varepsilon + \Delta\varepsilon$ were obtained, with $\Delta\varepsilon$ being typically $\lesssim$2 milliRydbergs. Angular momentum decomposed densities of states were calculated similarly, but the number of $\vec{k}$-points giving eigenvalues between ε and $\varepsilon + \Delta\varepsilon$ was weighted according to the percent contribution of the corresponding angular momentum components to the total charge within a Wigner-Seitz sphere surrounding the atomic site. The charge density $\rho(r) = \psi^*\psi$ inside the muffin-tin spheres was expanded as

$$\rho(\vec{r}) = \sum \rho_{\ell m} Y_{\ell m}(\theta\phi) \ .$$

Nonvanishing terms in this expansion occur for ℓ,m = (00), (20), (40), (45) at the (D_{3d}) Zr_1 site, (00), (20), (40), (33) for (D_{3h}) Zr_2, and (00), (20) for Al (also D_{3h}).

C. Results and Discussion

The total and angular momentum decomposed partial densities of states curves are shown in Figures 4.2, 4.3a-c and a table of eigenvalues obtained at the higher symmetry Brillouin zone points in Table 4.1. One of the more immediately noticeable features of the DOS curves is that, except for Al s-type states, there are no clear cut energy ranges where states of different angular momentum components tend to concentrate. A noticeable band gap is also obvious separating states in the energy range 0 → 0.2 Rydbergs which might be referred to as 'valence band' states from those in the energy range 0.22 → E_F = 0.52 Rydbergs which could be called 'conduction band' states. The major contribution to the valence band comes from the Al s type contribution. This is an interesting contrast to existing band structure calculations for iron, cobalt, and nickel aluminides[54],[55] where no discernible gap between valence and conduction band states is apparent. This would indicate a substantially more covalent nature to the bonding in zirconium aluminides as compared to these later transition metal compounds. The angular momentum decomposed densities of states, when integrated over all energies up to the Fermi level, indicate that virtually 100% of the Al -s type states lie within the valence band and these Al s-states account for about 50% of the valence band population.

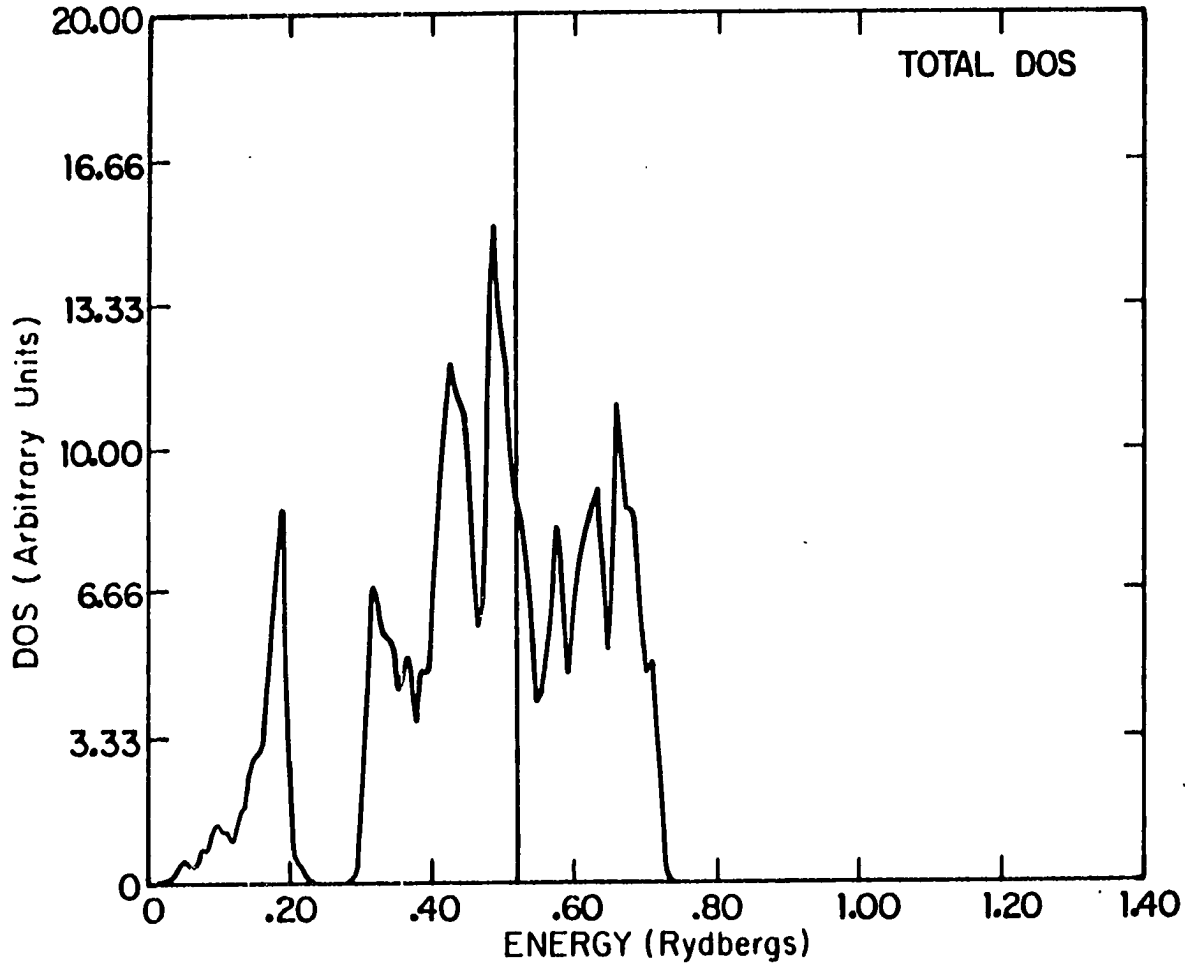

Figure 4.2. The total density of states of Zr_2Al

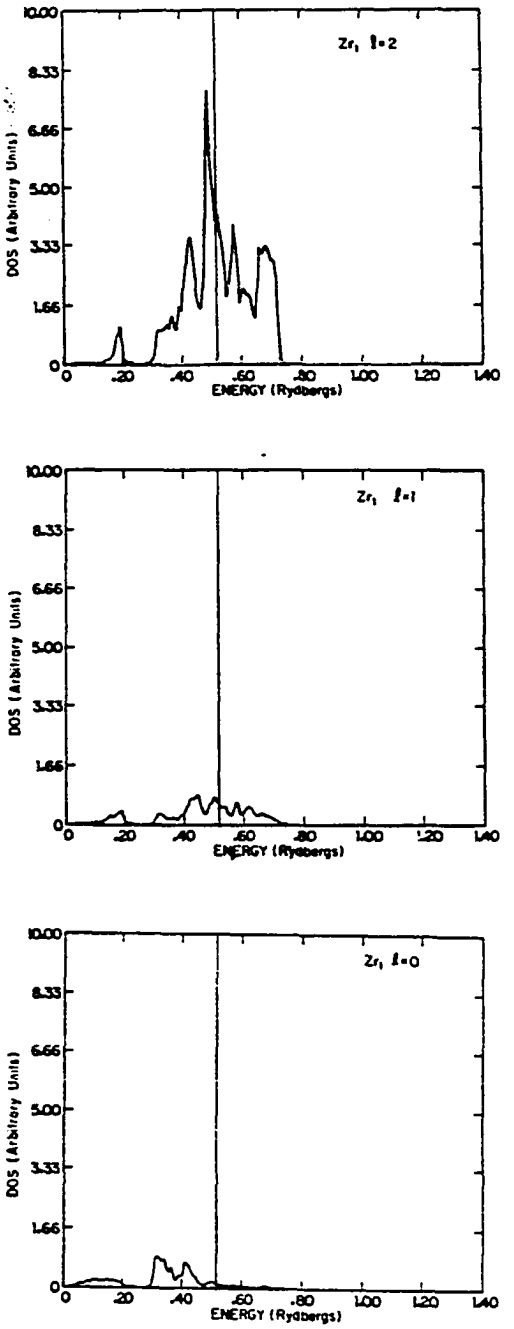

Figure 4.3a. LDDOS curves for the Zr_1 site

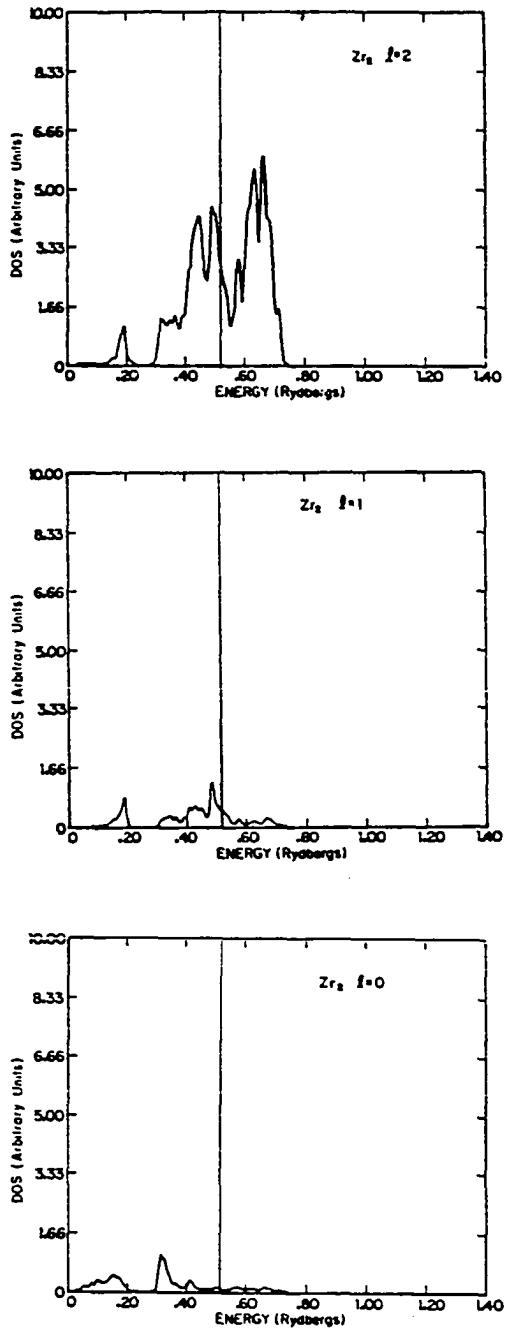

Figure 4.3b. LDDOS curves for the Zr_2 site

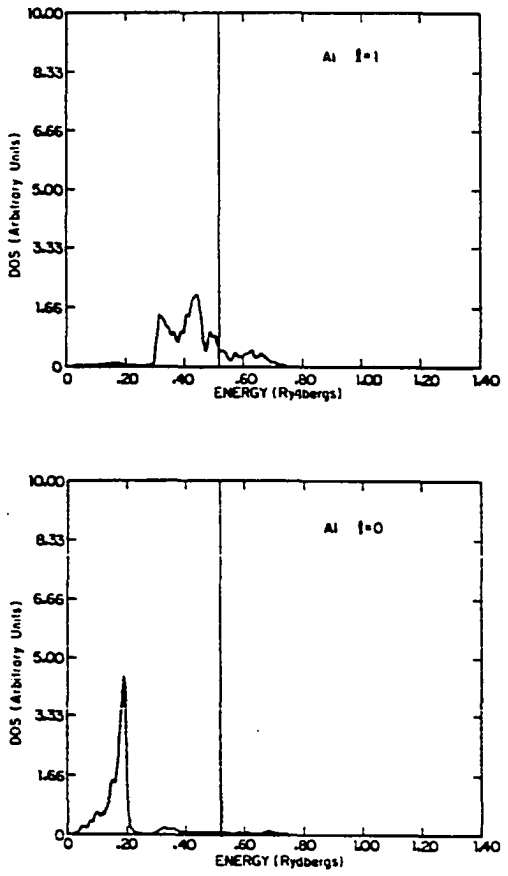

Figure 4.3c. LDDOS curves for the Al site

Table 4.1. Eigenvalues (Ryd) at high symmetry points

Γ	M	K	A	L	H
0.03645	0.15386	0.16365	0.11887	0.18994	0.19735
0.22553	0.15775	0.16370	0.11887	0.18994	0.19735
0.33569	0.30117	0.34069	0.36819	0.30027	0.33327
0.33575	0.37787	0.37050	0.36819	0.30027	0.33327
0.35840	0.41450	0.37053	0.36819	0.44196	0.39360
0.41928	0.42960	0.41624	0.36819	0.44196	0.39360
0.41995	0.46159	0.44954	0.41864	0.44825	0.43339
0.41999	0.48250	0.44957	0.41864	0.44825	0.43339
0.46699	0.50002	0.48293	0.48028	0.50587	0.52112
0.46702	0.50602	0.53287	0.48028	0.50587	0.52112
0.48095	0.50752	0.53296	0.48035	0.50847	0.52746
0.48100	0.50758	0.57553	0.48035	0.50847	0.52746
0.63764	0.55210	0.58019	0.64732	0.57734	0.54744
0.63764	0.57861	0.58029	0.64732	0.57734	0.54744
0.66734	0.62065	0.59580	0.70774	0.61233	0.62247
0.72342	0.62186	0.65125	0.70774	0.61233	0.62247
0.72349	0.65701	0.65141	0.70774	0.67015	0.67930
0.72770	0.69738	0.66235	0.70774	0.67015	0.67930

The conduction band, on the other hand, is composed mainly of Zr_1 and Zr_2 d-type states with a smaller contribution from Al-p. Integrating the partial DOS curves up to the band gap yields the following electron occupations

electrons in Wigner-Seitz sphere

Al s	Al p	Zr_1s	Zr_1p	Zr_1d	Zr_2s	Zr_2p	Zr_2d
1.0020	0.2560	0.1296	0.1060	0.1552	0.2102	0.1668	0.1789

and to the Fermi level the following

electrons in WS sphere

Al s	Al p	Zr_1s	Z_1p	Zr_1d	Zr_2s	Zr_2p	Zr_2d
1.0751	1.2960	0.5903	0.5847	3.0420	0.5243	0.6704	2.9647 .

It is somewhat dubious to attempt to determine charge transfer between the muffin-tin spheres using the results of a nonself-consistent calculation, but an attempt can be made nevertheless. The total charge due to occupied valence and conduction band states was found to be 2.898 electrons within the Zr_1 MT sphere, 2.802 in the Zr_2 MT sphere, and 1.507 electrons in the Al MT sphere. The corresponding values obtained by overlapping the atomic charge densities were 2.781, 2.786, and 1.878 electrons, respectively. The Al MT spheres appear to lose charge mostly to the interstitial region with only part of the loss being picked up by zirconium. Charge transfer form Al to Zr is opposite to what might be predicted on the basis of Pauling electronegativities, the electronegativity of Zr is 1.4 and aluminum 1.5. Charge transfer from Al to Ti

(opposite to electronegativity) and other first row transition metals has been observed experimentally, however, by Wenger and Steinemann[56], and filling of the d-band of a transition metal by aluminum electrons can be ascertained from the magnetic properties of Fe, Co and Ni aluminides.[57] Thus, the observed direction of charge transfer is not completely unlikely. A possible flaw in the bonding model of Miedema[41] discussed previously is that, based on electronegativity differences, it predicts a charge transfer from Zr to Al.

In order to investigate the directionality of the bonding between the different atoms in Zr_2Al, the charge density within the muffin-tin spheres were calculated by summing the absolute squares $\psi^*\psi$ of the one electron eigenfunctions over the occupied states in the valence ($0 < E < 0.22$ Ryd) and conduction ($0.22 < E < 0.52$ Ryd) bands. The charge densities $\rho(r,\theta,\phi)$ thus obtained were plotted as a function of direction with the radius r fixed on the surface of a muffin-tin sphere. Fixing one of the angles in addition to the radius enabled construction of polar graphs of the charge density in various planes passing through the center of an atomic sphere such as the xz, xz, yz planes. The plots thus obtained are shown in Figures 4.4, 4.5 for the valence band states and Figures 4.6-4.8 for occupied conduction band states. Plots of the charge density around an aluminum atom are not shown since these were found to show only minor deviations from sphericity and are therefore not useful in discussing the directional nature of the bonding.

The major interactions in the valence band were found, not surprisingly to be direct zirconium-aluminum σ and π-type interactions.

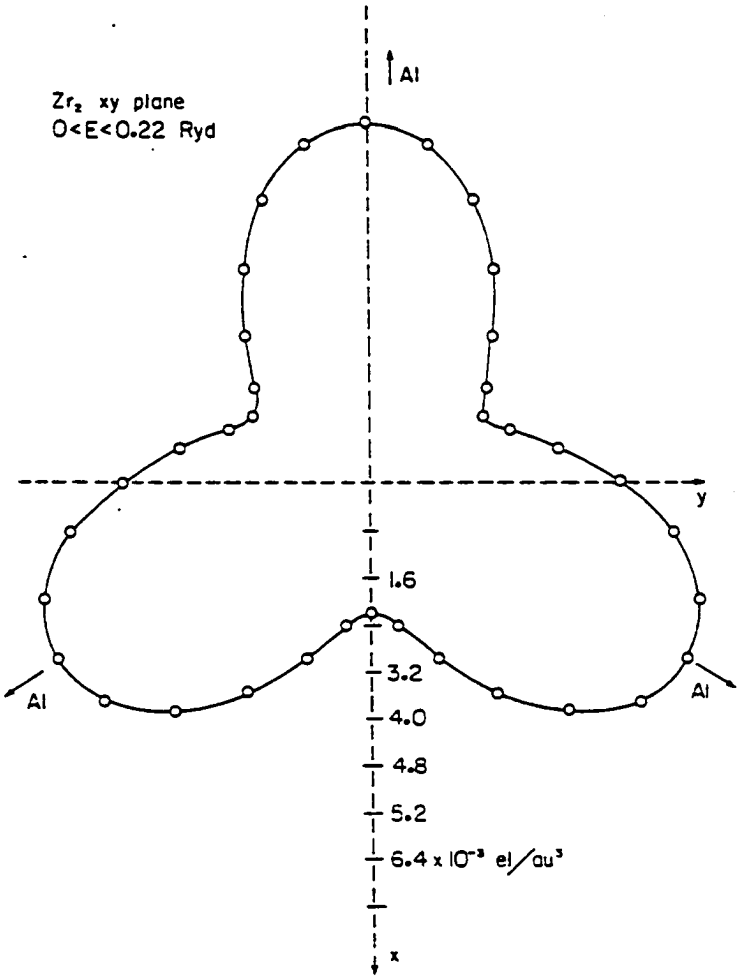

Figure 4.4. The charge density around a Zr_2 atom in the xy plane due to occupied states in the valence band

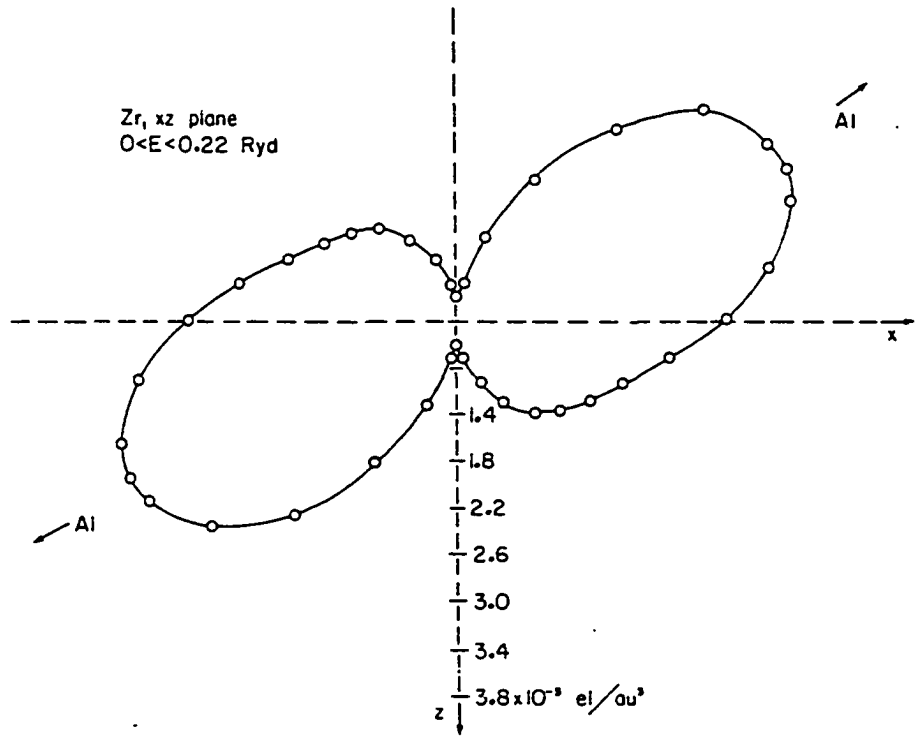

Figure 4.5. The charge density around a Zr_1 atom in the xz plane due to occupied valence band states

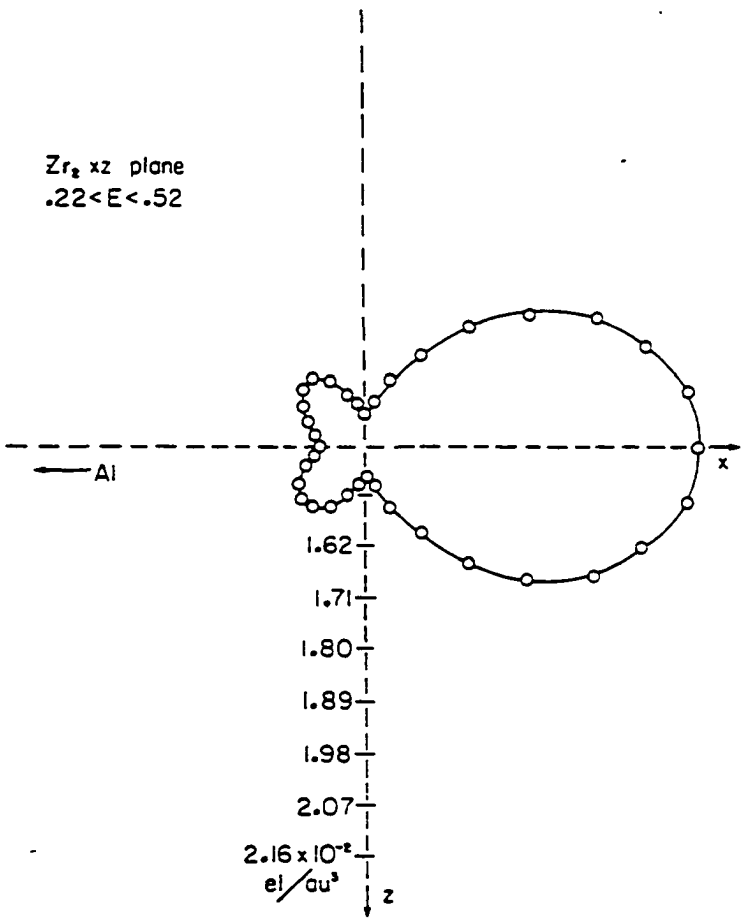

Figure 4.6. The charge density around a Zr_2 atom in the xz plane due to occupied states in the conduction band

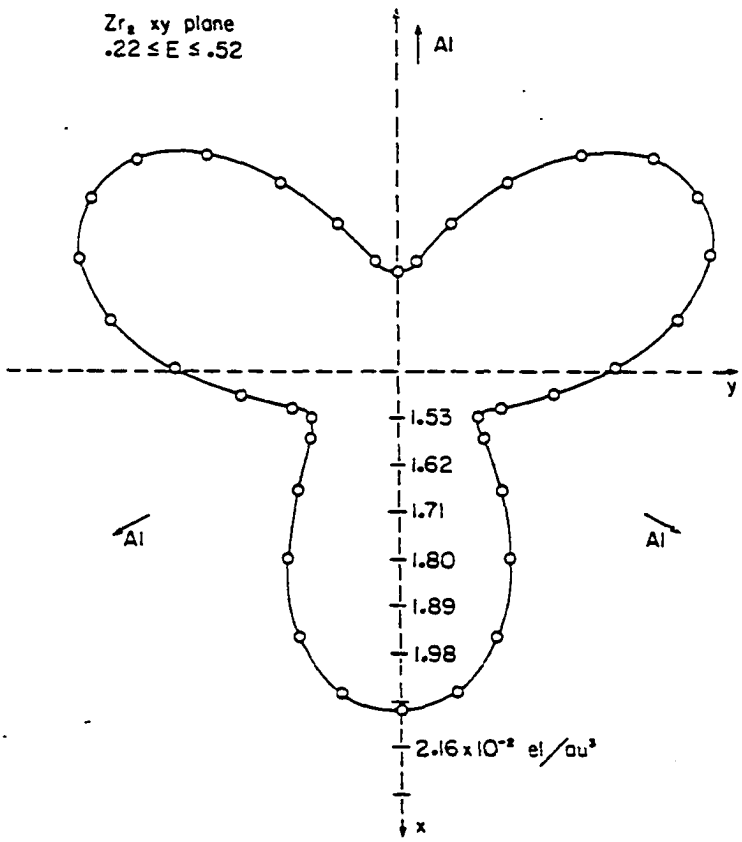

Figure 4.7. The charge density at the surface of the Zr_2 sphere in the xy plane due to occupied conduction band states

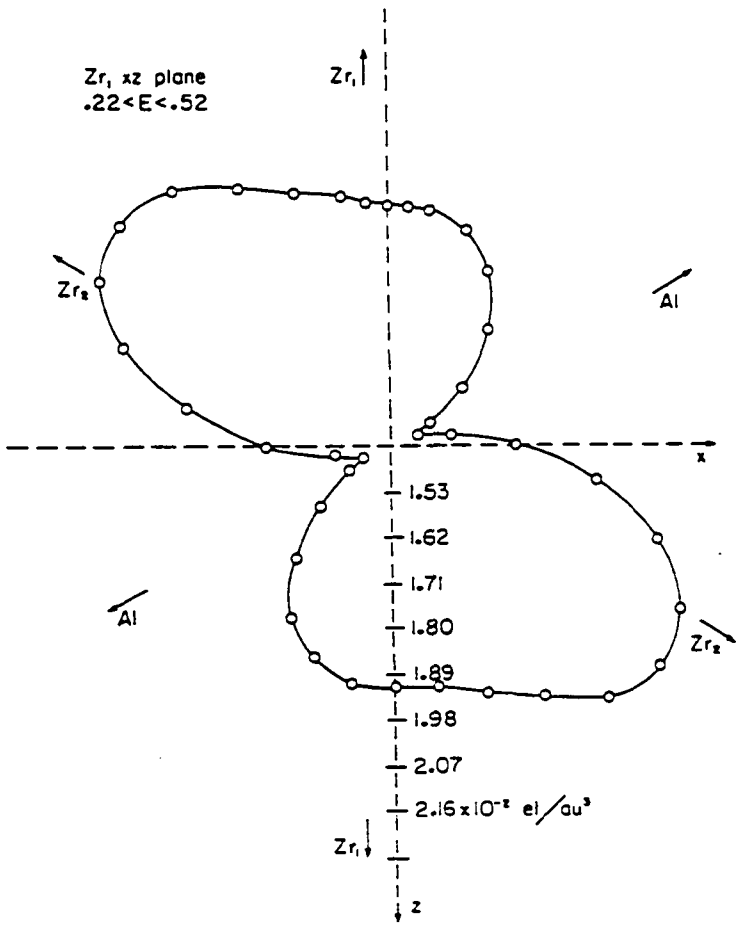

Figure 4.8. The charge density at the surface of the Zr_1 sphere in the xz plane due to occupied conduction band states

Figure 4.4 shows evidence of direct Zr_2-Al σ bonding in the small hexagonal nets, the charge density around a Zr_2 atom is maximized in the xy plane in the direction of an aluminum atom. The charge density at the surface of the Zr_1 sphere in the xz plane is shown in Figure 4.5. The charge density around the Zr_1 atom is maximized in the direction of the aluminum atoms in the hexagonal nets immediately above or below the Zr_1 atom. There is a small charge build up in the direction of the Zr_2 atoms in the hexagonal nets above and below the Zr_1 atom. There is a maximum in the charge density around a Zr_1 atom along the z-axis, the direction of the next nearest Zr_1 atom in the Zr_1 columns. The principal interactions in the valence band then appear to be intralayer Zr_2-Al bonding and interlayer Zr_1-Al bonding. No evidence is seen of any substantial Zr-Zr interactions in the valence band levels.

In the conduction band, interactions of a different type can be found. Plots of the charge density around the Zr_2 atom in the xz and xy planes are shown in Figures 4.6 throught 4.7. The charge density around the Zr_2 is shown in these figures to again maximize in the plane of the small Zr_2-Al hexagonal nets (the xy plane). The direction of the maxima are in this case towards the center of the hexagons, with minima in the direction of the Al atoms in the same plane. The charge density at the surface of the Zr_1 sphere also has different features, as shown in Figure 4.8, which plots the charge around the Zr_1 atom in the xz plane. There is a significant build up of charge in the direction of the Zr_2 atoms in the layers above and below the Zr_1 atom, with some charge also directed along the z axis towards the neighboring atoms in the Zr_1 column. There

is again a minima towards the Al atoms. The maxima in the charge density around the Zr_1 atom is in fact directed between the positions of neighboring Zr_1 and Zr_2 atoms, probably because the charge density along the Zr_1-Zr_1 and Zr_2-Zr_2 directions superimposes to create a maximum in this position. The interactions in the conduction band can be described as three center Zr_2-Zr_2 interlayer bonding in the small hexagonal nets, Zr_1-Zr_2 interlayer bonding and to a somewhat lesser extent Zr_1-Zr_1 bonding along the z-axis.

The bonding interactions in Zr_2Al can thus be summarized as follows. In the valence band, zirconium to aluminum bonding takes place; evidence is seen in the charge density plots of Zr_2-Al bonding in the xy planes and Zr_1-Al interlayer bonding. In the conduction band, the interactions appear to be Zr-Zr bonding; a three-centered bond appears between Zr_2 atoms in the plane of the Zr_2-Al hexagonal nets (xy plane) and evidence is seen of Zr_1-Zr_2 interlayer and to a lesser extent Zr_1-Zr_1 bonding along the c-axis. The fact that, in the conduction band, charge density minima are observed in the direction of aluminum atoms and that the DOS plots show a significant density of Al p states in the conduction band would seem to suggest that the Al p-orbitals are essentially nonbonding. This is a contrast to previous calculations of the electronic structure of early transition metal sulfides[44-46] which show the sulfur p-type states contributing to valence band interactions in these metallic sulfides. A three-centered Zr-Zr bonding interaction has been observed in ZrS of the WC type[44] however, and is quite similar to the Zr_2-Zr_2 three-centered bond observed in the conduction band of Ni_2In type Zr_2Al.

Some of the main structural features of Zr_2Al, such as alternating Zr-Al nets with columns of Zr atoms running through the nets, can be found in other Zr-Al compounds such as Zr_5Al_3 (W_5Si_3-type and Mn_5Si_3 type), Zr_4Al_3, and Zr_5Al_4 (Ti_5Ga_4 type). The factors stabilizing Zr_2Al, such as the intralayer Zr_2-Al and interlayer Zr_1-Al and Zr_1-Zr_2 interactions can be presumed to occur in these other compounds as well. It is also interesting to use the results of this calculation as an attempted test to the Brewer-Engel correlation of crystal structure with electronic configuration. The coordination of the various atoms in the Zr_2Al-type structure resembles most closely the hcp structure of a pure metal; considering only the Zr atoms the structure appears as a double hexagonal ABAC... type of stacking and considering only aluminum atoms the structure appears as an ordinary hcp ABAB... type. The Brewer-Engel correlation would then predict ~2 s, p-type electrons per atom. The integration of the partial DOS curves indicates there are approximately 1.18 s,p electrons on each zirconium atom and 2.37 on each aluminum, or an overall average of 1.57 s,p electrons per atom if no distinction is made between types of atoms. The applicability of the correlation of this regard is somewhat questionable.

V. FINAL SUMMARY AND CONCLUSIONS

All of the intermediate phases previously reported in the zirconium-aluminum system were observed during the course of this investigation. The existence of the majority of these is well-established so efforts were concentrated primarily on some of the more controversial, particularly in the central region of the phase diagram. The existence of ZrAl was reconfirmed and an impurity analysis indicates it to be a binary, not a Hf stabilized ternary. The existence and nonexistence of Zr_5Al_4 and Zr_4Al_3, respectively at temperatures in excess of about 1000°C was confirmed.

Thermodynamic data for the entire Zr-Al system were collected in high temperature vaporization experiments. Aluminum vapor pressure data collected across the system were used to derive enthalpies of formation of seven zirconium-aluminum compounds. The results of these experiments are the only such data available for this system.

A nonself-consistent band structure calculation for the compound Zr_2Al was performed. A substantial degree of covalent interaction was found, with Zr-Al bonding taking place in valence-band type states and Zr-Zr interactions in the conduction band. A three centered Zr-Zr interaction in the conduction band, similar to that previously observed in a similar calculation for ZrS, was also found in Zr_2Al.

An attempt can be made to evaluate the relative successes of the current study and the remaining uncertainties about the Zr-Al phase relationships and thermodynamics. Some unsuccessful experimental

undertakings might also be mentioned in this context. The heat treatment experiments performed with sample compositions near the center of the Zr-Al phase served to verify the major phase diagram features in this area, especially those reported by Potschke and Schubert who indicated that the high temperature phase Zr_5Al_4 decomposed eutectoidally at nearly the same temperature at which Zr_4Al_3 formed peritectoidally (Figure 1.2), and reported observing the alleged ternary phase "$Zr_5Al_3O_x$" over a significant range of composition (~50 to 63 at %). The annealing/X-ray diffraction experiments described in Section II revealed an apparent Ti_5Ga_4-type phase, presumably Zr_5Al_4, in samples of nominal composition 81 wt % Zr (55 atomic %) cooled from temperatures higher than ~1200°C, and a Zr_4Al_3 phase in the samples cooled from temperatures below ~1000°C. The powder patterns of samples cooled from temperatures between ~1000°C and ~1200°C were very complicated, with another hexagonal phase quite like the reported Mn_5Si_3-type "$Zr_5Al_3O_x$" phase appearing along with Zr_5Al_4. The appearance of this new phase, coupled with the fact that the non-metallic impurities in the samples used are rather low, that the appearance and disappearance of the phases Zr_4Al_3, Zr_5Al_4, and the supposed Mn_5Si_3 type ternary "$Zr_5Al_3O_x$" were reversible with heat treatment, and that the Ti_5Ga_4 type structure of Zr_5Al_4 is quite closely related to the Mn_5Si_3 type structure seem to suggest that Zr_5Al_4 orders on cooling from high temperature to form another phase also with a structure quite closely related to the Mn_5Si_3 structure. Both Zr_5Al_4 of the Ta_5Ga_4 type and the new Mn_5Si_3 type phase then decompose on further cooling. The supposed ternary "$Zr_5Al_3O_x$" phase observed in this system may thus be

a binary phase with a very limited temperature range of stability, and it seems unlikely that Zr_5Al_4 decomposes eutectoidally into ZrAl and Zr_4Al_3 as suggested by Potschke and Schubert.

The thermodynamic properties measured and derived herein are substantially complete covering compositions across the entire Zr-Al system and provide the only basic experimental data available for this system. The primary data are aluminum partial pressures measured at different temperatures and Zr/Al ratios. Experiments were often hampered by the low volatility of aluminum in the various solid samples used which made both weight-loss and mass-spectrometer measurements difficult and data for some of the more zirconium-rich compositions were collected over relatively narrow ($\leq$ 100°C) temperature ranges. Other experimental methods might be used to confirm and extend the results of this study. The enthalpies of formation of the various compounds could possibly be measured more accurately by direct reaction calorimetry. An experimental determination of zirconium activities in the Zr-Al system, perhaps by an electrochemical means, would provide data to complement the aluminum vapor pressure data measured herein by Knudsen cell techniques. In fact, numerous attempts were made during the course of this study to construct a solid state galvanic cell of the type

$$\underline{Zr}(Al), ZrO_2 \mid ThO_2(Y_2O_3) \mid Ni, NiO$$

in which a Y_2O_3 doped ThO_2 solid electrolyte would serve as an O^{2-} ionic conductor and the virtual cell reaction would become

$$\underline{Zr}(Al)(s) + 2NiO(s) = ZrO_2(s) + 2Ni(s).$$

Measurements of the voltage produced by this cell at various temperatures

(~1100 to 1300 K) should in principle permit evaluation of zirconium activities in the Zr(Al) alloy. Stable voltages and relative measurements were never obtained, however, probably due to a partial reduction of the ThO_2 based electrolyte at the Zr(Al), ZrO_2 electrode and a resulting degradation of its electrolytic properties. Alternative cells incorporating solid electrolytes based on CaF_2 or β'-alumina could possibly prove more functional in measuring Zr activities in Zr-Al alloys.

The band structure calculation performed on the compound Zr_2Al provided insight into the bonding in the Zr-Al compounds. Perhaps the most interesting feature emerging from the calculation is the clean energy separation between Zr-Al interactions which were found to occur in valence band type states and Zr-Zr interactions in conduction band states. It may also be worth noting that the thermodynamic results described herein show that the most stable Zr-Al compositions are on the aluminum rich side of the phase diagram. This seems to correlate with the band structure results showing that Zr-Al interactions occur in the lower energy states. Presumably, the more aluminum-rich compounds involve more extensive Zr-Al bonding and since these bonding interactions occur in the valence band states the thermodynamic stability of the more aluminum-rich compounds is enhanced relative to the Zr-rich compounds. Experimental confirmation of the electronic structure calculations is unfortunately lacking. Numerous attempts were made to examine core and valence level photoelectron spectra of several Zr-Al compositions. Surface contamination of the samples used hampered the measurements, core level spectra invariably showed what appeared to be "oxide" contamination

of the samples, and accurate valence band spectra could not be obtained. The only method available for cleaning the sample in situ was by means of argon ion bombardment, which causes undesirable changes in the sample surface. It was noted, however, that the apparent binding energies of the zirconium core levels were independent of the Zr/Al ratio, for example a Zr $3d_{5/2}$ binding energy of 178.5 eV was observed for pure Zr and for Zr-Al samples of nominal compositions Zr_2Al, ZrAl, and $ZrAl_2$.

VI. REFERENCES

1. Brauer, G. Z. Anorg. Chem. 1939, 242. 1.
2. Wilson, C. G. Acta Cryst. 1959, 12, 660.
3. Renouf, T. J.; Beevers, C. A. Acta Cryst. 1961, 14, 469.
4. Spooner, F. J.; Wilson, C. G. Acta Cryst. 1962, 15, 621.
5. Schubert K.; Anantharaman, T. R.; Ata, H. O. K.; Meisner, H.-G.; Potschke, M.; Robteutscher, W.; Stolz, E. Naturwiss. 1960, 47, 512.
6. Wilson, C. G.; Thomas, D. K.; Spooner, F. T. Acta Cryst. 1960, 13, 56.
7. Wilson, C. G.; Spooner, F. J. Acta Cryst. 1960, 13, 358.
8. Edshammar, L. E.; Andersson, S. Acta Chem. Scand. 1960, 14, 56.
9. Wilson, C. G.; Sams, D. Acta Cryst. 1961, 14, 71.
10. Keeler, J. H.; Mallery, J. H. J. Metals, 1955, 7, 394.
11. Wilson, C. G.; Sams, D.; Renouf, T. J. Acta Cryst. 1959, 12, 947.
12. Pearson, W. B. "A Handbook of Lattice Spacings and Structures of Metals and Alloys", Pergamon: New York, 1967.
13. Fink, W. L.; Willey, L. A. Trans. Am. Inst. Mining and Metallurgical Engineers 1939, 133, 69.
14. McPhersen, D. J.; Hansen, M. Trans. Am. Soc. Metals 1954, 46, 554.
15. Hansen, M. "Constitution of Binary Alloys", McGraw-Hill: New York, 1958.
16. Hultgren, R.; Orr, R. L.; Anderson, D. P.; Kelley, K. K. "Selected Values of Thermodynamic Properties of Metals and Alloys", Wiley & Sons, Inc.: New York, 1963.
17. Kubashewski, O. in "Atomic Energy Review, Zirconium: Physicochemical Properties of its Compounds and Alloys"; International Atomic Energy Agency: Vienna, 1976; special issue No. 6.
18. Edshammar, L. E. Acta Chem. Scand. 1962, 16, 20.

19. Nowotny, H. et al. Mh. Chemie 1959, 90, 15.

20. Potschke, M.; Schubert, K. Z. Metallkde 1962, 53, 548.

21. Schneider, A.; Klotz, H.; Stendel, J.; Strauss, G. Pure Appl. Chem. 1961, 2, 13.

22. Clark, C. M.; Smith, D. K.; Johnson, G. J. "A Fortran IV Program for Calculating X-Ray Powder Diffraction Patterns--Version 5", Department of Geosciences, Pennsylvania State University, University Park, PA, 1973.

23. Takusagawa, F. Ames Laboratory, Iowa State University, unpublished research, 1976.

24. Knudsen, M. Ann. Physik. 1909, 29, 179.

25. Cater, E. D. in "Techniques of Metal Research"; R. F. Bunshah, Ed.; Wiley-Interscience: New York, 1970; Vol. IV, Part 1, Chapter 2A.

26. Grimley, R. T. in "The Characterization of High Temperature Vapors"; J. L. Margrave, Ed.; Wiley & Sons, Inc.: New York, 1967; Chapter 8.

27. Schiffman, R. A.; Franzen, H. F.; Ziegler, R. J. High Temperature Science 1982, 15, 69.

28. Shilo, I.; Franzen, H. F.; Schiffman, R. A. J. Electrochem. Soc. 1982, 129, 1608.

29. Shilo, I.; Franzen, H. F. J. Electrochem. Soc. 1982, 129, 2613.

30. Lewis, G. N.; Randall, M. "Thermodynamics"; revised by Leo Brewer, K. S. Pitzer; McGraw-Hill: New York, 1961.

31. Cubiciotti, D. J. Phys. Chem. 1966, 70, 2410.

32. Kubaschewski, O.; Evans, E. L.; Alcock, C. B. "Metallurgical Thermochemistry", 4th ed.; Pergamon: New York, 1967.

33. Hultgren, R.; Desai, P. D.; Hawkins, D. T.; Gleisser, M.; Kelley, K. K.; Wagner, D. D. "Selected Values of Thermodynamic Properties of the Elements", Wiley & Sons, Inc.: New York, 1963.

34. Beauchamp, K. G.; Yuen, C. K. "Digital Methods for Signal Analysis", George Allen & Unwin: Boston, 1979; Chapters 2, 5 and 6.

35. Savitsky, A.; Golay, M. J. E. Anal. Chem. 1964, 36, 1627.

36. Kaufmann, L.; Nesor, H. NASA Contract NAS-3-17304, Report, 1974.

37. Hoch, M.; Russell, R. J. Metall. Trans. 1971, 2, 2627.

38. Brewer, L. Science, 1968, 161, 115.

39. Brewer, L.; Wengert, P. R. Metall. Trans. 1973, 4, 83.

40. Miedema, A. R.; Boom, R.; deBoer, F. R. J. Less-Common Met. 1975, 41, 283.

41. Miedema, A. R.; de Chatel, P. F.; deBoer, F. R. Physica B 1980, 100, 1.

42. Griffith, J. S. J. Inorg. Nucl. Chem. 1956, 3, 15.

43. Miedema, A. R. Philips Technical Review, 1976, 36, 217.

44. Nguyen, Thuy-Hoa Ph.D. Dissertation, Iowa State University, Ames, IA, 1980.

45. Nguyen, Thuy-Hoa; Franzen, H.; Harmon, B. N. J. Chem. Phys. 1980, 73, 425.

46. Nakahara, J.; Franzen, H.; Misemer, D. K. J. Chem. Phys. 1982, 76(8), 4080.

47. Köhn, W.; Rostoker, N. Phys. Rev. 1954, 94, 1111.

48. Ashcroft, N. W.; Mermin, N. D. "Solid State Physics", Holt, Rinehart and Winston: New York, 1976; Chapters 8 and 11.

49. Ham, F. S.; Segall, B. Phys. Rev. 1961, 124, 1786.

50. Hermann, F.; Skillman, S. "Atomic Structure Calculations", Prentice Hall: Englewood Cliffs, New Jersey, 1963.

51. Matheiss, L. F. Phys. Rev. 1963, 133, 184.

52. Lowdin, P. O. Adv. Phys. 1956, 6, 1.

53. Slater, J. C. Phys. Rev. 1951, 81, 385.

54. Moruzzi, V. L.; Williams, A. R.; Janak, J. F. Phys. Rev. B, 1974, 10, 4856.

55. Johnson, K. H.; Connolly, J. W. D. "Electronic Density of States"; L. H. Bennett, Ed.; NBS Spec. Publication 323, 1971.

56. Wenger, A.; Steinemann, S. Helvetica Physica Acta 1974, 47, 321.

57. Poex, G.; Wucher, J. J. Phys. et le Radium, 1956, 17, 454.

ACKNOWLEDGEMENTS

Thanks are due to various colleagues who provided support during the course of this research. Several Ames Lab Postdoctoral Fellows, particularly Robert Schiffman, Ilan Shilo, and Bernd Harbrecht provided advice which helped improve the author's experimental technique. The assistance of James Anderegg of the Ames Laboratory in almost all matters ranging from instrumentation and computer programming to more mundane problems involving plumbing, electrical wiring, and "finding the leak" was quite valuable. The guidance and moral support provided throughout by Professor H. F. Franzen is deeply appreciated, as are the efforts of Shirley Standley in typing and preparing this dissertation.

VIII. APPENDIX A: SELECTED OBSERVED VS CALCULATED POWDER PATTERNS OF Zr-Al PHASES

(All powder patterns were obtained with a Guinier focusing camera, Cu K-Alpha radiation λ = 1.5406 Å, NBS Si internal standard)

(vs = very strong, m = moderate, w = weak, etc.)

THE OBSERVED POWDER PATTERN OF Zr_4Al_3

$2\Theta_{obs}$	Q_{obs}	Q_{calc}	I_{obs}	I_{calc}	hkℓ
16.36	341.0	342.7	WB	16.0	001
18.80	449.7	453.1	MWB	14.3	100
25.06	793.4	795.8	WB	14.3	101
32.96	1356.2	1359.6	S	96 .6	110
37.10	1706.1	1702.0	S	53.7	111
38.27	1811.0	1812.5	S	16.4	200
38.45	1827.4	1823.8	S	100.0	102
41.88	2152.8	2155.2	M	25.7	201
51.56	3187.6	3183.2	M	18.9	202
58.95	4080.2	4078.2	M	20.4	300
61.70	4432.7	4420.8	MWB	13.9	301
61.70	4432.7	4443.3	MWB	13.9	113
62.58	4546.0	4542.6	MB	55.4	212
65.37	4915.6	4896.5	W	8.1	203
69.17	5430.1	5437.6	MS	24.3	220
71.63	5771.5	5780.3	VVW	2.4	221
75.09	6259.3	6255.9	VVW	1.8	213
79.14	6840.0	6842.0	W	22.4	114
82.00	7255.3	7261.4	WB	34.0	312
82.00	7255.3	7250.1	WB	34.0	400

Lattice parameters: a = 5.424(1) Å
c = 5.405(2) Å

THE OBSERVED POWDER PATTERN OF $ZrAl_3$

$2\Theta_{obs}$	Q_{obs}	Q_{calc}	I_{obs}	I_{calc}	hkℓ
204.83	316.1	3.17.7	M	15.7	004
227.23	388.1	389.3	MS	29.7	101
27.055	547.1	548.2	M	11.5	103
31.512	737.3	738.9	M	11.6	110
34.118	860.5	865.9	MS	17.1	105
37.901	1054.6	1056.7	S	100.0	114
41.775	1271.2	1270.8	MS	18.1	008
45.181	1475.7	1477.9	MS	31.8	200
50.141	1795.5	1795.6	MW	6.5	204
51.090	1859.5	1867.3	MW	7.4	211
52.850	1980.5	1977.9	M	8.1	109
53.307	2012.5	2009.8	MW	4.6	118
53.501	2025.9	2026.1	W	4.0	213
57.924	2344.7	2343.8	MW	8.6	215
63.250	2749.6	2748.8	MS	25.1	208
65.867	2955.6	2955.9	M	12.5	220
69.822	3275.1	3273.6	W	3.0	224
72.016	3456.0	3455.8	W	8.1	2.9
73.719	3598.5	3598.3	M	16.8	1,1,12
74.919	3699.2	3694.8	W	2.9	310
75.216	3723.9	3725.3	W	5.2	1,0,13
78.622	4013.5	4012.5	MS	36.9	314
81.079	4224.8	4226.7	M	16.9	228

Lattice parameters: a = 4.0074(7) Å
c = 17.286(4) Å

THE OBSERVED POWDER PATTERN OF $ZrAl_2$

$2\Theta_{obs}$	Q_{obs}	Q_{calc}	I_{obs}	I_{calc}	hkℓ
19.45	480.9	478.4	M	22.4	100
20.41	529.1	522.8	W	14.1	002
22.05	616.6	609.1	M	15.6	101
34.01	1441.4	1435.2	S	70.2	110
36.59	1661.2	1654.8	S	100.0	103
39.42	1917.1	1913.6	M	15.7	200
39.89	1960.8	1958.0	S	92.3	112
40.81	2048.6	2044.3	S	43.2	201
41.26	2091.7	2091.4	MW	5.0	004
46.00	2572.7	2569.8	W	2.6	104
50.70	3089.5	3090.0	M	8.4	203
52.90	3343.1	3348.8	M	2.9	210
54.05	3479.2	3479.6	M	3.8	211
56.27	3747.7	3746.2	MS	16.8	105
57.25	3867.4	3871.7	M	6.5	212
60.69	4301.8	4305.7	MS	15.4	300
62.44	4528.0	4525.2	S	48.1	213
63.75	4700.0	4705.5	MS	4.5	006
64.71	4826.4	4828.5	S	26.9	302
67.35	5181.7	5181.4	S	34.3	205
71.40	5738.7	5740.9	S	27.6	220
74.24	6138.4	6140.8	M	3.4	116
74.80	6217.4	6219.3	M	1.8	310
75.13	6264.0	6263.7	M	3.7	222
75.77	6354.7	6350.0	M	1.6	311
77.62	6619.6	6616.6	S	19.1	215

Lattice parameters: a = 5.2792(7) Å
c = 8.747(2) Å

THE OBSERVED POWDER PATTERN OF Zr_5Al_4

$2\Theta_{obs}$	Q_{obs}	Q_{calc}	I_{obs}	I_{calc}	hkℓ
12.07	186.4	186.7	VW	5.5	100
20.95	556.8	559.9	VW	3.6	110
34.31	747.3	746.5	M	12.1	200
26.13	860.9	858.9	MS	47.5	111
30.87	1193.4	1195.8	M	4.3	002
32.39	1310.9	1306.4	M	12.2	210
33.24	1378.8	1382.4	M	9.8	102
35.98	1607.4	1605.3	M	32.0	211
36.90	1687.9	1679.7	S	90.5	300
37.65	1754.9	1755.7	S	100.0	112
52.16	3257.1	3250.4	VW	7.5	113
53.66	3433.5	3435.3	W	32.7	222
57.11	3850.2	3844.9	VW	10.4	321
64.41	4786.6	4783.2	W	9.3	004
66.82	5109.3	5116.7	W	3.1	313
66.82	5109.3	5114.9	W	28.0	412

Lattice parameters: a = 8.452(2) Å
c = 5.784(2) Å

THE OBSERVED POWDER PATTERN OF Zr_2Al_3

$2\Theta_{obs}$	Q_{obs}	Q_{calc}	I_{obs}	I_{calc}	hkℓ
19.44	480.1	480.4	MS	27.1	111
22.43	637.5	638.9	MS	26.6	220
26.56	889.3	892.5	S	46.8	131
31.66	1254.4	1256.9	S	45.9	240
32.81	1344.2	1346.2	S	62.1	311
34.57	1487.8	1488.8	MS	45.1	022
37.21	1715.3	1715.7	S	48.8	202
37.21	1715.3	1716.6	VS	100.0	151
37.65	1754.3	1758.2	S	43.6	331
39.53	1926.8	1921.7	S	51.8	222
43.25	2288.7	2287.1	W	6.0	260
46.05	2578.7	2582.3	W	8.6	351
49.49	2952.5	2952.7	M	19.8	171
50.32	3046.5	3046.1	W	5.0	113
50.59	3077.0	3077.7	MW	7.7	511
51.10	3134.9	3137.0	W	4.0	062
52.47	3293.6	3296.3	W	3.3	080
53.86	3457.6	3458.1	M	16.8	133
54.14	3489.6	3489.7	M	12.9	531
54.90	3581.4	3585.7	MW	10.4	460
56.15	3732.2	3729.2	M	15.4	280
57.03	3840.8	3838.4	M	34.3	442
57.58	3908.6	3911.8	W	8.0	313
59.12	4101.7	4101.9	W	11.5	620
60.55	4283.9	4282.2	MW	19.7	153
60.86	4323.7	4313.8	W	5.5	551
63.03	4605.0	4600.9	W	5.1	191
63.90	4719.0	4719.9	W		640
66.19	5024.0	5027.9	W	5.9	282

Lattice parameters: a = 9.617(2) Å
b = 13.934(3) Å
c = 5.584(1) Å

THE OBSERVED POWDER PATTERN OF ZrAl
~76 wt % Zr SAMPLE ANNEALED AT 1250°C

$2\theta_{obs}$	Q_{obs}	Q_{calc}	I_{obs}	I_{calc}	hkℓ
16.18	333.8	337.2	M	13.5	020
26.46	882.7	884.7	MS	43.3	021
27.73	967.4	968.8	W	6.0	110
32.87	1348.7	1348.7	M	13.7	040
34.92	1516.8	1516.3	S	100.0	111
36.38	1641.9	1643.2	S	49.3	130
39.18	1894.4	1896.2	M	44.8	041
42.22	2186.2	2190.0	M	25.7	002
49.88	2996.5	2991.9	W	7.4	150
50.22	3035.0	3034.6	W	4.9	060
54.46	3540.8	3539.4	MS	16.2	151
56.97	3833.2	3833.2	MS	30.4	132
61.70	4431.2	4422.8	MW	9.9	221
65.12	4880.8	4886.9	W	4.7	240
66.18	5022.8	5015.0	MW	8.4	170
67.42	5190.7	5181.9	MW	7.2	152
70.15	5565.6	5562.5	MW	9.3	171
71.35	5731.8	5728.2	MW	14.6	202
72.52	5896.0	5896.4	MW	16.6	113
72.80	5934.3	5942.4	MW	10.7	081
77.27	6569.0	6572.7	VW	9.0	260
80.73	7069.0	6076.9	W	6.9	242
81.66	7204.9	7205.0	W	12.6	172

Lattice parameters: a = 3.362(1) Å
b = 10.892(3) Å
c = 4.274(2) Å

THE "Mn_5Si_3 TYPE" PHASE OBSERVED IN AN 81 Wt % SAMPLE ANNEALED AT 1200°C

$2\Theta_{obs}$	hkℓ	Q_{obs}	Q_{calc}	I_{obs}	I_{calc}	Overlapping reflections
21.64	110	5940	5981	w	12.6	
25.11	200	7965	7975	m	20.6	
26.87	111	9099	9093	m	24.1	
31.53	002	12440	12447	w	7.0	
33.44	210	13946	13955	ms	52.9	
34.07	102	14460	14441	ms	40.7	
37.12	211	17074	17068	s	100.0	
38.10	300	17952	17943	mvb	24.4	
38.65	112	18453	18429	s	65.3	
49.91	103	29997	30001	vw	0.0	ZrAl, Zr_5Al_4
50.24	302	30368	30391	w	6.3	
51.59	400	31913	31899	vw	4.3	
55.36	222	36369	36372	mb	23.3	
57.01	312	38386	38365	msb	7.4	Zr_5Al_4, ZrAl
59.80	140	41873	41867	mvb	28.1	
61.73	402	44360	44346	mb	26.5	
65.91	500	49877	49841	wb	3.4	
67.35	104	51820	51784	wvb	2.6	ZrAl
71.05	331	56907	56940	w	13.4	
72.55	421	58999	58934	w	0.4	ZrAl
74.89	502	62302	62289	w	21.2	
77.61	332	66181	66276	w	16.8	
78.67	304	67706	67734	vw	8.5	

Lattice parameters: a = 8.435 (2) (Å)
c = 5.786 (3) (Å)

IX. APPENDIX B: MEASURED ALUMINUM PARTIAL PRESSURES OVER THE VARIOUS TWO-PHASE REGIONS

Al PARTIAL PRESSURES OVER $ZrAl_3$, $ZrAl_2$ REGION

DEG K	I (AMPS)	P (ATM)	DH298 (CAL)
1578.	4.970E-09	6.509E-08	84813.838
1551.	3.230E-09	4.158E-08	84838.047
1530.	2.300E-09	2.921E-08	84831.967
1511.	1.870E-09	2.094E-08	84840.078
1458.	6.600E-10	7.987E-07	84827.109
1563.	3.800E-08	4.670E-06	85090.398
1298.	2.200E-11	2.372E-08	85107.727
1563.	3.860E-09	5.008E-08	84873.838
1537.	2.580E-09	3.291E-08	84831.523
1524.	2.110E-09	2.669E-08	84792.297
1458.	6.680E-10	8.084E-07	84792.211
1510.	1.660E-08	2.080E-08	84807.266
1563.	4.030E-09	5.228E-08	84739.977
1550.	3.220E-08	4.143E-08	84796.297
1419.	3.150E-10	3.710E-07	84841.797
1438.	4.520E-10	5.395E-07	84847.898
1449.	5.540E-10	6.683E-07	84854.070
1510.	1.670E-08	2.093E-08	84789.242
1577.	4.920E-09	6.440E-08	84797.227
1578.	4.880E-09	6.383E-08	84774.469
1818.	8.830E-09	1.198E-05	84763.109
1509.	1.620E-08	2.029E-08	84829.539
1648.	1.450E-08	1.981E-05	84582.523
1670.	2.030E-03	2.814E-05	84563.078
1471.	8.200E-10	1.001E-08	84880.984
1510.	1.630E-08	2.043E-08	84861.884
1550.	3.180E-08	4.065E-08	84854.219
1405.	2.280E-10	2.659E-07	84978.063
1380.	1.360E-10	1.558E-07	85007.922
1354.	8.000E-11	8.991E-08	84962.547
1328.	4.100E-11	4.519E-08	85222.083
1393.	1.820E-10	2.104E-07	84936.500
1418.	3.050E-10	3.592E-07	84932.758
1432.	3.890E-10	4.623E-07	84951.766
1444.	5.040E-10	6.041E-07	84858.469
1458.	6.450E-10	7.805E-07	84893.711
1470.	8.330E-10	1.018E-08	84782.555
1483.	1.040E-08	1.280E-08	84809.977
1498.	1.290E-08	1.802E-08	84844.336
1509.	1.820E-08	2.029E-08	84829.539
1522.	2.050E-08	2.590E-08	84778.930
1535.	2.410E-08	3.070E-08	84939.766
1548.	3.170E-08	4.078E-08	84795.148
1561.	3.880E-08	5.027E-08	84760.039
1575.	4.800E-08	8.275E-08	84777.859
1589.	5.970E-08	7.874E-08	84765.844
1601.	7.250E-08	8.634E-08	84721.836
1628.	1.120E-08	1.513E-05	84592.945
1673.	2.040E-08	2.833E-05	84691.848
1647.	1.380E-08	1.888E-05	84780.227

Al PARTIAL PRESSURES OVER $ZrAl_2$, Zr_2Al_3 REGION

DEG K	I (AMPS)	P (ATM)	DH298 (CAL)
1536.	7.900E-10	1.007E-06	88393.820
1508.	4.850E-10	6.070E-07	88392.375
1508.	4.870E-10	6.095E-07	88380.047
1482.	2.930E-10	3.804E-07	88488.430
1455.	1.720E-10	2.077E-07	88355.898
1430.	1.080E-10	1.282E-07	88484.500
1408.	8.400E-11	7.469E-08	88582.781
1535.	8.200E-10	1.045E-06	88227.945
1581.	1.290E-09	1.671E-06	88175.617
1590.	2.110E-09	2.785E-06	88099.594
1615.	3.230E-08	4.330E-08	87979.547
1646.	5.320E-09	7.268E-06	87861.875
1673.	7.970E-09	1.107E-05	87805.945
1499.	4.100E-10	5.101E-07	88412.711
1471.	2.350E-10	2.869E-07	88533.758
1589.	2.030E-09	2.677E-06	88171.711
1590.	2.050E-09	2.705E-06	88190.742
1561.	1.130E-09	1.464E-06	88586.359
1563.	1.220E-09	1.583E-06	88451.008
1562.	1.180E-09	1.530E-06	88503.305
1534.	7.600E-10	9.676E-07	88407.438
1534.	7.800E-10	9.931E-07	88328.266
1508.	4.810E-10	6.020E-07	88417.195
1481.	2.910E-10	3.577E-07	88454.125
1456.	1.700E-10	2.054E-07	88845.408
1432.	1.080E-10	1.284E-07	88597.984
1444.	1.370E-10	1.642E-07	88595.908
1470.	2.400E-10	2.928E-07	88417.297
1499.	4.180E-10	5.201E-07	88355.158
1577.	1.690E-09	2.212E-06	88145.625
1590.	2.070E-09	2.732E-06	88160.063
1615.	3.150E-08	4.222E-08	88060.031
1605.	2.620E-09	3.490E-08	88157.408
1646.	5.090E-09	6.954E-08	88006.414
1534.	7.500E-10	9.549E-07	88447.820
1535.	7.980E-10	1.014E-08	88318.547
1577.	1.710E-09	2.238E-06	88108.758
1615.	3.140E-09	4.209E-06	88070.227
1648.	5.290E-08	7.227E-06	87880.367
1561.	1.290E-09	1.671E-08	88175.617
1562.	1.200E-08	1.556E-08	88451.141
1535.	7.400E-10	9.428E-07	88541.047

Al PARTIAL PRESSURES OVER Zr_2Al_3, ZrAl REGION

DEG K	I (AMPS)	P (ATM)	DH298 (CAL)
1338.	1.049E-11	4.000E-09	92280.375
1343.	1.344E-11	5.143E-09	91939.588
1348.	1.412E-11	5.424E-09	92124.688
1353.	1.604E-11	6.184E-09	92098.961
1358.	1.723E-11	6.670E-09	92220.338
1363.	2.244E-11	8.718E-09	91819.758
1368.	2.239E-11	8.730E-09	92137.773
1373.	2.397E-11	9.378E-09	92264.023
1378.	2.549E-11	1.001E-08	92406.594
1383.	3.009E-11	1.186E-08	92260.047
1388.	3.435E-11	1.359E-08	92203.563
1393.	3.970E-11	1.578E-08	92109.742
1398.	4.328E-11	1.725E-08	92174.939
1403.	4.847E-11	1.858E-08	92281.063
1408.	5.421E-11	2.175E-08	92153.617
1413.	6.157E-11	2.479E-08	92098.023
1418.	6.779E-11	2.740E-08	92127.141
1423.	7.589E-11	3.078E-08	92107.211
1428.	8.410E-11	3.423E-08	92113.906
1433.	9.430E-11	3.851E-08	92084.656
1438.	1.046E-10	4.288E-08	92082.852
1443.	1.170E-10	4.812E-08	92056.844
1448.	1.289E-10	5.320E-08	92071.156
1453.	1.439E-10	5.958E-08	92046.070
1458.	1.605E-10	6.671E-08	92019.320
1463.	1.778E-10	7.412E-08	92012.820
1468.	1.976E-10	8.265E-08	91993.203
1473.	2.179E-10	9.148E-08	91993.281

Al PARTIAL PRESSURES OVER Zr_2Al_3, Zr_5Al_4 REGION

DEG K	I (AMPS)	P (ATM)	DH298 (CAL)
1503.	3.765E-10	1.613E-07	92074.711
1508.	4.179E-10	1.796E-07	92041.359
1513.	4.816E-10	1.990E-07	92021.039
1518.	5.098E-10	2.205E-07	91999.133
1523.	5.578E-10	2.421E-07	92003.102
1528.	8.079E-10	2.647E-07	92017.203
1533.	6.700E-10	2.927E-07	91995.289
1538.	7.280E-10	3.191E-07	92014.477
1543.	7.848E-10	3.451E-07	92056.609
1548.	8.601E-10	3.795E-07	92045.898
1553.	9.374E-10	4.149E-07	92050.625
1558.	1.027E-09	4.562E-07	92036.148
1563.	1.114E-09	4.960E-07	92054.320
1568.	1.217E-09	5.437E-07	92045.531
1573.	1.329E-09	5.952E-07	92038.977
1578.	1.452E-09	6.530E-07	92023.516
1583.	1.575E-09	7.105E-07	92032.477
1588.	1.719E-09	7.779E-07	92019.797
1593.	1.857E-09	8.431E-07	92037.250
1598.	2.027E-09	9.230E-07	92020.930
1603.	2.211E-09	1.010E-08	92004.078
1608.	2.237E-09	1.025E-08	92226.383
1613.	2.613E-09	1.201E-08	91987.141
1618.	2.829E-09	1.304E-08	91989.297
1623.	3.081E-09	1.425E-08	91970.563
1628.	3.368E-09	1.563E-08	91937.352
1633.	3.650E-09	1.699E-08	91931.531
1638.	3.968E-09	1.852E-08	91912.914
1643.	4.302E-09	2.015E-08	91901.430
1648.	4.683E-09	2.200E-08	91875.320
1653.	5.060E-09	2.384E-08	91871.508
1658.	5.514E-09	2.605E-08	91838.563
1663.	5.981E-09	2.825E-08	91829.641
1668.	6.449E-09	3.068E-08	91816.398
1673.	8.934E-09	3.306E-08	91822.375

Al PARTIAL PRESSURES OVER Zr_5Al_4, Zr_3Al_2 REGION

DEG K	I (AMPS)	P (ATM)	DH298 (CAL)
1519.	1.038E-10	4.101E-08	97161.063
1524.	1.113E-10	4.412E-08	97230.234
1529.	1.266E-10	5.035E-08	97118.727
1534.	1.347E-10	5.373E-08	97209.329
1539.	1.468E-10	5.871E-09	97226.219
1543.	1.560E-10	6.259E-08	97316.570
1549.	1.685E-10	8.702E-08	97392.299
1553.	1.840E-10	7.428E-08	97360.570
1558.	2.054E-10	8.319E-08	97293.938
1563.	2.160E-10	8.774E-08	97412.008
1567.	2.295E-10	9.353E-08	97495.453
1572.	2.611E-10	1.067E-07	97364.719
1577.	2.740E-10	1.123E-07	97484.531
1582.	3.009E-10	1.238E-07	97460.492
1587.	3.173E-10	1.309E-07	97562.734
1591.	3.489E-10	1.444E-07	97531.172
1596.	3.678E-10	1.526E-07	97631.680
1601.	3.993E-10	1.662E-07	97636.633
1608.	4.275E-10	1.785E-07	97684.789
1611.	4.498E-10	1.883E-07	97787.914
1615.	4.980E-10	2.092E-07	97725.680
1620.	5.380E-10	2.266E-07	97740.547
1625.	5.800E-10	2.450E-07	97760.555
1630.	8.250E-10	2.648E-07	97780.438

Al PARTIAL PRESSURES OVER Zr_3Al_2, Zr_5Al_3 REGION

DEG K	I (AMPS)	P (ATM)	DH298 (CAL)
1464.	1.763E-11	6.941E-09	98961.453
1469.	2.135E-11	8.437E-09	98713.680
1474.	2.273E-11	9.011E-09	98840.703
1479.	2.423E-11	9.638E-09	98961.914
1484.	2.700E-11	1.078E-08	98950.408
1489.	3.090E-11	1.238E-08	98858.289
1494.	3.302E-11	1.327E-08	98968.430
1499.	3.925E-11	1.583E-08	98756.852
1504.	4.287E-11	1.735E-08	98795.781
1509.	4.543E-11	1.844E-08	98924.438
1514.	5.230E-11	2.130E-08	98801.648
1519.	5.617E-11	2.295E-08	98885.539
1524.	6.310E-11	2.587E-08	98832.305
1529.	6.575E-11	2.704E-08	99004.805
1534.	7.168E-11	2.958E-08	99038.734
1539.	7.908E-11	3.274E-08	99034.203
1544.	9.080E-11	3.763E-08	98911.602
1549.	1.014E-10	4.224E-08	98859.055
1554.	1.089E-10	4.551E-08	98930.727
1559.	1.155E-10	4.845E-08	99038.281
1584.	1.303E-10	5.481E-08	98955.344
1569.	1.396E-10	5.891E-08	99029.518
1574.	1.541E-10	6.525E-08	99008.203
1579.	1.695E-10	7.201E-08	98996.088
1584.	1.878E-10	8.002E-08	98959.969
1589.	1.996E-10	8.531E-08	99052.898
1594.	2.198E-10	8.425E-08	99031.375

Al PARTIAL PRESSURES OVER Zr_5Al_3, Zr(ss) REGION

DEG K	I (AMPS)	P (ATM)	DH298 (CAL)
1493.	1.035E-11	4.402E-09	102177.508
1498.	1.135E-11	4.847E-09	102216.430
1503.	1.290E-11	5.527E-09	102148.969
1508.	1.410E-11	6.061E-09	102195.768
1513.	1.574E-11	6.786E-09	102178.336
1518.	1.730E-11	7.486E-09	102203.328
1523.	1.914E-11	8.309E-09	102207.633
1528.	2.112E-11	9.198E-09	102217.641
1533.	2.349E-11	1.026E-08	102202.016
1538.	2.590E-11	1.135E-08	102209.750
1543.	2.854E-11	1.255E-08	102217.773
1548.	3.151E-11	1.390E-08	102217.391
1553.	3.490E-11	1.545E-08	102204.719
1558.	3.869E-11	1.718E-08	102187.422
1563.	4.229E-11	1.884E-08	102212.438
1568.	4.669E-11	2.086E-08	102203.908
1573.	5.146E-11	2.307E-08	102198.008
1578.	5.648E-11	2.540E-08	102203.734